Evaluation of an OpenSees Layered Shell Model for Simulating Flexure-Controlled Reinforced Concrete Walls

Joshua Stokley

A thesis

submitted in partial fulfillment of the

requirements for the degree of

Master of Science in Civil Engineering

University of Washington

2023

Reading Committee:

Laura Lowes

Pedro Arduino

Paolo Calvi

Program Authorized to Offer Degree:

Civil & Environmental Engineering

University of Washington

Abstract

Evaluation of Existing Nonlinear Finite Element Modeling Software for Simulation and Calibration of RC walls

Joshua Stokley

Chair of the Supervisory Committee:

Laura Lowes

Civil & Environmental Engineering

Reinforced concrete walls are used commonly in mid- and high-rise buildings to resist lateral loads; typically, concrete walls have three-dimensional configurations to maximize stiffness and strength and to accommodate architectural constraints. Seismic design, evaluation, and retrofit of concrete wall buildings often requires nonlinear analysis to predict performance, assessment of earthquake risk for regions and individual buildings often requires nonlinear analysis to predict damage, loss of functionality, and repair time and cost. The research presents here used high-performance cloud-computing resources to calibrate an OpenSees model for simulating the earthquake response of planar walls. Jupyter notebooks were used to create and run OpenSees models of individual walls included in a published experimental dataset, and Jupyter notebooks were used to define error functions for the model calibration effort. Creation of an efficient research workflow was enabled by use of the NHERI SimCenter quoFEM software. Computational time was reduced by using cloud computing resources provided by the NHERI DesignSafe-CI facility. Results of the effort include recommendations for modeling walls to provide accurate simulation of response and the creation of the Jupyter notebooks can support future projects.

TABLE OF CONTENTS

LIST OF FIGURES

LIST OF TABLES

Chapter 1. Introduction

Reinforced concrete walls are used in commonly in buildings to resist lateral forces resulting from wind and earthquakes; walls can easily and efficiently be designed to provide high lateral strength and stiffness. In regions of high seismicity, walls are designed to exhibit flexure-controlled response under earthquake loading. Under service-level lateral loading, flexure-controlled walls are expected to exhibit modest cracking in the regions of high flexural demand; under design-level loading, walls are expected to exhibit significant damage, including concrete cracking and spalling as well as buckling and yielding of reinforcing steel. The *American Concrete Institute (ACI) Concrete Design Code 318* [1] provides requirements for detailing concrete walls so that damaged walls maintain lateral and axial load-carrying capacity at large deformation demand, and ASCE-7 specifies wind, earthquake and other demands to be used in wall design. Both ACI 318 and ASCE-7 provide requirements for analysis to determine demands used in design of individual walls; though, local jurisdictions often supplemented these requirements, for example in regions of high seismicity on the UW West Coast the design of walls in tall buildings requires nonlinear analysis using suites of site-specific ground motion records to demonstrate acceptable performance under service- and design-level lateral loading.

Current design requirements and standards of practice for design and construction of walls were developed primarily using data from laboratory tests of wall specimens with relatively simple configurations, very simple load patterns and quasi-static loading. An experimental data set assembled and published by Shegay[21] includes 142, with only 33 walls being used in this research. Expanding this experimental data set substantially to include laboratory data for walls with distributed earthquake loading and a variety of complex configurations that are representative of current design practice is not viable, given that there are few testing facilities that have the physical size, equipment capacity, control software to support representative loading scenarios, and instrumentation to accomplish high-resolution monitoring of specimen deformation. However, numerical modeling, using models that have been validated using experimental data, can be used to advance design of nonplanar walls and walls with complex configurations subjected to complex load patters.

The current study seeks to advance numerical modeling of reinforced concrete walls for use in i) performance-based design of tall walled buildings, which requires nonlinear dynamic analyses to demonstrate that a proposed design will exhibit acceptable performance under wind as well as service-level loading and design-level earthquake loading and ii) research to advance understanding of the earthquake behavior and performance on walls with complex configurations and, ultimately, to generate data to advance design requirements and performance-based design processes. Specifically, the study i) employs a series of Jupyter notebooks that assemble and convert a MATLAB database to python, model RC walls, post process to visualize simulated results, and provide error functions to determine accuracy of simulations, ii) quantify uncertainty of key parameters through the use of online resources like TACC and DesignSafe through the means of sensitivity studies on QuoFEM, and iii) Give recommendations on shell element formulations and values for key parameters.

Various wall specimens have been investigated in the lab to understand these failure modes and many modeling techniques have been developed to best represent the response of these walls through simulations. Though some of these techniques do a great job representing some of the aspects of the experimental results, they fail to meet the mark on certain responses like prediction of stiffness, strength, deformation capacity, and localization of failure. Part of this is due to the uncertainty in variables that are defined in the material models and the capabilities of the modeling techniques being used. To better represent the responses of these wall specimens, a mutli-layer shell element analysis was implemented, and sensitivity analyses were used to optimize uncertainty.

1.1 Research Objectives

The primary objectives of the research presented in this thesis are:

1. Develop a modeling technique that makes use of 3D continuum shell elements to accurately predict stiffness, strength, deformation capacity, failure mode, and cyclic response of wall test specimens.
2. Provide recommendation between two shell models studied in previous work.

3. Conduct sensitivity and parameter studies to optimize the shear retention factor and crushing energy ratio of the concrete and the strain hardening ratio and steel buckling rupture strain of the steel.
4. To provide recommendations for the said variables in the context of the multi-layer shell element model.

1.2 Organization

These research activities and results are presented in this thesis as follows:

Chapter 2 introduces the experimental data set used in the current study as well as the three subsets of this dataset that are used to support i) preliminary evaluation and calibration of the model, ii) calibration of the model, and iii) validation of the calibrated model. A series of error functions are defined to support model calibration.

Chapter 3 reviews nonlinear response models that have been used previously by practicing engineers and university researchers as well as presents the layered shell element and associated material model used in the current study. shell element formulation and the material models are introduced and represented. A series of preliminary analyses using dataset #1 investigates model configuration (preferred element size, smeared versus discrete reinforcing steel, and mesh sensitivity) to give a recommendation of a shell element.

Chapter 4 introduces tools and resources used in this study. Online resources like NHERI, TACC, and SimCenter are referenced and the Jupyter notebooks created for this study are discussed in greater detail. The use of QuoFEM's sensitivity analysis and parameter estimations are explained.

Chapter 5 starts with simulated runs of four walls with baseline values of the key parameters to understand how these parameters affect the outcome of the error functions. A calibrated study is conducted on a larger list of walls to determine best values of these parameters that are then used on a different set of walls to validate results.

Chapter 2. Experimental Data Used for Model Calibration and Validation

2.1 Introduction

This chapter presents the experimental data used for model evaluation, calibration, and validation. Experimental data were sought that characterize the behavior of planar walls, exhibiting flexure-controlled response, when subjected to quasi-static cyclic lateral loading and constant axial loading. The data set compiled by Shegay et al. [21] and published in the NHERI DesignSafe Data Depot [18] was found to provide comprehensive design and performance data for 48 planar walls meeting these criteria. In this Chapter, Section 2.1 presents the Shegay et al. data set, Section 2.2 describes behavior of the slender planar wall test specimens used in the current study, and Section 2.3 presents the MATLAB data structure created by Shegay as well as discusses how this data structure is ported to python for use in the current study.

2.2 Experimental Data

Previous research, Lowes [10] shows that code-compliant slender walls typically exhibit flexure-controlled response when subjected to cyclic lateral loading and modest axial load. Previous research shows also that walls with high shear demand, high axial load, or non-planar configurations that results in high localized compression demand, may exhibit flexure-controlled response or flexure-shear-controlled response with low ductility. While the layered shell element consider in the current study is appropriate for modeling the response and failure of planar and non-planar concrete walls exhibiting the full range of ductile and non-ductile response modes, this preliminary study focusses on the simplest wall configuration and wall response modes: planar walls exhibiting tension- and compression-controlled flexural failure.

A first step in the research process was to assemble an experimental data set comprising planar wall test specimens, with a breadth of design characteristics, exhibiting flexure-controlled response in the laboratory. The wall data set published by Shegay et al. in the DesignSafe Data

Depot [18] was found to meet the data needs of the project. The Shegay data set provides design details and measured response data for 142 concrete walls with a wide range of configurations and design details. For the current study, only planar walls with a thickness greater than 4 inches, without spliced reinforcing steel and with a shear span ratio (height from foundation to the point of shear load application divided by the length of the wall) greater than 1.5 were used; planar wall not meeting these criteria were considered to have a high likelihood of exhibiting reduced deformation capacity and/or a failure mode other than flexure due to confinement. Figure 2.1 shows the distribution of nine design parameters, considered to be particularly influential in determining wall behavior and performance, for the 33 walls planar walls, from 11 experimental test programs, that met the requirements for inclusion in the current study. Appendix A provides the data presented in Figure 2.1 for the experimental test program.

As shown in Figure 2.1, the walls are divided into two sets, a calibration set and a validation set. All walls were included in either the calibration set or the validation set. Both have walls with a range of axial load ratios, shear span and cross-sectional aspect ratios. In terms of each experimental wall programs, programs with two or less walls were grouped together into the calibration or validation set. Programs with three or more were split up between the calibration and validation sets.

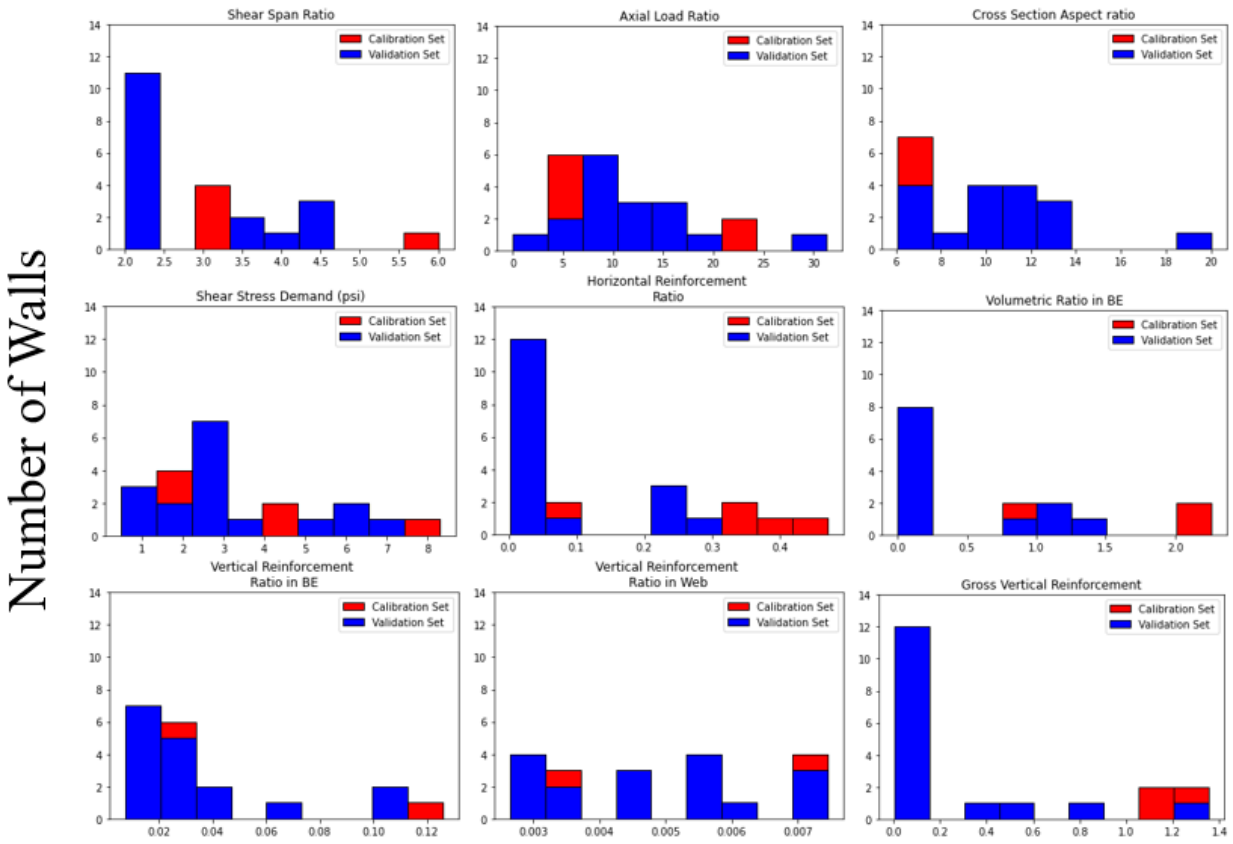

Figure 2.1 *Wall design parameters bar charts for calibration and validation sets*

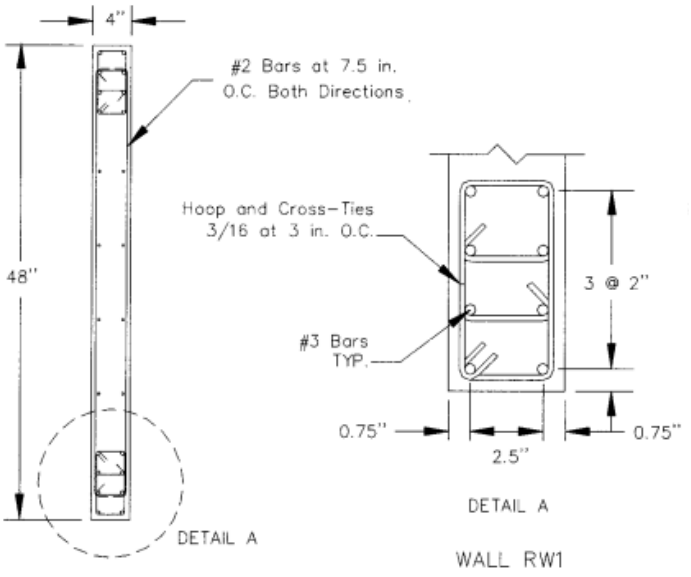

Figure 2.2 *Boundary reinforcement detail*

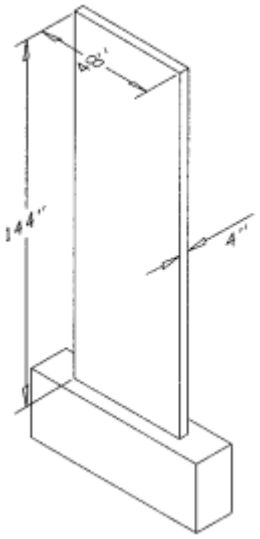

Figure 2.3 *Three dimensional view*

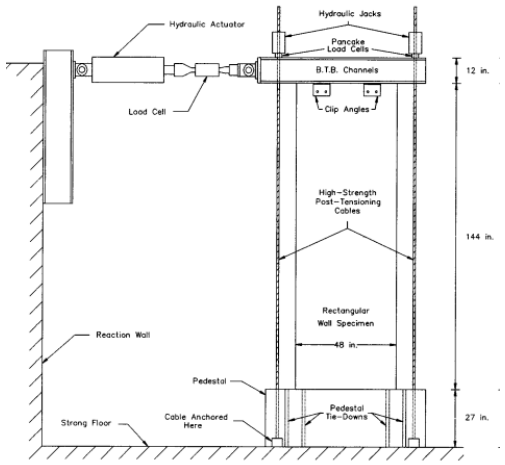

Figure 2.4 *Specimen set up*

- Shear Span Ratio: Effective height divided by length of wall. The effective height can be defined as the base moment of the wall divided by the base shear of the wall. The length of the wall in terms of RW1 is 48 inches as shown in figure 2.2.
- Axial Load Ratio: The vertical load applied on top of the wall (see figure 2.4 where this load is applied by the hydraulic jacks) divided by the concrete compressive strength, thickness of the wall (see figure 2.3 where the thickness is 4 inches), and the length of the wall.

- Cross Section Aspect Ratio: Length of the wall divided by the thickness of the wall.
- Shear Stress Demand: Maximum shear force attained in the test divided by the thickness of the wall, length of the wall, and the square root of the compressive strength of the concrete.
- Horizontal Reinforcement ratio: Area of horizontal reinforcement divided by spacing the horizontal reinforcement layers and thickness of the wall. In figure 2.2, the horizontal bar used in the web are #2 bars and the spacing is 7.5 inches.
- Volumetric Ratio in BE: Volume of one layer of hoops/ties in boundary region divided by the length of the boundary region, spacing of the hoops, and thickness of the wall. In figure 2.2, the length of the boundary region is roughly 4 inches, spacing of the hoops is 3 inches.
- Vertical Reinforcement Ratio in BE: Area of longitudinal reinforcement in the BE divided length of the boundary and thickness of the wall.
- Vertical Reinforcement Ratio in Web: Area of longitudinal reinforcement in the web divided by length of wall, thickness of wall minus two multiplied length of the boundary multiplied by thickness of the wall.
- Gross Vertical Reinforcement: Area of all longitudinal reinforcement divided by length of wall and thickness of wall.

2.3 Summary of Experimental Tests

- Dazio et al. (2009): Six reinforced concrete walls were tested to investigate the impact on deformation capacity of vertical reinforcement ratio and strain capacity. Wall designs were consistent with existing construction in Europe, and walls were representative of mid-rise construction with relatively low axial load ratio. Results of laboratory testing show that deformation and ductility capacity is reduced with low reinforcement ratios and use of low ductility reinforcing steel.

- Liu (2004): The experimental program was designed to investigate the impact of concrete compressive strength on wall performance for specimens subjected to cyclic lateral load

protocols. Two walls were tested; the walls were identical in design with the exception that they were constructed using concrete with different compressive strength.

- Lowes et al. (2011): The experimental program investigated the earthquake response of mid-rise slender walls designed using ACI 318-14. Four planar wall specimens were tested; test specimens differed with respect to a splice at the base of the wall, shear stress demand and use of uniformly distributed reinforcement versus a reinforcement layout with heavily reinforced boundary elements and a lightly reinforced web region. Walls without splices sustained damage at the base of the wall; walls with splices sustained damage at both the top of the splice and the base of the wall, with the critical region depending on the shear demand. Shear demand also affected response; a moderate increase in shear demand resulted in the failure mechanism changing from bar fracture to flexure–compression failure of the boundary elements.
- Thomsen et al. (1995): The research assess the performance of walls designed using a displacement-based design approach. Four walls were developed (Two T-shaped cross sections and two of which are rectangular cross sections) and the walls were tested with constant axial load and reverse cyclic lateral loads. Walls were designed using ACI 318-89, and test variables comprised wall shape, transverse steel configuration, and the distribution of web steel. Test results indicated that displacement-based design procedures resulted in acceptable performance and enabled the use of reduced transverse reinforcement.

- Oh et al. (2002): Three planar reinforced concrete wall specimens were tested under constant axial load and quasi-static cyclic lateral loading to investigate the impact of boundary element detailing on deformation capacity under simulated earthquake loading. Walls were representative of construction in Korea and Chile, had a vertical height to length ratio of 2.0, and differed on the basis boundary element transverse.
- Shegay et al. (2019): Experimental testing was done to understand the impact of axial load ratio on flexure controlled walls with rectangular cross sections. Variables that were changed are the use of crossties, the length of the boundary element, and using full hoops versus crossties in the boundary element. The reference wall designed to the standard of NZS 3101:2006-A2 and A3. In all walls, the full axial load was sustained following

lateral load failure. However, once lateral load capacity was lost, walls sustained axial load for at most one additional drift cycle.

- Zhang et al. (2000): At the time of this experiment, little research has been done on the behavior of RC walls under high axial load. In the laboratory walls were designed to be subjected to high axial load and reverse cyclic loading designed to the standard of ACI 318-95 and JGJ 3-91. When comparing the ACI and Chinese code, they found that walls subjected to an axial load ratio of 0.25 were same with the predicted strength of the Chinese code but were 6% higher when using an axial load ratio of 0.35. ACI were found to be conservative on the results. The ALR of 0.35 resulted in out of plane buckling with low ductility while the walls with an ALR of 0.25 exhibited crushing in the boundary elements.
- Segura et al. (2017): The experimental program investigated the theory that thin, code-compliant walls may be susceptible to compression failure prior to achieving expected lateral deformation capacity. Seven walls were subjected to reversed cyclic lateral loads and constant axial load. The specimens represented approximately the bottom 1.5 stories of an eight-story cantilever wall. The first phase of testing (WP1-WP4) was conducted to identify potential deficiencies in current provisions. Test variables for the phase 1 specimens included the configuration of boundary longitudinal reinforcement, quantity and arrangement of boundary transverse reinforcement, and compression depth (influence by axial load, quantity of longitudinal reinforcement, and wall cross-section). For the second phase of testing (WP5-WP7), walls were designed either with thicker cross-sections or improved boundary transverse reinforcement details.
- Tran et al. (2012): The experimental program was designed to evaluate the impact of shear span, axial load ratio, and peak shear stress on wall response for specimens with a relatively low cross sectional aspect ratio (CSAR = 8.0). The parameters were varied as follows: shear spans from 1.5 to 2.0, ALRs from 2.5% to 7.5%, and peak shear stresses from roughly $4\sqrt{f'c}$ to $8\sqrt{f'c}$ psi ($0.33\sqrt{f'c}$ -$0.66\sqrt{f'c}$ MPa).

- Lu et al. (2017): investigated the performance of lightly reinforced concrete walls subjected to constant axial and reverse-cyclic lateral loading. Results supported revision of minimum reinforcement limits in the NZ 3101.

2.4 Data Structures Used for the Wall Data Set

The Shegay et al. [21] dataset was found to be particularly valuable to the current study because, in addition to providing a comprehensive data set, the Shegay data presents the data in a highly structured format that greatly facilitates scripted data extraction. Specifically, data are provided as a structured MATLAB file. The top level of the data structure contains the main branches stem all the variables needed to create a model of a wall. Below is a summarized version of each top-level branch. The following pages visualize the data structure in a tree format. For more information about each variable, see appendix C.

- 'Authors': Representative author of the study
- 'SpecimenID': Specimen ID as classified by author
- 'UniqueID': Unique specimen ID - amalgamation of Author and SpecimenID
- 'WallType': Shape and steel layout of wall
- 'Geometry': Wall geometrical details
- 'Reinf': Wall reinforcement detailing
- 'Material': Material information for the steel and concrete
- 'Loading': Information on the loading conditions on the test wall during the experiment
- 'ExperimentalData': Experimental results summary data
- 'SectionAnalysis': Data useful for construction a fiber section of the wall to perform analysis (e.g., for moment curvature analysis)

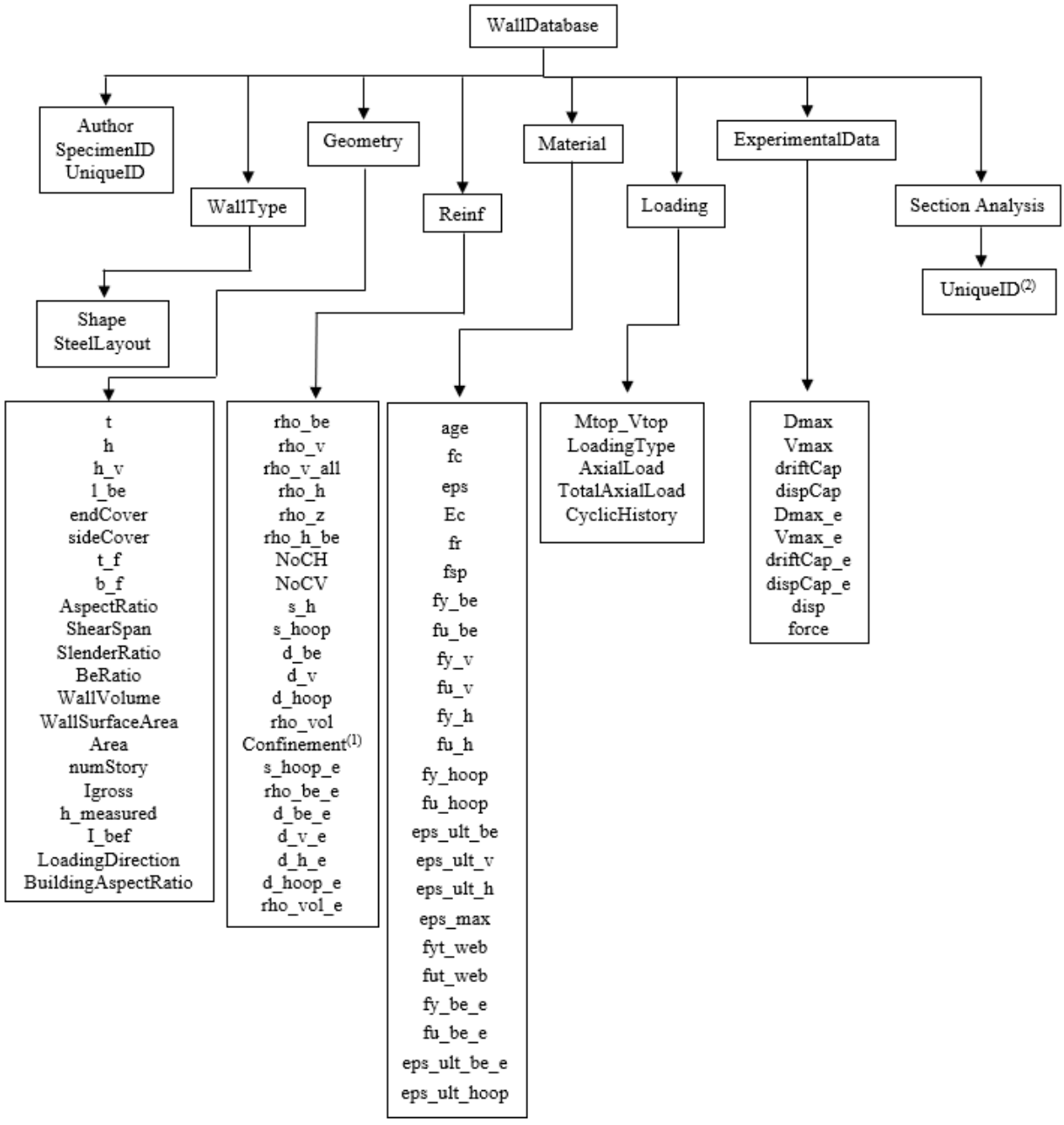

Figure 2.5 *Matlab structure of Shegay database*

(1) and (2) extended trees shown on next page.

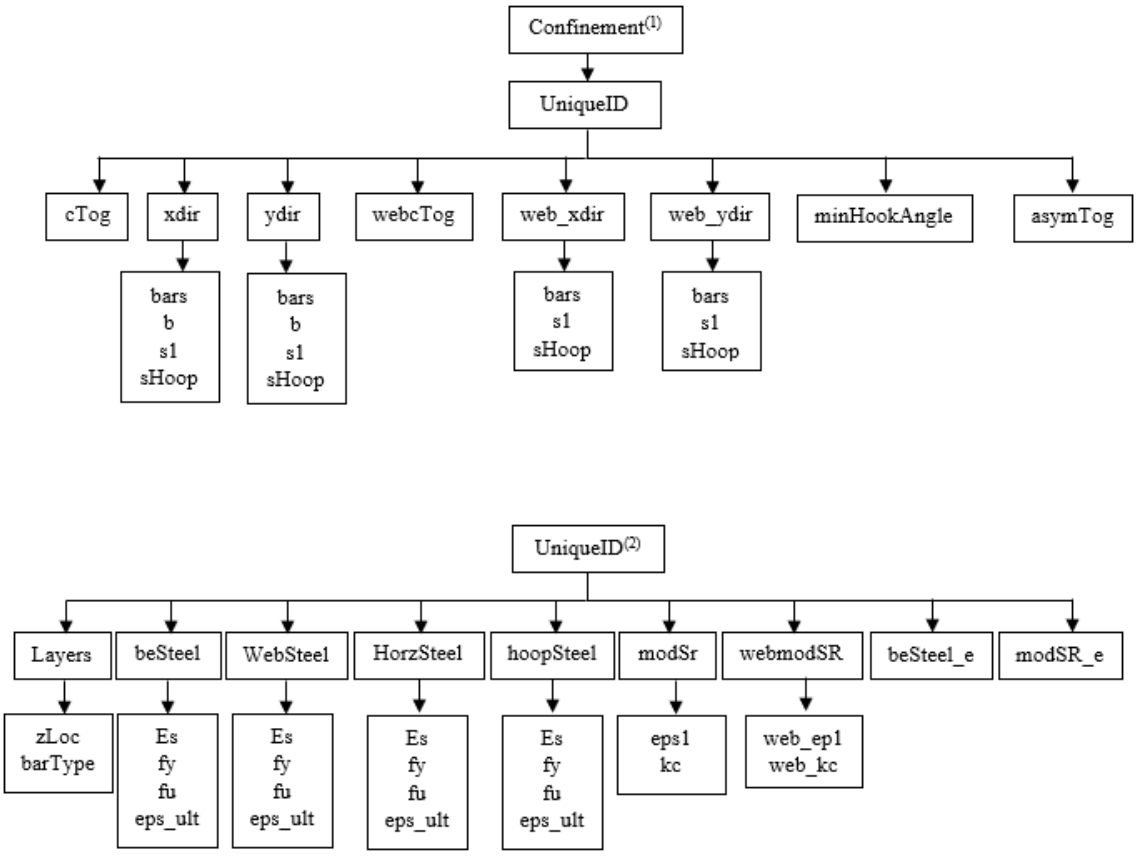

Figure 2.6 *Extended Matlab structure of Shegay database*

2.5 Conclusions

The review of the literature is split into two sets of walls as described as the calibration and validation set. The tests that were conducted each of the papers exhibit primary failure and behavior modes. The data set published by Shegay et al. [18] was used to support the current research effort. This data set provides comprehensive data (i.e. specimen design, material properties, loading and response) for a large number of planar wall tests conducted around the world during the last 30 years. These data are presented in a structured format, specifically a hierarchical MATLAB data structure, which facilitates their reuse for the current research project. The next chapter will cover previous finite element models that were used in the modeling of RC walls and introduce the shell element formulation, material models of the

concrete and steel, and conduct mesh sensitivity tests to determine an accurate and cost-efficient mesh and give a recommendation for the shell element model that will be used to for non-linear finite element studies of the calibration and validation set.

Chapter 3. Wall Modeling

This chapter reviews commonly used approaches for modeling the nonlinear response of flexure-controlled concrete walls, presents the layered shell element models and associated material models that are available for use in the OpenSees platform, and presents the results of investigative studies to identify a preferred layered-shell element model. Section 3.1 reviews element formulations and material models used in past research studies by others to simulate the response of reinforced concrete walls exhibiting flexure-controlled response. Section 3.2 presents layered shell element models and two-dimensional material models developed by Lu et al. [8] for use with these models that are available in OpenSees. Sections 3.3 present the results of simulations to investigate the impact on simulated response of multiple modeling decisions, including shell element formulation, the level of mesh refinement, the use of discrete versus smeared vertical reinforcing steel, and inclusion of cover concrete at the ends of the wall. The chapter concludes with identification of a preferred modeling approach.

3.1 Element Formulations Used Previously by Others

Previous research has developed, calibrated, and applied a variety of modeling approaches to simulate the response of reinforced concrete walls exhibiting flexure-controlled response when subjected to constant axial load and quasi-static cyclic and lateral loading. Table 3.1 was put together by Pugh [17] lists modeling approaches used commonly, the strengths and weaknesses of these approaches, and representative research studies in which models were calibrated, evaluated and applied.

Table 3.1 previous wall modeling approaches

Model Type	Strengths	Weaknesses	Example Applications
Either Fiber-Hinge Model or Lumped-Plasticity Fiber-Type Beam-Column Element	• Computationally efficient • Provides accurate prediction of strength for planar and nonplanar walls • Can be calibrated to accurate simulation of deformation capacity, regardless of assumed hinge length	• Assumption that plane sections remain plane • Does not account for flexure-shear interaction • Cannot simulate distributed inelasticity. • Location of yielding defined a priori based on location of plastic hinge. • Elastic elements must be calibrated to provide accurate simulation of stiffness.	**Berry et al. 2008**
Regularized Distributed-Plasticity Beam-Column Element w/ Fiber Section	• Computationally efficient • Provides accurate prediction of strength, and stiffness. • Can be calibrated and regularized to enable accurate simulation of deformation capacity • Provides accurate simulation of distributed yielding.	• Assumption that plane sections remain plane • Uses two-node line elements to model 3 geometry • Cannot simulate flexure-shear interaction	**Pugh 2012**
Multi-Vertical Line Element	• Computationally efficient • Provides accurate prediction of strength and stiffness • Can be calibrated and regularized to enable accurate, mesh-independent simulation of deformation capacity. • Provides simulation of flexure-shear interaction	• Assumption that plane sections remain plane • Uses two-node line elements to model 3D geometry • Has not been calibrated to provide accurate simulation of deformation capacity. • Does not provide simulation of flexure-shear interaction	**Orakcal and Wallace 2006**
2D Continuum Model using VecTor2	• Does not assume that plane sections remain plane; simulated flexure-shear interaction • Provides accurate prediction of strength	• Computationally expensive • Does not provide an accurate prediction of stiffness • Difficult to calibrate material models to achieve accurate, mesh independent, simulation of deformation capacity • Can simulated distributed yielding	**Palermo and Vecchio 2007, Pugh 2012**
Perform3D Fiber Shell Element	• Can be calibrated to provide accurate prediction of stiffness, strength and deformation capacity. • 2D shell elements can be used to model 3D geometry	Computationally expensive • Flexure and shear response are decoupled • Requires use of unconfined and confined concrete material models	**NIST 2013**
3D Continuum Analysis	• Does not require the assumptions about stress and strain fields that are used in the above models. • Previous research demonstrates potential for accurate prediction of strength, strength, deformation capacity, and failure mode • Uses 3D elements to model 3D geometry • Can simulate distributed inelastic action and localization of failure	• Computationally expensive	**Lowes, Lehman and Whitman**

Layered Shell	• Does not require the assumptions about stress and strain fields that are used in the above models. • Previous research demonstrates potential for accurate prediction of strength, strength, deformation capacity, and failure mode • Compatible with truss elements and Beam-Column Element • Use of two and three dimensional geometries	• Computationally expensive	**Lu et al**

3.2 OpenSees Layered Shell Element: Introduction and Formulation

The information presented in Table 3.1 suggests the potential for layered shell elements to be an ideal modeling approach for planar and non-planar reinforced concrete walls. These models offer the potential for accurate simulation of response for walls with two- and three-dimensional geometries and multi-dimensional stress and strain fields as well as substantially reduced computational demand in comparison with solid element models. However, given the assumptions embedded in this model, additional research is required to develop recommendations for using the model and to validate the model for simulation of walls with a range of design parameters.

The current study employs the OpenSees software platform and the two-dimensional layered shell elements and concrete and steel constitutive models available for use with this platform. OpenSees was chosen for use because it is widely used by the earthquake engineering research community to simulate the response of structural and geotechnical systems subjected to quasi-static cyclic and dynamic earthquake loading. The current version of OpenSees (OpenSees 3.3.0) includes three shell element formulations (MITC4, DKGQ, and NLDKGQ), tools for creating layered shell materials appropriate for use with these shell element formulations a two-dimensional concrete constitutive model (plane stress user material), and multiple one-dimensional steel material (e.g., Steel02) models. The following paragraphs discuss these.

All three of the four-node, multi-layer shell elements available in OpenSees 3.3.0 (MITC4 [5], DKGQ [8], and NLDKGQ [8]) were considered in the current study. These layered shell elements can be used to provide a simplified representation of the 3D nonlinear behavior of thin reinforced concrete elements, such as walls, by neglecting stress-strain response in the through-

thickness direction and representing the in-plane response of different through-thickness layers (e.g., cover concrete, confining steel, confined core concrete) by discretizing the component into multiple bonded layers in the through the thickness direction. Figure 3.1 shows an idealization of a layered shell element.

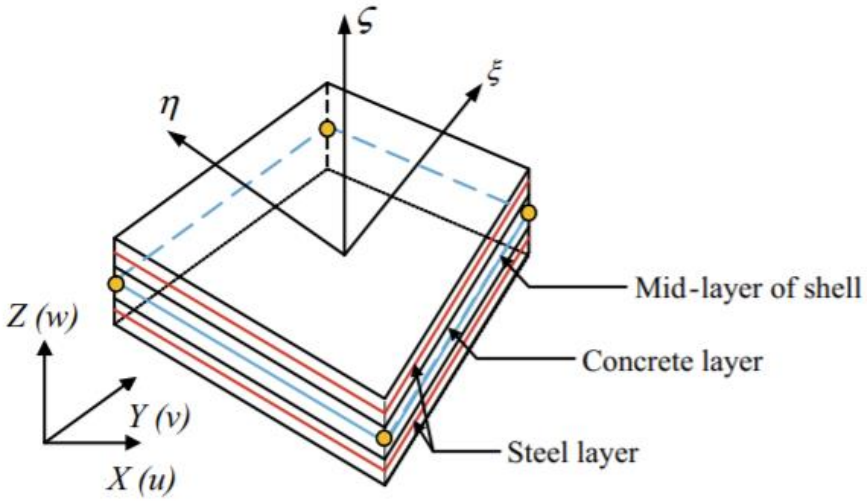

Figure 3.1 *Multi-layer shell element [5]*

In a layered shell element, the axial strains and curvature of the middle layer are calculated at the quadrature points using the nodal rotations and displacements. For each layer, strains are computed at the quadrature points using middle-layer strains and curvatures and the assumption that plane sections remain plane. Stresses are computed for each layer, at each quadrature point, using quadrature point strains and specified material model parameters and history variable values [8].

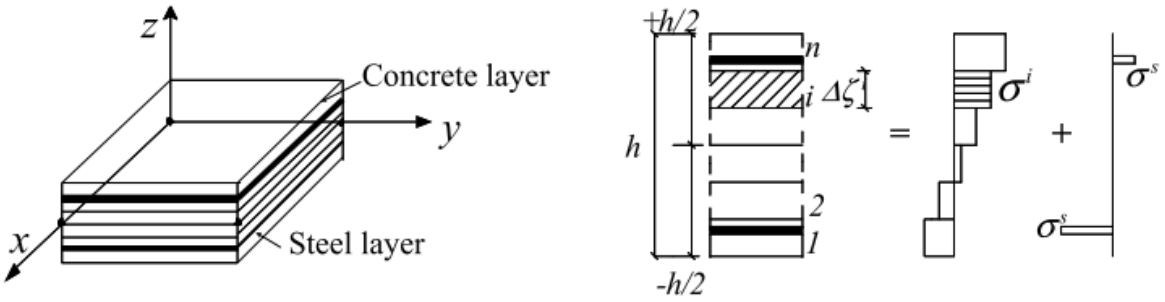

Figure 3.2*: visual of steel and concrete layers and stress/strain profiles*

This study investigates use of two shell element formulations available in the OpenSees platform, DKGQ and MITC4, for use in simulating the response of reinforced concrete walls. Lu investigated application of the MITC4 element and concluded that the element formulation posed too many computational issues; specifically, he found that the element exhibited shear locking and artificial stiffness when used with the MITC4. As a result, he formulated two new shell elements, DKGQ and NLDKGQ. Figure 3.3 shows compares simulation results of a column collapse analysis generated using the MITC4 and DKGQ element formulations.

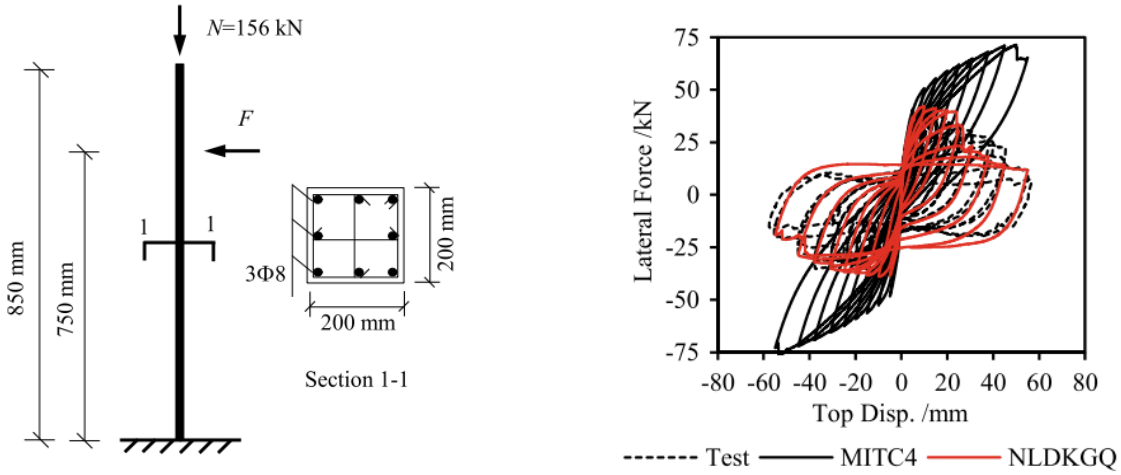

Figure 3.3*: RC column collapse simulation setup and results*

The MITC4 is a 4-node flat shell element that employs mixed interpolation and tensorial components. It uses a bilinear isoparametric formulation in combination with modified shear interpolation. Compared to other shell elements, MITC4 improves thin plate bending [8]. The MITC4 calculates the in-plane strain components which are linear while assuming that the shear strain in the transverse direction is constant.

The DKGQ element is a 4-node flat shell elements that combines a planar membrane element formulation with a plate bending element as seen in Figure 3.4. As Lu stated that MITC4 has a locking problem, the DKQ element does not. The DKQ element has one transitional DOF around the z axis and two rotational DOFs around the x and y axes per node. The GQ12 element which is the plane membrane element, has two transitional DOFs around the x and y axes and one rotational DOF around the z axis which makes a total of 6 DOFs per node compared to the MITC4 element which only has 5 DOFs per node. The NLDKGQ formulation builds on the

DKGQ formulation to provide more accurate simulation of components exhibiting large rotations and deformations and, thus, geometric nonlinearities through use of a Lagrangian formulation. There are no large deformations in the experimental walls used in this study thus the DKQG formulation is assumed to be appropriate for the current study.

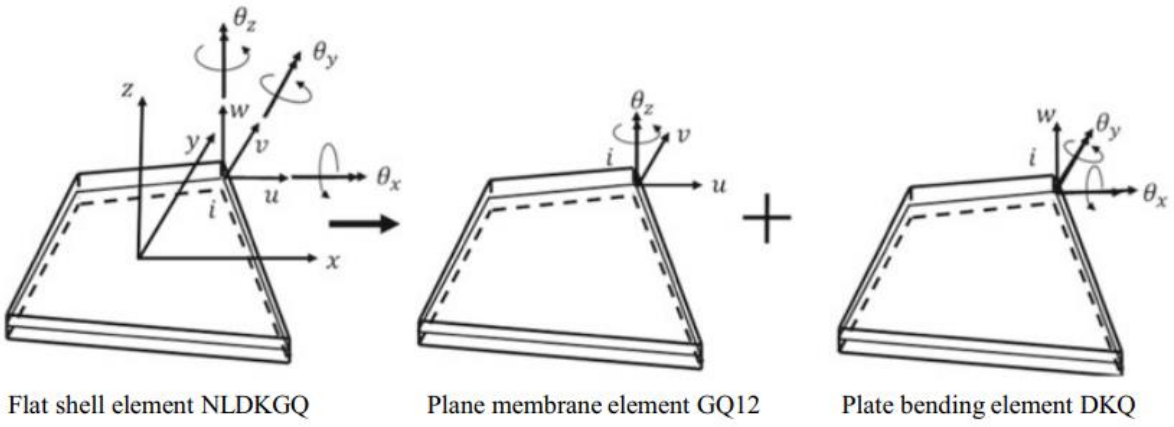

Figure 3.4*: Visualization of DOFs for NLDKGQ*

3.3 Material Models for Concrete and Reinforcing Steel

Use of a layered shell element to simulate the response of a reinforced concrete wall requires definition of two-dimensional material models that simulate the response of the confined and unconfined concrete layers as well as horizontal reinforcing confining steel. For concrete, a two-dimensional concrete constitutive material model is incorporated into the layered shell element using the *PlaneStressUserMaterial* function, which supplements that two-dimensional concrete model with *PlateFromPlaneStress* to fully define concrete layered shell region. The concrete material model assumes elastic response until cracking, a fixed crack orientation, and post-racking response defined by a 1D confined or unconfined concrete stress-strain model perpendicular to the crack surface and a shear-friction model parallel to the crack surface. For reinforcing steel, the one-dimensional steel material model is incorporated into the layered shell element using the *Steel02* with *PlateRebar*. The Reinforcing steel material response is modeled using a simple 1D hysteretic model with strain capacity in tension and compression calibrated to provide accurate simulation of strength loss due to bar fracture or buckle. The subsequent sections provide a detailed description of the material models.

Material models and the OpenSees commands that support use of these with the layered shell element are discussed below.

3.3.1 Plane Stress Concrete Constitutive Model

Lu et al. [8] developed and implemented in the OpenSees platform a two-dimension plane stress concrete constitutive model; this model is appropriate for use with layered shell elements. The model simulates concrete response as elastic to the point of concrete cracking, when principal tensile stress exceeds concrete tensile strength. Once concrete cracking occurs, concrete is considered to be orthotropic, with concrete response defined by one-dimensional stress strain response models in the direction normal and parallel to the fixed crack surface. To minimize mesh sensitivity associated with material softening, the softening portion of the concrete stress-strain response curve, both in compression and in tension, is defined using a mesh dependent length and a measure of energy dissipation associate with damage [8].

Cracked concrete response in the direction normal to the crack plane is defined per Figure 3.5, with concrete compressive strength defined by the experimental data sets and all other model parameters defined as follows:

Concrete elastic modulus $E_c = 57000\sqrt{f_c}$ psi ($E_c = 47000\sqrt{f_c}$ MPa) per [1] *(Eq 3.1)*

Concrete tensile strength, $f_t = 4\sqrt{f_c}$ psi ($f_t = 0.056\sqrt{f_c}$ MPa) per [1] *(Eq 3.2)*

Concrete fracture energy, which defines the area under the post peak concrete tension curve, is defined as:

$G_t = (0.174(D_{max})^2 - 0.0727D_{max} + 0.149)(\frac{f_c}{1450})^{0.7}$ lb/in [11] *(Eq 3.3)*

($G_t = (0.0469(D_{max})^2 - 0.5D_{max} + 26)(\frac{f_c}{10})^{0.7}$ N/m)

where D_{max} is the maximum aggregate size, which is defined as 0.5 inches (12.5 mm) for the current study.

Concrete fracture ultimate strain is defined as: $\varepsilon_{tu} = \frac{f_t}{E_c} + \frac{2G_t}{L_E f_t}$ [10] *(Eq 3.4)*

Concrete strain at maximum compressive strength: $\varepsilon_p = \frac{f_c}{E_c}$ [10] *(Eq 3.5)*

Concrete residual strength:

$f_{res} = 0.2f_c$ for confined concrete [10] *(Eq 3.6)*

$f_{res} = 0.01f_c$ for unconfined concrete [10] *(Eq 3.7)*

Concrete strain at residual strength is defined per previous studies [10] as

$\varepsilon_{res} = \frac{2G_f}{(\delta+1)f_p L_E} + \varepsilon_p \frac{\delta+1}{2}$ [10] *(Eq 3.8)*

where,

δ = the ratio of residual compression capacity to maximum compression strength, defined equal to 0.2 for confined concrete and 0 for unconfined concrete per [10]

L_E = the length of the element in the minimum principal stress direction at the onset of crushing, which is assumed to be equal to the vertical height of the element

G_f is the unconfined concrete crushing energy:

$G_f = 0.0134f_c$ kips/in ($G_f = 2f_c$ N/mm) [10] *(Eq 3.9)*

Confined concrete has been shown to have greater strength and strain at peak strength as well as greater crushing energy [11]. This is simulated by increasing concrete compressive strength and increasing compressive strain at peak strength per Saatcioglu and Razvi (1992) [19] and increasing crushing energy per Marafi [10]. Specifically,

$f_{cc} = k_c f_c$ *(Eq 3.10)*

$\varepsilon_{cc} = k_c \varepsilon_c$ *(Eq 3.11)*

Where k_c is a confinement factor for the boundary region [19] *(Eq 3.12)*

$G_{fcc} = 2.2G_{fc}$ as calibrated by Marafi [10] *(Eq 3.13)*

Concrete response parallel to the crack surface is defined as linear elastic with shear stiffness reduced to represent slip on the crack surface:

$\tau = G\,\beta\,\gamma$ *(Eq 3.14)*

where

$G = \frac{E_c}{2(1+\nu)}$ is the concrete elastic shear modulus, with ν = 0.2 [1]

β is the shear retention factor

γ is the shear deformation in the direction parallel to the crack surface

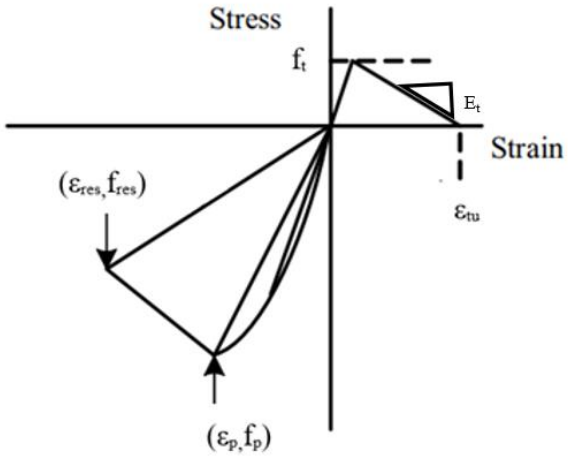

Figure 3.5*: Concrete stress-strain response model perpendicular to the crack surface*

As the principal tensile stresses start to exceed the concretes tensile strength, cracks began to form, and the concrete is then treated as orthotropic. Shear stiffness then starts to deteriorate based on the shear modulus and shear retention factor for aggregate interlocking.

As the wall develops primary and secondary cracks under loading, it follows the equation 6 when determining stresses:

$$[\sigma] = \begin{vmatrix} 1-d_1 & 0 \\ 0 & 1-d_2 \end{vmatrix} D_e \varepsilon_c \qquad \textit{(Eq 3.15)}$$

Where d_1 and d_2 are the damage parameters calculated by damage evolution curves under tension and compression. These values are either 1 or 0. When primary cracks occur at an integration point, d_1 goes to 1 and as secondary cracks occur, d_2 goes to 1. σ and ε_c are the stress

and strains in the direction of the principal stresses. D_e represents the elastic constitutive matrix [8].

3.3.2 Modeling reinforcing steel

Reinforcing steel is modeled in two ways, as a smeared horizontal steel layer within the layered shell element and using vertical truss elements. The material response of all steel is modeled using the OpenSees *Steel02* material model, which is based on the Giuffré-Menegotto-Pinto model, with response parameters defined using measured response quantities and strain capacity in tension and compression reduced to account for the impact of cyclic bar buckling and loss of restraint due to concrete crushing. The material model is paired with *PlateRebar* which is derived from the uniaxial materials for rebars (Mazzoni et al. 2006) and modeled at the angle of which the steel is placed. For instance, the transverse bar angle would be zero as it is modeled across the cross section.

Horizontal reinforcement, which provides confinement of boundary element concrete and contributes to wall shear capacity, is modeled as a single steel layer within the layered shell element that has stiffness and strength only in the horizontal direction. Layer thickness is computed as the total area of horizontal steel within the wall divided by the total effective height of the wall. Since, for the test specimens considered, confining reinforcement and horizontal shear reinforcement does not vary over the height of the wall, all elements within the boundary element region of the wall have one horizontal steel layer thickness and all elements within the web region of the wall have a second horizontal steel layer thickness.

Vertical steel, which determines wall strength based on its area, material properties and horizontal location within the wall cross-section, is modeled discretely using truss elements. When the vertical steel is smeared into the shell it doesn't behave accordingly, the location of the vertical steel reinforcement drives the mesh size. Figure 3.9-3.11 below shows the range of mesh configurations are the base of wall simulated as part of this study.

The steel model requires as input steel yield strength, initial elastic modulus, strain-hardening ratio; these quantities are provided for each wall in the Shegay data set. The model requires also R0, CR1 and CR2. Figures 3.6 and 3.7 show hysteretic behavior with and without isotropic

hardening in compression and tension. Figure 3.8 shows a comparison of a monotonic envelope with different values of R0 (recommendation is a value between 10 and 20).

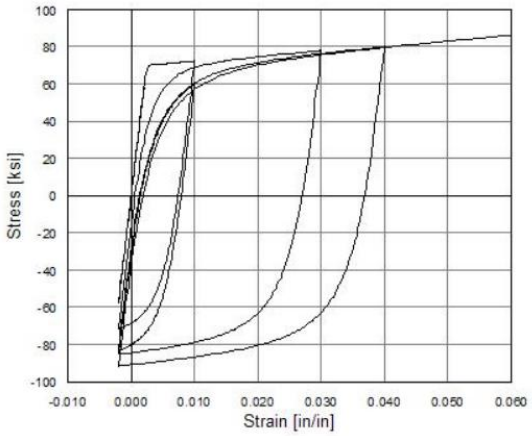

Figure 3.6 *Hysteretic Behavior of Model with Isotropic Hardening in Compression*

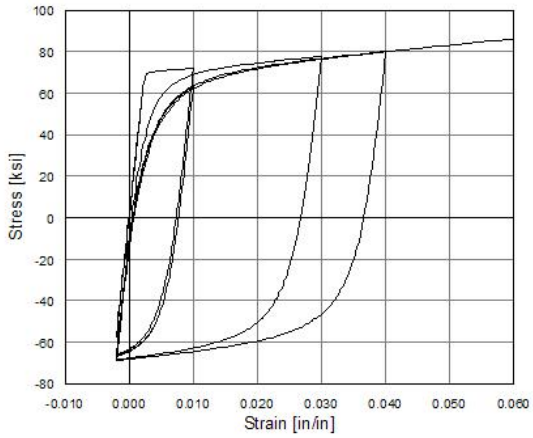

Figure 3.7 *Hysteretic Behavior of Model w/o Isotropic Hardening*

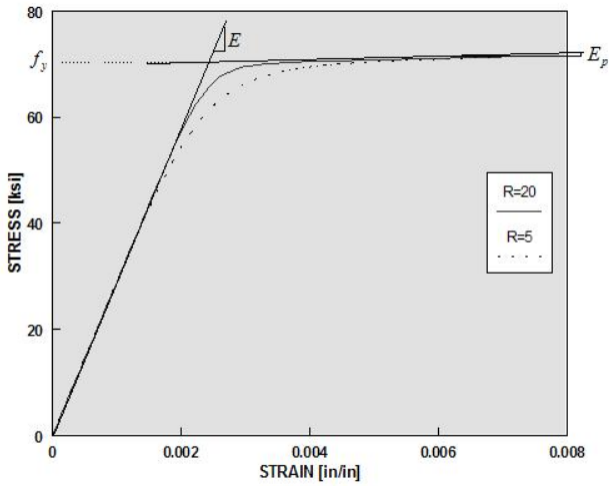

Figure 3.8 *Stress vs Strain material model*

Following the recommendations of Pugh [17] and Marafi [10], the OpenSees MinMax wrapper is used to establish compression and tension strain limits. In compression this limit is defined at the point the concrete reaches crushing strain, and in tension this limit is defined as the steel rupture strain.

3.4 Model Development

To speed modeling the large number of the walls included in the Shegay database, two Jupyter notebooks were created to automate modeling building directly from the Shegay database. These notebooks are published here …. Includes link to facilitate reuse by the community. The first notebook extracts from the MATLAB data structures the data required for modeling each wall and stores these data in a structured python array. The second notebook uses the python array to create a tcl script that builds the OpenSees model of the wall and executes an OpenSees analysis; the second notebook is split into nine sections that correspond to a different step in the OpenSees analysis process:

- Section 1: Initialize the model
    - The model is defined to be three-dimensional with one rotational and one translational degree of freedom per axis.
    - The variables, for which uncertainty will be considered, are defined

- Section 2: Define location of nodes
    - Nodes are placed at the locations of the vertical reinforcing bars along the horizontal length of the wall.
        - If element length vs height of the wall results in too coarse of a mesh, additional nodes are placed to optimize the mesh of the wall.
    - The height of each element is equal to the length of the nodes in boundary to create square elements up the wall. This usually results in rectangular elements in the web because if every element were square, it would be too computationally expensive to run.
    - Note that wall specimens were modeled from the top of the foundation to the height at which lateral displacement was measured. If the height at which lateral displacement was measured did not correspond to the height at which lateral load was applied, then loading was applied at the top of the wall model as a lateral load plus and an overturning moment.
- Section 3: Define material models and their variables
    - Unconfined and confined concrete crushing energy and fracture energy are computed

  Material models are defined.

- Section 4: Create the layered shell element
    - The shell element comprises 5 layers: 2 cover concrete layers , 2 transverse steel layers, and 1 core concrete layer.
    - The cover concrete thickness is defined using data provided by the researcher.
    - Transverse steel thickness is calculated as total layers of transverse steel multiplied by the area of the steel divided by the height of the wall.
    - The cover concrete and steel thicknesses are subtracted from the total thickness of the wall to determine the thickness of the core concrete layer.
- Section 5: Define the elements
    - There are usually two sections that are defined, the boundary and the web. Based on how many nodes are in the boundary, the script will print out the elements for the left side of the boundary, then for the entire web region, and lastly for the right

side of the boundary. This process is repeated until the elements reach the last row of nodes.

    - The Shegay database has variables that define each boundary region on either side of the wall or if the wall only consists of unconfined concrete. This will be taken into account if a wall is only unconfined concrete or if the boundary regions vary in confinement or amount of steel.

- Section 6: Define constraints
    - The bottom row of nodes are fixed for all degrees of freedom.
- Section 7: Define recorders
    - Two recorders are created to store reaction forces in the x-direction for the bottom row of nodes and displacements in the x-direction for the top row of nodes. These data are used to generate base shear and wall drift histories as well as to enable creation of base shear force versus wall drift response histories.
    - A second group of recorders stores stress and strain histories (more on these in chapter 4) for the middle layer of concrete at the four gauss points for all layered shell elements in the model. The Movies are created using these data that show normal as well as principal stress and strain fields; these movies to provide understanding of wall response and failure modes.
    - A third group of recorders stores the concrete crack angle, for the middle layer of concrete, at each the gauss points in the element. Movies are created to visualize the progression and orientation of concrete cracking; these movies supplement stress and strain-field movies and provide further understanding of wall behavior. and
    - A final group of recorders stores stress and strain data for all of vertical steel truss. These data are used to determine onset of steel yielding as well as strength loss due to fracture or buckling.
- Section 8: Define and apply wall axial load
    - The Shegay data base includes the compressive axial load applied to the wall during laboratory testing; for all walls used in this study, a constant axial load was applied in the laboratory.

    - A uniformly distributed axial load pattern, applied to the nodes at the top of the wall model, was created to represent the axial load applied in the laboratory.
    - This uniform axial load pattern was applied, to the nodes at the top of the model, via load control, with X steps used to apply the total axial load applied in the laboratory.
- Section 9: Define the cyclic lateral displacement history and conduct the analysis.
    - A cyclic lateral displacement history was defined for each test specimen by extracting, from the measured displacement history included in the Shegay database, peak displacements for each half cycle (i.e., maximum positive and minimum negative displacement for each full displacement cycle) and then creating a simulated displacement history that progressed from half peak to half peak using a displacement step magnitude of 0.01 inches.
    - A lateral load pattern was created in the OpenSees model to represent the lateral load applied in the laboratory. For specimens for which lateral load was applied and lateral load was measured at the same height, this lateral load pattern comprised a uniformly distributed lateral loads applied to the nodes at the top of the specimen. For specimens for which the heights of lateral load application and lateral displacement measurement were not the same, the "lateral load pattern comprised lateral load plus a linearly distributed vertical load appropriately scaled to appropriately represent the moment applied at the top of model.
    - Lateral load (or lateral load plus moment) was applied under displacement control to achieve the measured lateral displacement history.
- The last section of this notebook creates a reference file that holds variables needed for postprocessing:
    - Total nodes along the width of the wall
    - Total nodes along the width of the wall that are connected to a truss element
    - Total nodes in the file
    - Total elements in the file
    - Displacement peaks in the positive direction
    - Fracture strength of the concrete
    - total layers of elements in the file

- Unique ID of the wall
- File path to the folder of the wall
- File path to the tcl file

3.5 Model Evaluation

3.5.1 Mesh Sensitivity Study

A mesh sensitivity study was conducted to determine the maximum mesh size, and thus the minimum run time, that could be used to achieve 1) accurate simulation of strength, stiffness, deformation capacity and failure mode and 2) a high level of reliability with respect to simulations continuing through to onset of strength loss. Figures 3.9-3.11 below show one row of elements for the three levels of mesh refined considered. In these figures, i) heavy blue lines indicate shell element edges that align with the location of truss elements representing vertical reinforcing steel at the correct location within the wall cross section, ii) light blue lines indicate shell element edges that do not align with vertical steel, and iii) orange elements indicate shell elements composed of confined concrete heavy, smeared, horizontal confining reinforcement. It should be noted that these meshes do not include cover concrete at the ends of the wall; as discussed previously, including this concrete, which has a thickness of less than half an inch in most cases, was found in preliminary analyses to result in premature failure due to convergence issues. Additionally, it should be noted that vertical reinforcing steel is modeled using discrete truss elements as preliminary analyses, which followed the recommendations of Lu et al [8]. Mesh refinement studies were conducted using both the MITC4 and DKGQ elements; though subsequent analyses discussed later in this chapter identified DKGQ as the preferred element formulation. Data in figures 3.12 and 3.13 show normalized load versus drift histories for the three meshes.

Continuum element analysis is computationally expensive. To be able to efficiently run analyses accurately with the least amount of time possible, a mesh refinement study was conducted with the MITC4 and DKGQ elements to see how the height over length of an element ratio affects the outcome of the analysis and to determine a mesh that will be best suitable. The model has some restrictions on it which will affect the mesh size. The first restriction is that the nodal locations are placed based on the locations of the longitudinal bars. Since the longitudinal bars are

modelled as truss elements, their locations need at the correct placement to produce an accurate result of the wall. Also an assumption made with this model is that the cover concrete is ignored on the end of the wall as this would give elements with a high height to length element ratio causing convergence issues in the model. The three meshes that are used to show how the elements behave with figure 3.9 being the optimal mesh, figure 3.11 being a high height to length element ratio, and figure 3.10 being a low height to length ratio. The orange areas are the boundary elements, the gray area is the web region and the thick blue lines are the truss bars.

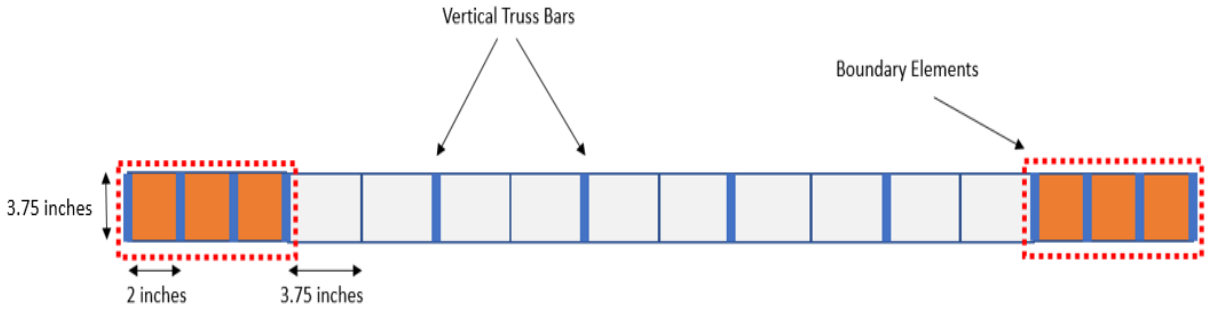

Figure 3.9. *mesh with h/l of 1 to 1.9*

Figure 3.10. *mesh with h/l of 0.5 to 1.5*

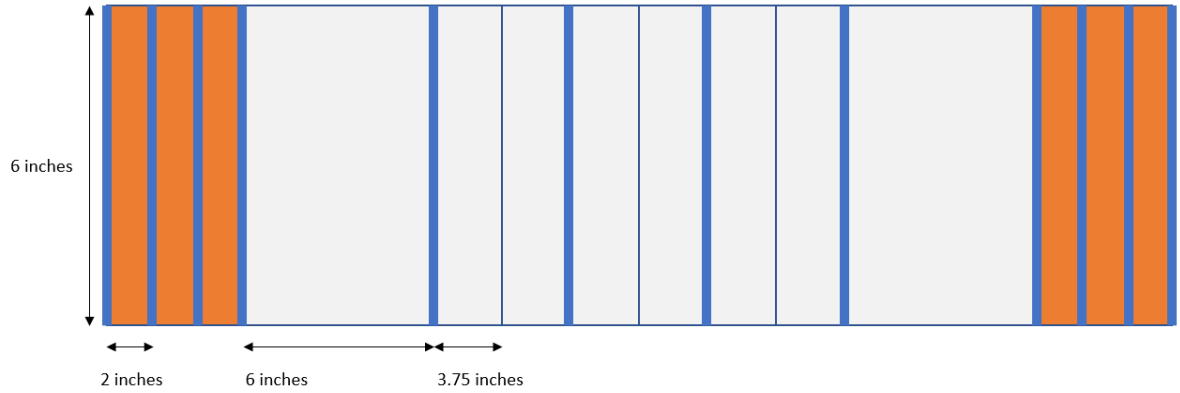

Figure 3.11. *mesh with h/l of 1 to 3*

Figure 3.12-3.13 show simulated and measured load versus drift histories for wall RW1 computed using baseline/reference concrete and steel material model parameters with the DKGQ elements and MITC4 element. For both element formulations, results for meshes with elements with height-to-length (h/l) ratios ranging from 1.0 to 3.0 perform better, with simulations including simulation of strength loss and continuing beyond the point at which strength loss was observed in the laboratory. Simulations conducted with elements with height-to-length (h/l) ratios of less than 1.0 exhibit numerical failure (i.e. solution algorithm fails to converge) at drift demand far below the drift at which strength loss was observed in the laboratory.

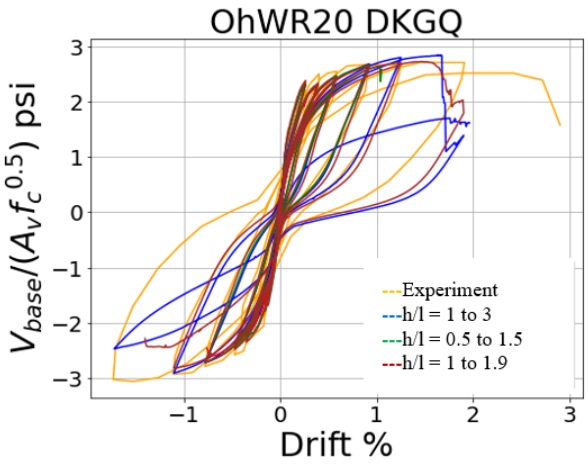

Figure 3.12. *Load-Displacement DKGQ*

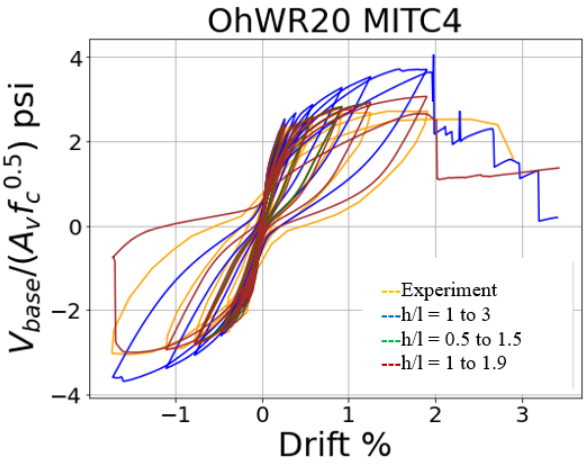

Figure 3.13 *Load-Displacement of MITC4*

Meshes for both elements suggests that a ratio below 1 of h/l results in convergence issues where meshes with an h/l ratio higher than 1 have similar drift capacities. It is evident in the MITC4 results that a higher ratio does result in shear locking, causing overstrength whereas in the DKGQ element, this is not seen.

3.5.2 Discrete vs Smeared Vertical Reinforcing Steel

Smearing vertical reinforcing steel has positive and negative consequences. For the current study, a primary benefit of smearing vertical reinforcement, is that this decouples the mesh from the vertical steel spacing and, thereby, provides substantially greatly flexibility in defining the mesh for the wall model. However, smearing the reinforcement necessarily reduces accuracy in simulate strength, as the full bar area is not accurately located.

3.5.3 Shell Element Recommendation

The above sections have the purpose of comparing the two shell elements so that we can give a recommendation of what shell element to use. Looking at the results of the mesh sensitivity analysis, the MITC4 is significantly overstrength compared to the DKGQ results. This is due to shear locking as discussed earlier. The concrete retains a significant amount of shear after cracking which results in a higher max strength. DKGQ was able to have similar results when it came to mesh 1 and 3 as they both failed +/- 2% drift. As Lu talked about in his research, his goal was to create an element that would not have the shear locking affect that is seen with the MITC4 element.

Both elements failed early on in mesh 2 which suggests that when an h/l element ratio of less than 1 dominates the cross section of the wall, this can cause premature failure or convergence issues so that mesh should be not be used at all. Regarding mesh 1 and 3, the results are different for MITC4, meaning that a very refined mesh will need to be used for MITC4 in order to accurately simulate the wall. For the DKGQ, since the results are similar, this can suggest that we can accurately simulate a model with a mesh that has an h/l element ratio between 1-2. This is an advantage as it will be computationally less expensive than the MITC4 element.

Because the MITC4 has shown to have a shear locking problem, overstrength issues, and less flexibility with mesh sizing; we recommend the DKGQ element as it does behave correctly, allows for less computational expense, and can accurately run locally compared to on QuoFEM. The rest of the research will now focus on using the DKGQ element in all the analyses.

3.5.4 Comparing Simulated and Measured Response via Error Functions

Multiple error functions were developed to quantify the accuracy with which OpenSees models simulated wall specimen response quantities measured in the laboratory. Error functions quantified the difference between simulated and measured strength, deformation capacity, and stiffness to yield.

A Jupyter notebook was developed for each error function. Each notebook determines the appropriate value of the response quantity of interest using the simulated and the measured data sets and computes the error function as

$$\%\ error = \sum \frac{|simulated\ value - experimental\ value|}{experimental\ value} x100 \qquad \textit{(Eq 3.17)}$$

Simulation error was quantified as follows:

- Stiffness error: Stiffness error was computed using the simulated and measured stiffness to the load at which first yield of the extreme vertical reinforcing bar. The Jupyter notebook created to determine this error includes the following process steps:
    1. Identify the "index point" (i.e. step number in the simulation) at which the extreme fiber of the concrete exceeds -0.003.
    2. Determine the base moment at that point which becomes Mn and find the displacement at that point
    3. Find on the measured points where it reaches that exact moment and pull the displacement. These values are compared.
- Max Strength error: The max strength corresponds to the point in the simulation at which the model sees the highest base shear. This is compared to the experimental max base shear.
- Displacement capacity error: The displacement capacity is determined at the point when the model loses 20% of its strength. There is a file that holds the experimental displacement capacities of all the walls and the corresponding experimental value is extracted and compared. Usually if the model is under/over performing the experimental displacement capacity, the crushing energy or steel rupture strain is lower/higher than needed. This error function is vital for estimating those exact parameters to best model the walls.

Figures 3.14-3.16 visually show the stiffness, max strength, and displacement capacity locations of a simulated run of RW2.

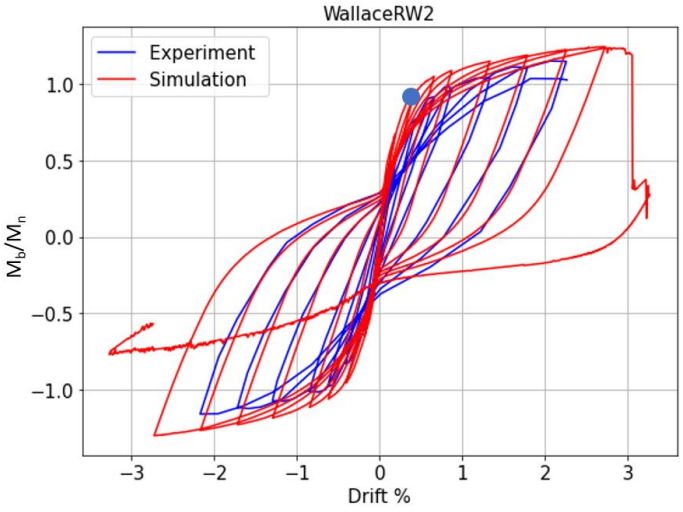

Figure 3.14. *stiffness point location with error of 20%*

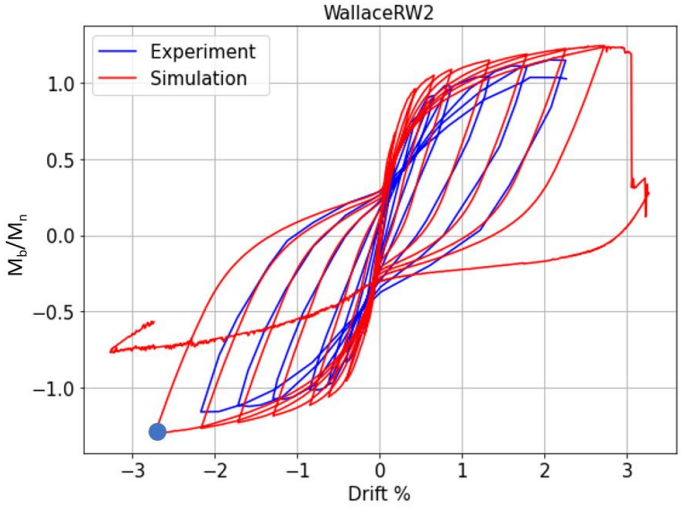

Figure 3.15. *max strength location with error of 16%*

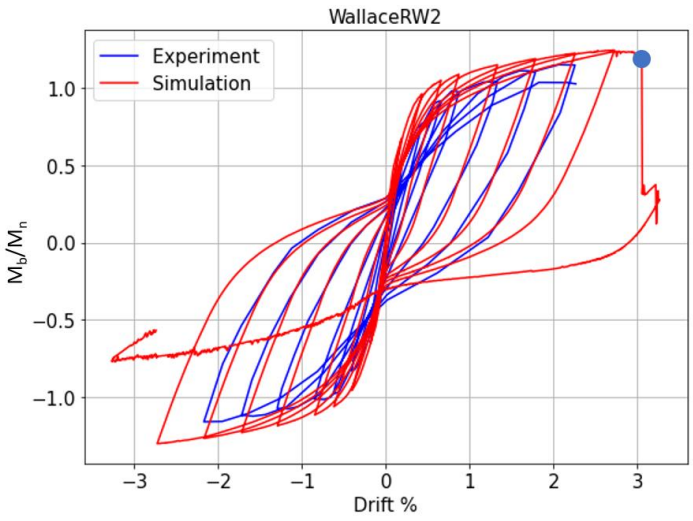

Figure 3.16. *drift capacity location with error of 35%*

3.5.5 Failure Modes

Previous research [17] concludes that flexure-controlled walls exhibit loss of lateral load resistance due to one of three failure modes: i) compression-buckling characterized by strength loss to do crushing of concrete at the extreme end of the wall and simultaneous buckling of reinforcing bars, ii) fracture of previously buckled reinforcing bars, or iii) crushing of concrete and buckling of reinforcing steel within the web of the wall at the boundary of the web and confined boundary element. The Shegay database includes categorization of wall failure mode in the laboratory based on these three failure modes; this study includes only walls exhibiting compression-buckling and bar-rupture failure modes.

To determine the simulated wall failure mode, simulated concrete and steel stress and strain histories, for extreme layered shell element and reinforcing bars and concrete were extracted from the recorders data sets. These data were processed to identify i) the simulation index point at which quadrature points, for the middle layer of confined concrete elements in the bottom rows of elements, develop compressive strains that exceed the strain at which residual compression strength is reached and ii) the index point at which reinforcing steel strains exceed the tension rupture strain.

Figure 3.17 shows data for RW2, for which both the simulated and observed failure mode was crushing-buckling. Figure 3.18 shows data for RW1, for which both the simulated and observed failure mode was bar rupture.

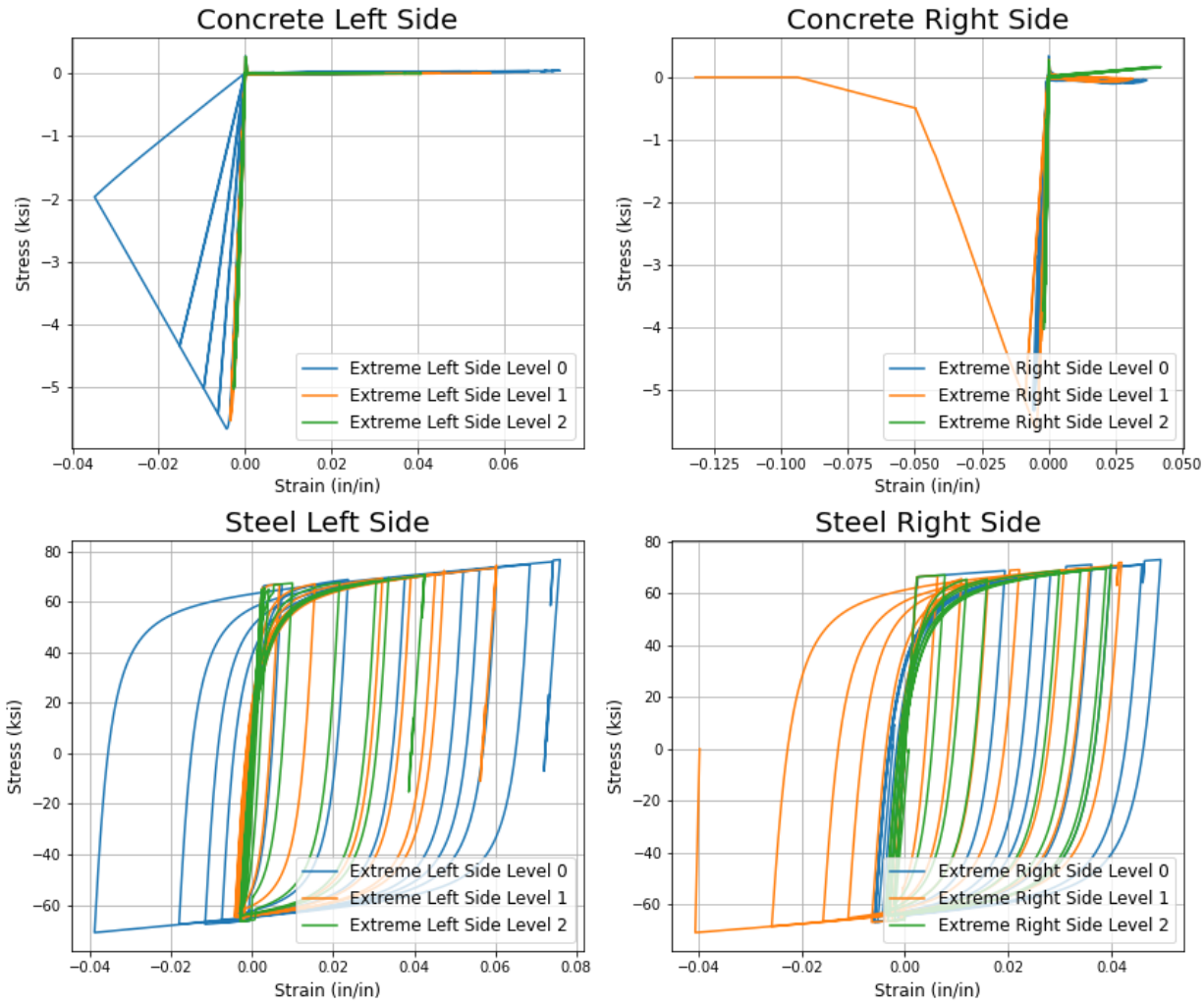

Figure 3.17. *Visualization of wall failure for Compression Buckling Failure*

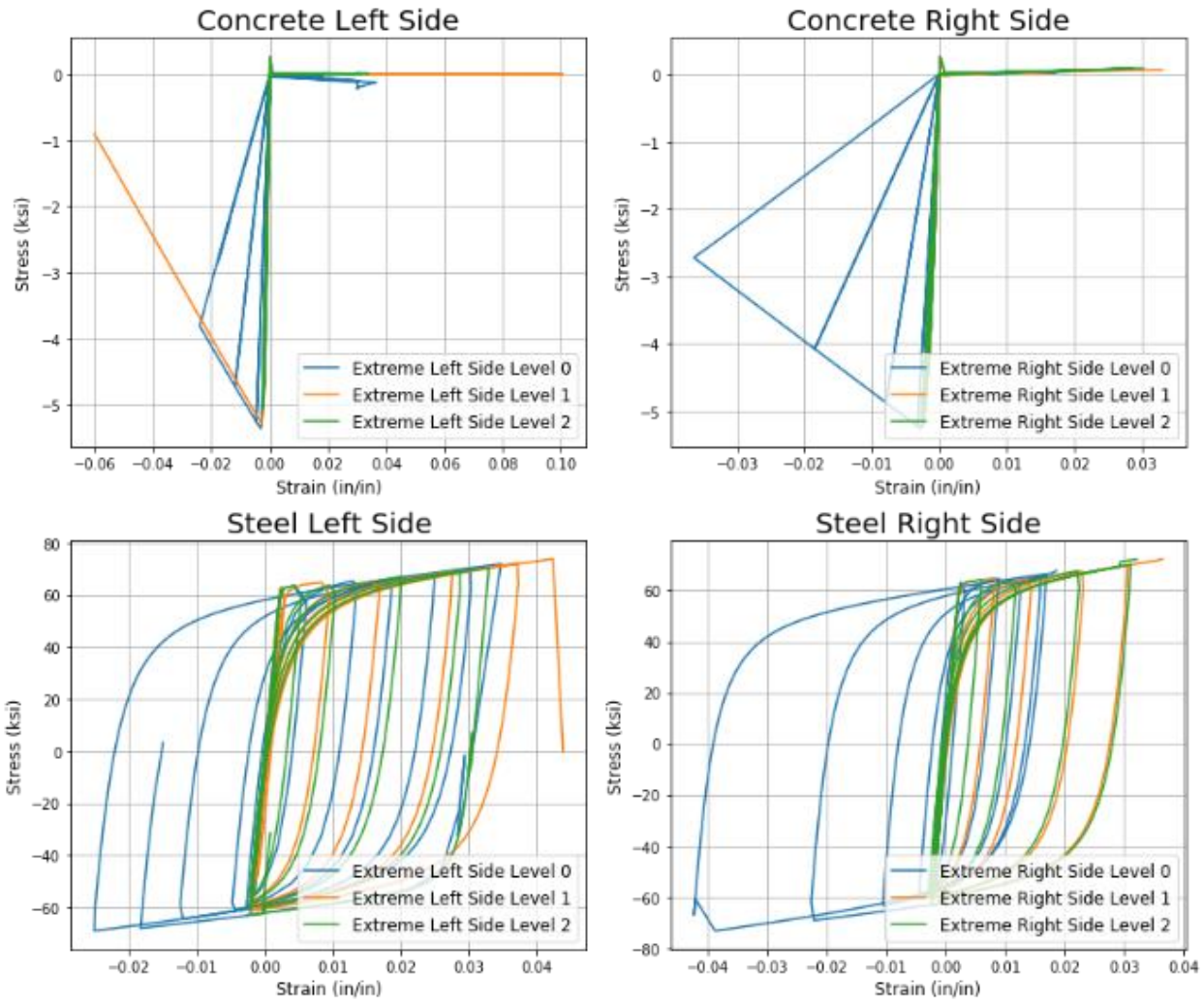

Figure 3.18. *Visualization of wall failure for bar Rupture Failure*

3.6 Conclusion

The material models and shell elements were introduced in this model with how the constitutive models are set up, how they work, and how they are incorporated into the shell element. Three shell elements were introduced; DKGQ, NLDKGQ, and MITC4. Their formulations were walked through and the DKGQ and MITC4 were compared side by side with three different meshes. Overall, the DKGQ was picked to be used in the rest of this research. This chapter also introduced what errors will be computed to help with the calibration of the dataset. The next chapter will introduce the software used and the Jupyter notebooks that were created for this research.

Chapter 4. Tools

4.1 Introduction

This chapter presents the computing infrastructure, software and computational workflows used to accomplish the research presented in this thesis. Three software packages were used to complete this project: i) the opensource finite element analysis platform OpenSees [12], for which finite element formulations and constitutive models were presented in Chapters 3, ii) the quoFEM software developed by NHERI Simcenter staff [18], which provides a user-friendly interface to iii) the Dakota software developed and maintained by the Dakota group at Sandia National Laboratories [22]. Use of these software platforms / packages was enabled via use of i) NHERI DesignSafe, which maintains the DataDepot [18] in which the Shegay [21] experimental data set is archived as well as provided research data storage and access to computing resources at the Texas Advanced Computing Center (TACC) [22] and ii) Jupyter Hub [18] / Jupyter notebooks [24] for model building, visualization of simulation results, and model assessment.

4.2 Computational Infrastructure

In 2015, the National Science Foundation (NSF) funded the Natural Hazard Engineering Research Infrastructure (NHERI) program to provide infrastructure to support natural hazard engineering research. The NHERI Simcenter is one of 11 research infrastructure facilities funded through the NSF NHERI program. The Simcenter "provides next-generation computational modeling and simulation software tools, user support, and educational materials to the natural hazards engineering research community with the goal of advancing the nation's capability to simulate the impact of natural hazards on structures, lifelines, and communities." [18]. This includes the following, which are relevant to the current study:

1. The Data Depot platform for publishing and archiving natural hazard data and/or accessing data published and archived by others.
2. Secure and expansive data storage space for data that are developed by natural hazard research teams during ongoing research projects, with the expectation that some of these data will ultimately be published in the Data Depot.
3. Access to software used like OpenSees, QuoFEM, Dakota, Jupyter notebook, and python.

4. Access to HPC resources at the Texas Advanced Computing including the Stampede2 supercomputer used in quoFEM.
5. The use of Jupyter hub on DesignSafe to utilize the Jupyter notebooks created for this research.

4.3 Software

The software used for this research are OpenSees [13], quoFEM[18], and Dakota[2] . The quoFEM software facilitates the use of Dakota, in conjunction with OpenSees, a software framework that was used to simulate nonlinear structural response to earthquake loading. This software is vital for the use of simulating nonlinear response of concrete models and calibrating uncertainty in parameters of these models.

Software developed by the Simcenter includes WE-UQ, EE-UQ and HYDRO-UQ, which enable users to simulate linear and nonlinear building response under wind, earthquake, and tsunami and storm surge wave loading, respectively, and quantify uncertainty in simulate response [18]. The current study uses the Simcenter quoFEM software, which Quantifies Uncertainty with Optimization for Finite Element Method applications, via a user-friendly interface to the Dakota software [2] and the HPC resources provided by DesignSafe. Specifically, quoFEM is used to accomplish parameter estimation and sensitivity analysis of OpenSees models.

OpenSees is the open-source software platform originally developed by Frank Mckenna [13] for simulating the earthquake response of structural and geotechnical systems. OpenSees can be used on a local machine or used through Jupyter hub in Simcenter (this will be discussed at the end of this chapter). The original framework has been greatly enhanced by community contributions of new element and material formulations, solution algorithms, and utilities. The current study employs OpenSees Version 3.3.0, compiled for use on the TACC Stampede2 supercomputer, and the DKGQ layered shell element, the 2D concrete material model and the utility functions that create 2D shell material layers that employ 1D constitutive models to simulate layer response. It should be noted that for some analyses, OpenSees compiled for use on Stampede provides slightly different results than does OpenSees compiled for use on a desktop computer running Windows version 3.3.0. Because of this, results on windows may defer slightly than that on quoFEM especially in the post strength loss region of a simulation. This can be due

to the application being compiled on different architectures which may have different order of instructions issued by the compilers as well as to which significant digit will be rounded off. There may be differences that haven't been noticed yet with the build which may also cause differences.

QuoFEM provides a user-friendly interface to the Dakota software. The Dakota software provides "iterative systems analysis methods, which include: optimization with gradient and non-gradient based methods; uncertainty quantification with sampling, reliability, stochastic expansion, and epistemic methods; parameter estimation using nonlinear least squares (deterministic) or Bayesian inference (stochastic); and sensitivity/variance analysis with design of experiments and parameter study methods" [2] for use in conjunction with a wide range of simulation tools. For the current study quoFEM is used to facilitate use of Dakota with OpenSees; specifically, to facilitate use of Dakota to accomplish a sensitivity analysis and parameter estimation for OpenSees models. The primary workflow for the current study comprises running quoFEM from the user's local desktop, with each quoFEM "run" comprising identification of random variables, creation of a Dakota input file to conduct the requested analyses and sending the job to nodes on the Stampede2 supercomputer. The quoFEM / Dakota analyses are i) sensitivity analysis and ii) parameter estimation. Section 4.4 provides further discussion of the probability and analysis theory and methods embedded in Dakota, the computational workflows, and the QuoFEM interface. Details of the use of quoFEM for the current project are provided in Section 4.3.

Jupyter notebooks and python are used to create tcl scripts that drive the OpenSees analyses. OpenSees was used rather than OpenSeesPy because at the time, the model that we wanted to use was unavailable through OpenSeesPy. Jupyter notebooks can be downloaded locally to a computer and used as a web application to create code and documentation. Jupyter Notebook is available through the DesignSafe cloud servers. So, any data that is stored in the data depot can be accessed through DesignSafe Jupyter hub and immediately analyzed. This can speed up one's workflow. Currently though QuoFEM is available as a desktop app which can slow down a workflow as the files needed to input into QuoFEM would need to be on the local drive but there will be a way for QuoFEM to be used through Jupyter notebook on DesignSafe. A discussion of the workflow, python code, and outputs of the Jupyter notebooks that were developed for this

research are in the next section of this chapter. Details of the use of Jupyter Notebooks for the current study are presented in Section 4.2.

4.4 Jupyter Notebooks

Three groups of Jupyter notebooks were create for this project; these groups i) create OpenSees models of the walls in the datasets and execute OpenSees simulations, ii) visualize simulation results, and iii) compute error functions characterizing the accuracy with which measured response is simulated. Individual notebooks are described below; these notebooks are published here: https://github.com/stokljos/thesis/notebooks.

4.4.1 Notebooks for OpenSees Simulations

The first group of two notebooks are used to accomplish OpenSees simulations of each wall in the data set. The first notebook maps the MATLAB data characterizing wall test specimens and loading protocols into python, and the second notebook creates OpenSees models of each wall as well as executes OpenSees analyses of each wall that mimics the laboratory loading. The second group of Jupyter notebooks comprises five notebooks that accomplish post processing of simulation data.

4.4.1.1 Notebook 1.1: MATLAB to Python

The primary function of Notebook 1.1 is to create a python list that stores all of the data from the Shegay MATLAB data structure that are required to build and execute an OpenSees analysis of the X planar walls that are used in the current study. For each wall in the Shegay dataset, this notebook creates a unique name and a unique index number; these identifiers are used throughout the analysis. The “unique name” is a combination of 1) the last name of the researcher who conducted the laboratory testing and published the laboratory data and 2) the identifier assigned to each wall specimen by the researcher. For example, Thomsen and Wallace [25] conducted laboratory testing and published laboratory data for a wall specimen that they identified as RW1; thus, this wall specimen is given the unique name “WallaceRW1”. Each wall specimen is assigned a unique index number, somewhat randomly, based on the order in which the data were entered into the Shegay MATLAB data structure. For example, the WallaceRW1 wall was assigned the index 33. When 33 is provided as input to Notebook 1.2, a python list is created that stores all relevant data for ‘WallaceRW1’ for use in subsequent notebooks.

The data that are retrieved from the MATLAB data structure and stored in the python list for use in model building include the following:

- **Wall geometry:** including height, thickness, in-plan length, shear span defined as the moment at the base of the wall divided by the shear at the base of the wall, thickness of cover concrete, and aspect ratio.
- **Reinforcement layout:** including, for horizontal and vertical bars, locations of the vertical bars, bar diameters, bar spacing of bars, and reinforcement ratios.
- **Steel material data:** including, for each unique bar size, yield strength, ultimate strength, strain at yield, and strain at ultimate strength.
- **Concrete material data**: including, concrete (boundary and web regions) like compressive strength and strain at compressive strength. Strength data of concrete is measured in the lab and strain data and boundary strength are calculated values.
- **Response data**, including axial load, lateral load, and displacement history.

4.4.1.2 Notebook 1.2: Build Out Model

This notebook takes a user input of the wall index (or for multiple walls, the user can create a list of indices of walls that can be ran through a for loop which is set up in the notebook). The output is a tcl script which is used to simulate in OpenSees.

As discussed, this notebook calls Notebook 1.1 with the input wall index to retrieve a python list of data characterizing the wall and the load and displacement histories employed in the laboratory.

Chapter two gives a summary of each section of the notebook 1.2 as well as the three other files that are created along with the model file which are a text file of the experimental displacement capacity, the experimental max strength, and a reference file that is used in the post processing script to give various information needed in those notebooks. The text files of the experimental results are used in quoFEM when comparing simulated outputs to experimental, which is discussed in further detail in section 4.3.

4.4.2 Notebooks for Post Processing

Notebooks 2.1 – 2.4 accomplish postprocessing of the OpenSees analysis data. Notebook 2.1 reads the xml files generated by OpenSees and extracts and processes the data that are used by three additional post processing notebooks (Notebooks 2.2-2.4).

4.4.2.1 Notebook 2.1: Xml Reader

Notebook 2.1 requires a single input, which is the reference file (This file is one of the text files created with the model, it will be placed in the same folder as the model). It will output extracted data from the simulation that is required for the following notebooks.

This notebook will create multiple arrays of data extracted from the xml files in a python variable; for the stress and strain concrete xml files, this notebook will extract stress/strain in the y, stress/strain in the x, and shear stress/strain and place the corresponding data in an array to be used by the following post processing notebooks. For the steel stress/strain xml files, this notebook will extract the stress/strain in the y.

Some of the output data from the simulation is recorded in an XML file. This is to save space as if it were recorded into a text file, the text file may be 2-5x larger than if it were recorded into an xml file. A typical xml file for stresses for the concrete can range from 200 MB to 1 GB and thousands of lines of data. In order to also save time parsing through data, notebook 2.1 was created to grab the data needed and transfer it to the other post processing notebooks.

The following are the names and summary of what is in each XML output files:

- FULLWALL_elementsmat1fib3sig.xml & FULLWALL_elementsmat1fib3eps.xml
    - Stress/Strain data at a single integration point of every single element in the wall
- FIRST3LEVELS_elementsmat1fib3sig.xml & FIRST3LEVELS_elementsmat1fib3sig.xml
    - Stress/Strain at a single integration point of the first 3 levels of elements in the wall. (This is to save time for post processing when a notebook doesn't not require every single stress and strain point on the wall).
- trusssig.xml & trussseps.xml
    - Stress/Strain of all vertical bars in the wall
- Crack_elementsmat1fib3crack.xml

- Records at which simulated step number the concrete cracks and at that point it also records the angle of the concrete crack in degrees from the horizontal axis.

Note 1: ‘mat1’ references an integration point of the element so with 4 integration points in an element there will be 4 total files; ‘mat1’, ‘mat2’, ‘mat3’, and ‘mat4’.

Note 2: ‘fib3’ references fiber 3 so all data from fiber 3 of the element is recorded. (Fiber 3 is picked because that concrete fiber in the middle of every wall).

Note 3: ‘sig’ references that it is a stress file and ‘eps’ references that it is a strain file.

The reference file (which is created when the model is created) contains numbers like how many nodes are across the base of the wall, total number of nodes in the wall, and total number of elements in the wall. Since the data is recorded based on the amount of elements in the wall, this information in the reference file is unique to each wall model and aids in parsing the data correctly. In a stress xml file for integration point 1 (lower left section of an element) a single line of data carries five stress values on every element in the wall. That single line is defined by an step sequence in the cyclic history. So, if it were a pushover analysis to 6 inches and the analysis is pushing the wall 0.01 inches per step and the wall has 500 elements, that is a total of 600 lines of data with 2,500 total values per line which comes to a total of 1.5 million values. For a cyclic analysis, that is being pushed +/- 1 inch, 2-inch, 3 inch….6 inches, that comes to a total of 10.5 million values. Many of these walls have more cyclic runs and ranges as well as upwards of 2000 elements so it is important to keep the computational expense as low as possible. When parsing through this data, the use of the number of elements from the reference file comes into play as we can know exactly how many values are in a single line.

4.4.2.2 Notebook 2.2: Visualization of load-displacement history

This notebook takes two output files, basereact.txt and topdisp.txt, from the simulations that are not xml files but text files, are used as input for this notebook. These files are the load reactions in the vertical direction at the base of the wall and the displacement in the horizontal direction of the top of the wall. Using these files, a simulated cyclic response can be generated. The experimental history of the measured response can be pulled from the MATLAB file. The graph is unitless and since the output for the histories are in kip for the y axis and inches for the x axis,

more information needs to be pulled to convert these axes to be unitless. The x axis will be converted to drift % and the y axis will be converted to Moment of the base of the wall divided by nominal moment of the wall. The displacement of the simulation will have the same peak displacements of the measured history, but the steps to those peaks will be different as the simulation is taking 0.01 inch increments.

Starting with the x axis, information needed is the height of the wall. Taking each displacement of the cyclic history and dividing it by the height and multiplying by 100 will give a percentage of drift. For the y axis, the information needed is the nominal moment of the wall (which is calculated and stored in a text file for every wall in the database) and the height of the wall. Taking each reactive force of the cyclic history and multiplying it by the height will give base moment and then dividing it by the nominal moment will produce a value of Moment base divided by nominal base.

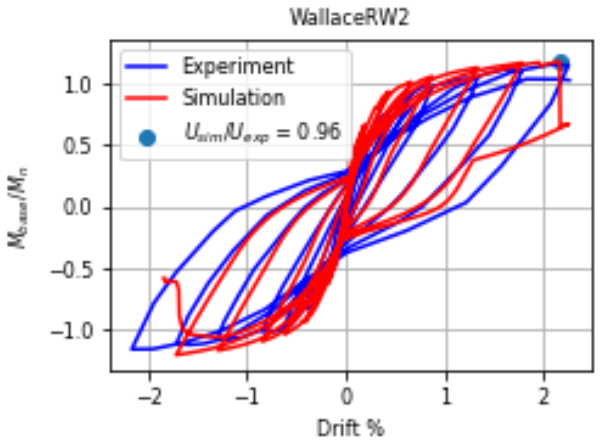

Figure 4.1 *Load-Drift Plot*

4.4.2.3 Notebook 2.3: Assessment of Wall Failure Mode

Notebook 2.3 takes as input the stress and strain histories at each quadrature point in each concrete element as well as the stress and strain histories for all vertical steel bars for the first 3 rows of elements. These data are used create plots showing the stress-strain histories for concrete element quadrature points and reinforcing steel elements near the bottom of the wall and at the horizontal ends of the wall, where material yielding and failure could be expected to occur. Notebook 2.3 provides as output plots of concrete quadrature point vertical stress-strain response and vertical reinforcing steel stress-strain response.

Notebook 2.3 also provides as output the simulate failure mode for the wall, which is defined as either concrete crushing and simultaneous reinforcement bucking (CB) or reinforcing steel fracture due to prior cycles of high compression strain demand, which could be expected to produce bar buckling (BR). Bar rupture failure is identified when a phase of monotonically increasing steel tensile strain produces a drop, to zero, of steel stress. Concrete crushing failure is identified when increasing concrete compressive strain demand results in loss of concrete compressive strength. In the laboratory, extreme concrete compression strain demand is typically accompanied by compression buckling of reinforcing steel; in the model reinforcing steel loses compressive strength at the compressive strain demand at which concrete compressive strength drops to the residual compression strength. Figures 4.2 show samples of simulated stress strain histories for quadrature points closest to the base of the wall in concrete elements at the horizonal perimeter of the wall and for vertical reinforcing steel elements near the base of the wall and at the horizontal ends of the wall. Simulated failure of concrete and steel was found to occur typically at the bottom most quadrature point and element, respectively; however considering data for several layers of quadrature points was found to be useful in evaluating wall response.

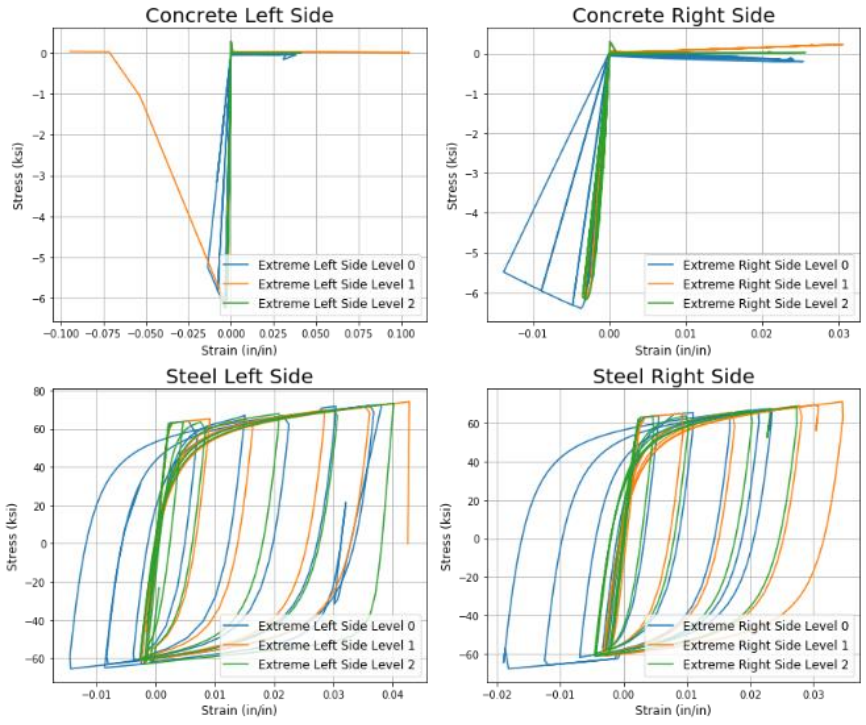

Figure 4.2 *Stress Strain of Concrete and Steel Extreme Fibers*

4.4.2.4 Notebook 2.4: Movies

Notebook 2.3 takes as input the stress and strain arrays generated by Notebook 2.1; these are the simulated stress and strain histories for every concrete element quadrature point and every reinforcing steel element. Notebook 2.3 creates an interactive plotting tool that can provide movies of the simulated concrete stress and strain field histories for the entire wall. The plotting interface comprises two plots of simulated concrete stress of strain fields placed side by side with a dropdown menu above each one to select which stress/strain value to be plotted and a slide bar at the bottom that identifies the point in the simulation history for which data are shown. The user can manually slide the bar to choose unique points during the simulation history or choose auto scroll, which slides through the cyclic history. The user can choose to view normal stress/strain is the vertical direction or shear stress/strain as well as minimum or maximum principal stresses and strains. This tool for visualizing simulation results enables the user to understand how these fields evolve as the wall is subjected to the cyclic displacement history and, thereby, provides improved understanding of the load-transfer mechanism and failure mode.

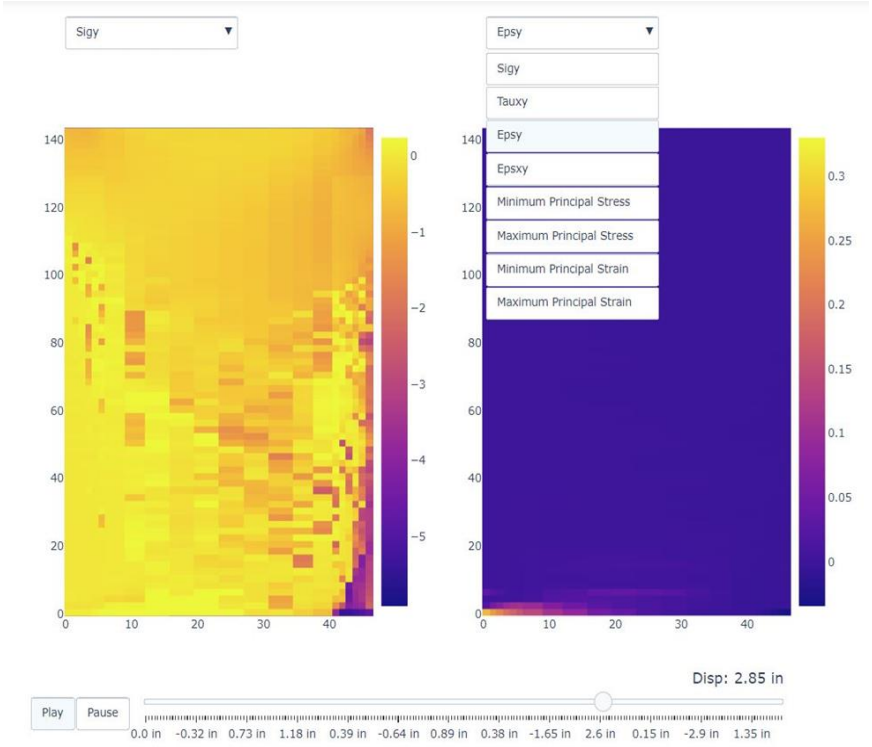

Figure 4.3 *Still of a Wall stress profile of drift history*

4.4.2.5 Notebook 2.5: Concrete Crack Angle

Notebook 2.5 takes as input the crack xml files and creates as output a figure showing the angle of the concrete crack at each cracked quadrature point at the end of the analysis. Figure 4.4 provides an example of the notebook output. These crack orientation data can be compare with crack patterns observed in the laboratory to evaluate the accuracy of the simulation. These data also provide understanding of the orientation of the principal stress fields at the point of crack initiation. The concrete material model includes two recorders that provide, for each quadrature point, i) output indicating whether or not the concrete has cracked and 2) the angle at which the concrete cracked. Notebook 2.5 builds an image of the wall mesh and then, at the location of quadrature points where these is a crack, creates a short line parallel oriented at the angle of the crack surface. It should be noted that within the material model, crack orientation is fixed, for the remainder of the analysis, once the crack forms.

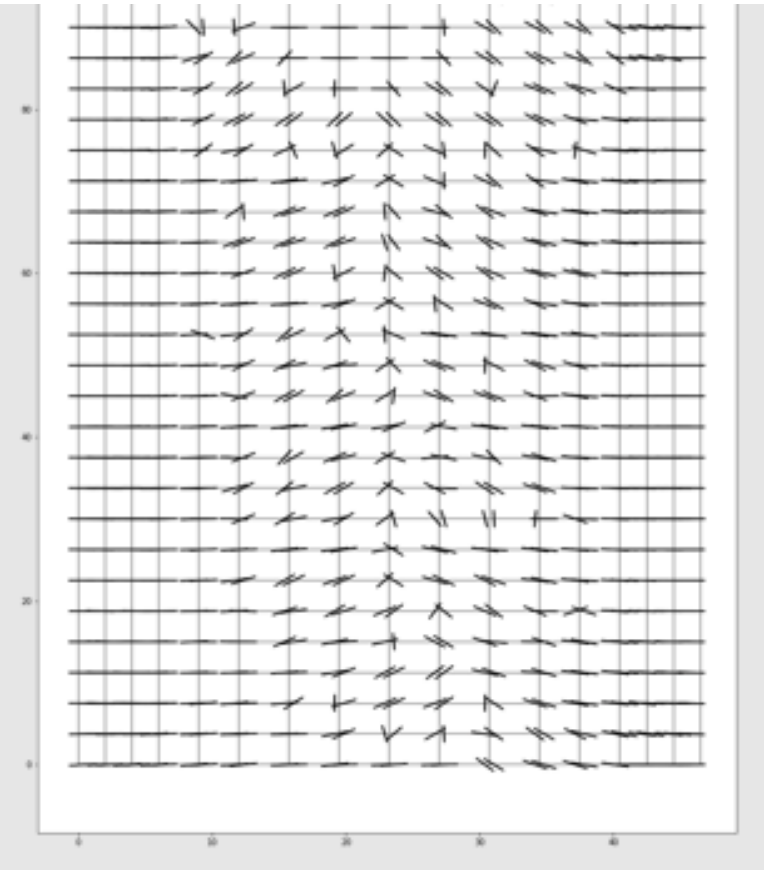

Figure 4.4 *Crack angle of elements*

4.4.3 Notebooks 3.1 through 3.4

The last group of Jupyter notebooks compute error functions that quantify the different between measured and simulated response quantities. There are four unique notebooks in this group that compute the different between the measured and simulated yield stiffness, maximum strength, displacement capacity, and envelope to the cyclic response history. Specifics of these notebooks follow:

- **Notebook 3.1: Yield Stiffness Error**. Initial stiffness is defined by the load-displacement point at which one of the concrete in the extreme fiber reach -0.003 per ACI code 318 [1]. The load at this displacement point is then compared to the load at the displacement point of the measured history. The error can be defined as:

$$Error_{stiffness} = \frac{k_{measured} - k_{simulated}}{k_{measured}}$$

- **Notebook 3.2: Maximum Strength Error**. Maximum strength error is defined using the absolute value of the maximum measured in either load direction. Notebook 3.2 searches through the measured data to find the maximum load sustained by the wall, in either the positive or negative direction, and then searches through the simulation data to find the maximum simulated load in the same load direction as the maximum measured load. The strength error is computed as follows:

$$Error_{load} = \frac{F_{max_{measured}} - F_{max_{simulated}}}{F_{max_{measured}}}$$

  with measured and simulated forces acting in the same load direction.

- **Notebook 3.3: Displacement Capacity Error**. Displacement capacity error is defined using the measured displacement at onset of strength loss in the laboratory; where strength loss is defined as the load-displacement point, on the envelope of the load-displacement history, where the displacement exceeds the displacement at maximum strength and simulated strength is less than 90% of maximum strength. Notebook 3.3 searches through the measured data to find the displacement at initiation of significant strength loss $\left(D_{max_{measured}}\right)$, searches through the simulation data to find the

displacement at which simulated onset of strength loss occurs in that same direction, and computes the displacement capacity error as follows:

$$Error_{load} = \frac{D_{max_{measured}} - D_{max_{simulated}}}{D_{max_{measured}}}$$

with measured and simulated forces acting in the same load direction.

4.4.4 Notebooks 3.4: quoFEM

The final Jupyter notebook creates quoFEM post processing script. This script duplicates code in Notebook 3.2 and 3.3 to determine simulated max strength and displacement capacity and provides as output the ratios of i) simulated maximum strength divided by measured maximum strength and ii) simulated displacement capacity divided by measured displacement capacity.

4.5 quoFEM

The quoFEM software developed by the NHERI Simcenter [18] was used to facilitate uncertainty quantification and model parameter estimation for the current study. QuoFEM provides a user-friendly interface to three uncertainty quantification and parameter estimation computational "engines": the Dakota software, which is developed and maintained by Sandia National Laboratory [2], as well as the SimCenterUQ [18] and UCSD-UQ [18] engines which were developed as part of the NHERI Simcenter project. The following will dive into the different algorithms used in this research for quoFEM.

4.5.1 Selection of quoFEM methods for use in the current study

QuoFEM provides a user-friendly interface to three uncertainty quantification (UQ) engines: Dakota, SimCenterUQ and UCSD-UQ.

QuoFEM utilize five methods from the Dakota engine; forward uncertainty propagation, reliability analysis, inverse problem, sensitivity analysis, and parameter estimation. The current study uses only sensitivity analysis and parameter estimation; these methods are discussed in the following sections.

4.5.2 quoFEM Sensitivity Analyses

Initially, quoFEM Sensitivity Analyses were performed, using the Nataf transformation algorithm, to assess the impact on simulated response, including response parameter of particular interest (Max strength) of variation in uncertain model parameter of the shear retention factor. The quoFEM software requires definition of the following to complete these analyses:

- name of the random variable
- distribution to be assigned to the variable and distribution parameters
- input file
- output file
- quantity of interest in the output file

For the current study, sensitivity analyses were conducted to assess the variability of the max strength of the model given uncertainty in model parameter shear retention factor, the response parameter were assumed to have uniform distribution. Figures 4.5 through 4.9 show definition of these quantities within the quoFEM GUI.

For example, in the case of this research, the quantity of interest is either max strength or displacement capacity errors. A walk through of visual representations can be found next with using the QuoFEM interface.

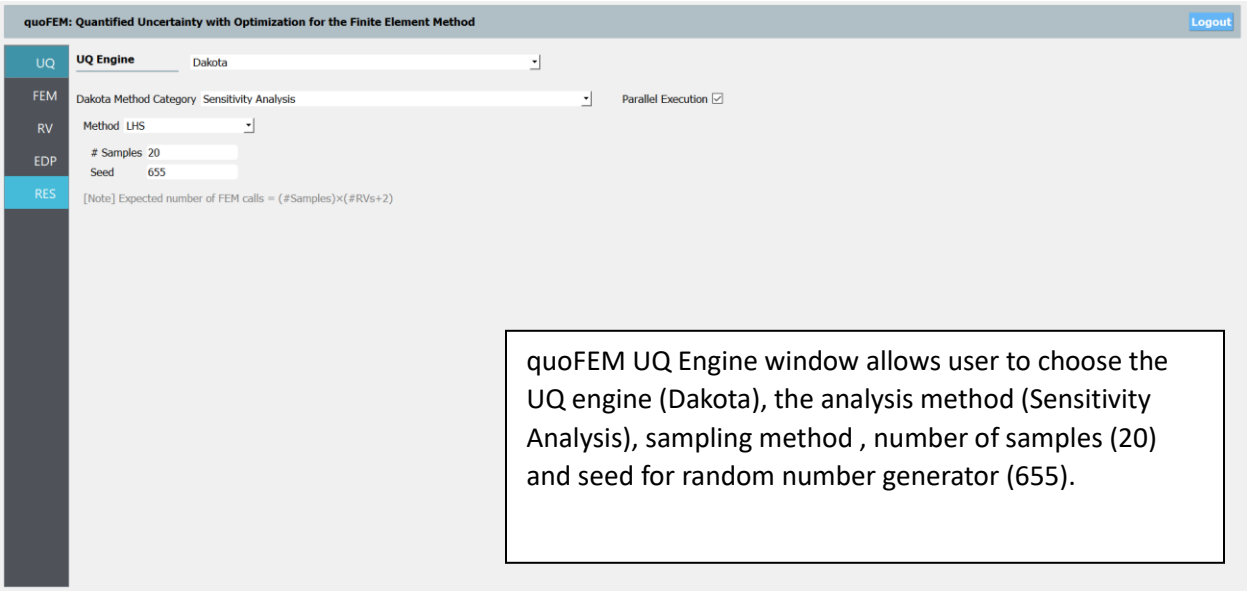

Figure 4.5 *Sensitivity set up*

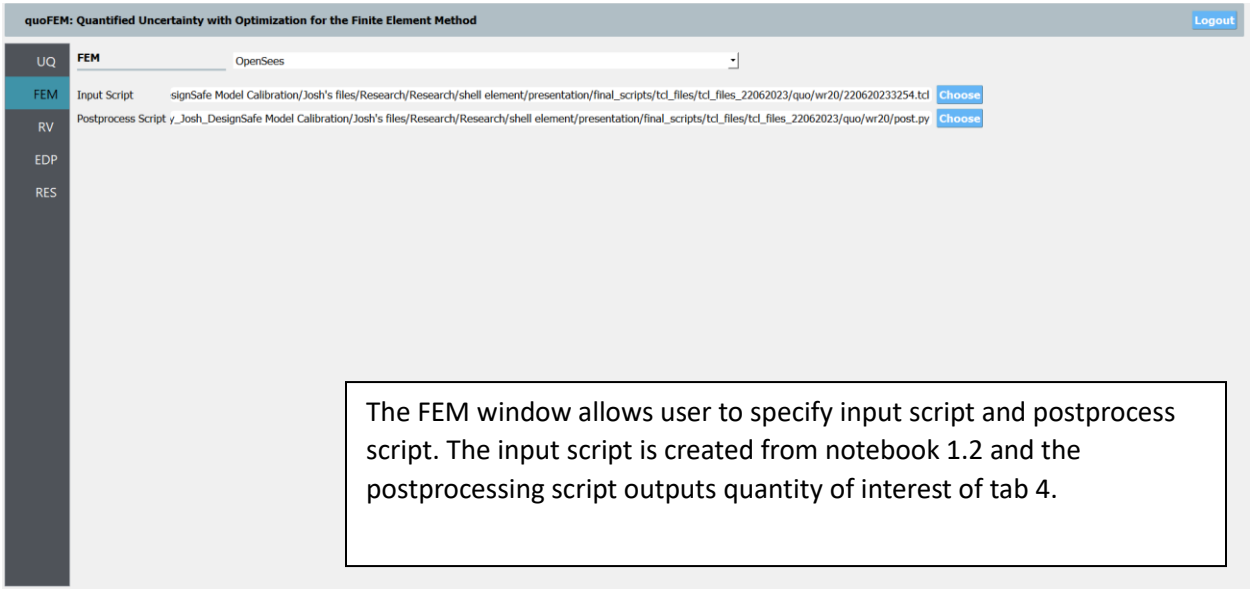

Figure 4.6 *Sensitivity FEM set up*

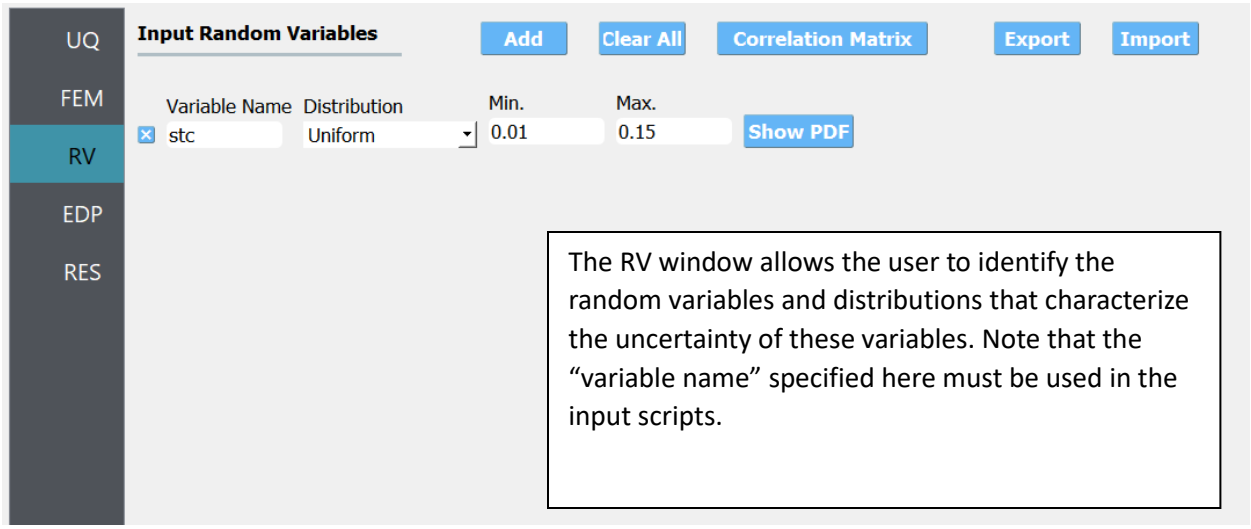

Figure 4.7 *Sensitivity Variable definition*

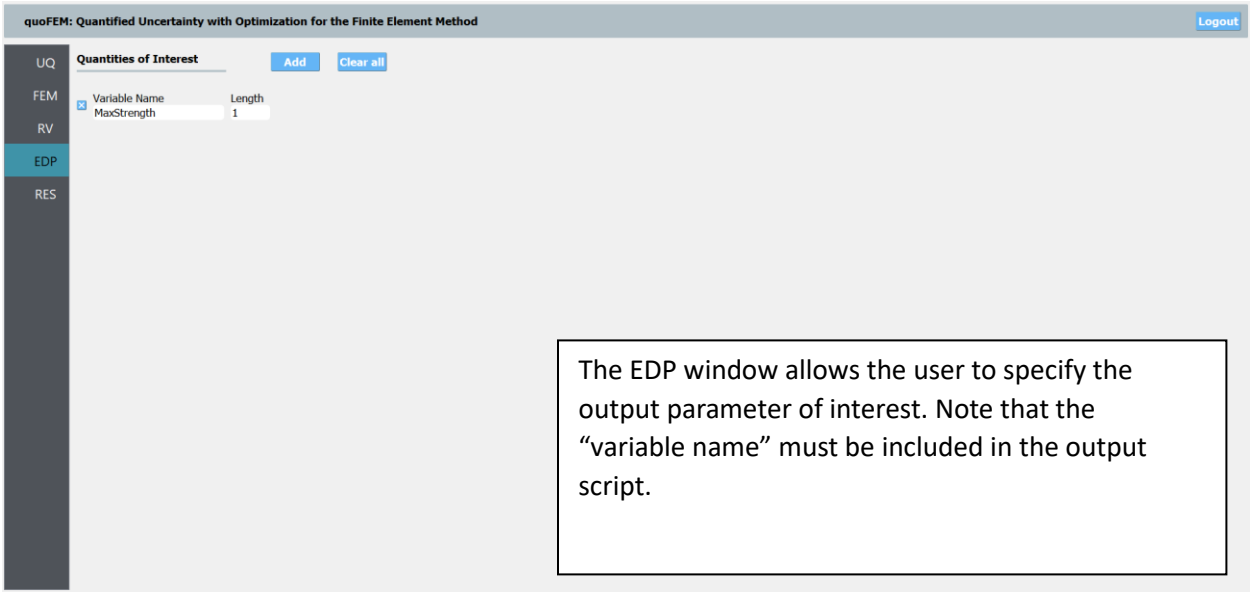

Figure 4.8 *Sensitivity QoI set up*

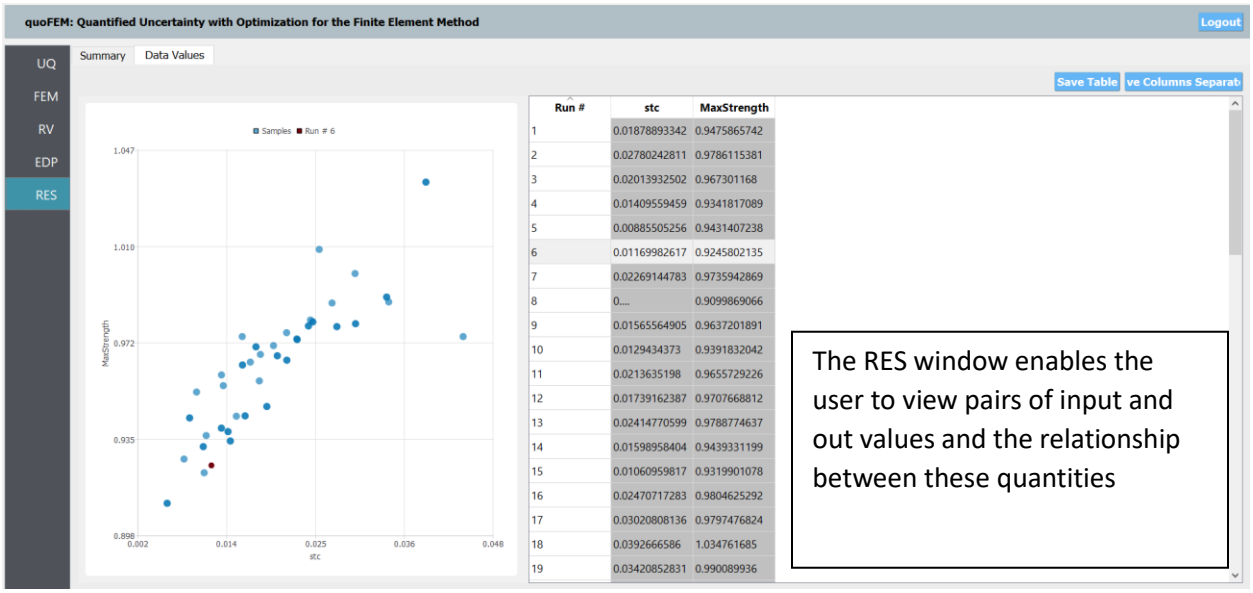

Figure 4.9 *Results*

A single run of a model can take 1 hour to as many as 5 hours depending on the size of the model script (This varies because of the number of elements per wall). Running a sensitivity analysis on a model that takes 5 hours and running 60 jobs on a single node with 30 processes will take around 10 hours. The results in figure 4.9 gives a quick representation of the data and can see how the model is sensitive to the parameter. Every simulated run is stored in a zip file on the

DesignSafe data depot. That file can be extracted and further post processing can be down through Jupyter to understand how certain parts of the model are behaving due to the change in the parameter.

4.5.3 quoFEM Parameter Estimation

A gradient based parameter estimation uses algorithms to optimize the random variables to find the best value for those variables in regard to the quantity of interest. This method is based on non-linear least squares to minimize the sum of the squared errors between the calibrated data and the simulated data. The two algorithms that can be chosen are OPT++GuassNewton or NL2SOL. The output that is being compared to is the displacement capacity and this is being tested by changing parameters with uncertainty that effect that outcome (steel rupture strain ratio and crushing energy ratio).

The first algorithm consists of the Guass-Newton Hessian approximation with full Newton optimization algorithms. The exact objective function value, exact objective function gradient, and the approximate objective function Hessian are defined from the least squares term values and gradients and are passed to the full-Newton optimizer. As for all of the Newton-based optimization algorithms in OPT++, unconstrained, bound-constrained, and generally-constrained problems are supported. However, for the generally-constrained case, a derivative order mismatch exists in that the nonlinear interior point full Newton algorithm will require second-order information for the nonlinear constraints whereas the GuassNewton approximation only requires first order information for the least squares terms. [2]

The NL2SOL algorithm [2] is a secant-based least-squares algorithm that is q-superlinearly convergent. It adaptively chooses between the Gauss-Newton Hessian approximation and this approximation augmented by a correction term from a secant update. NL2SOL tends to be more robust (than conventional Gauss-Newton approaches) for nonlinear functions and “large residual” problems, i.e., least-squares problems for which the residuals do not tend towards zero at the solution. [2]

When setting up a parameter estimation on quoFEM, it follows the sensitivity analysis workflow except for the first tab which will define the parameter estimation. The method will either be OPT++GuassNewton or NL2SOL, then max iterations of the estimation can be set and a

convergence tolerance. The user will also add a calibration file which will hold the value(s) of the result the user is trying to get to for the output of the post processing file.

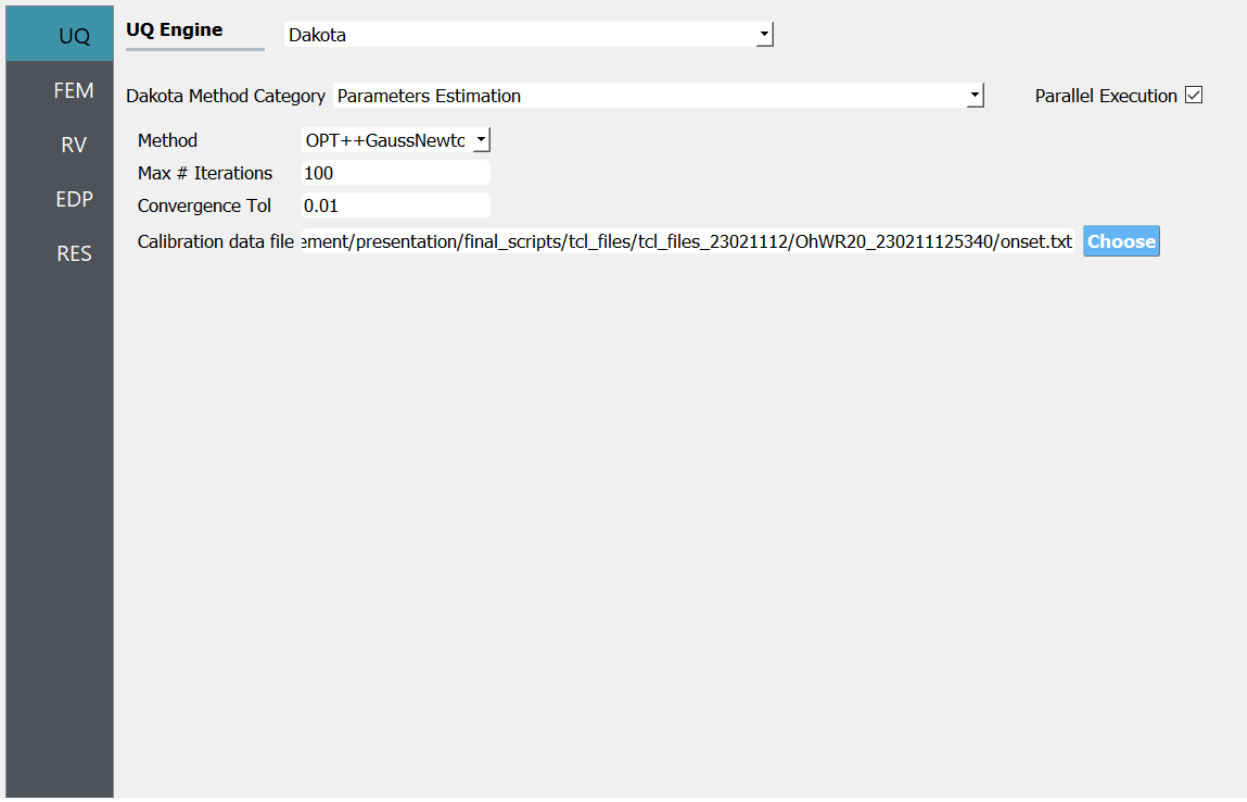

Figure 4.10 *Parameter Estimation set up*

In the instance of using a model where the parameters cannot be reliably estimated, there is the gradient free parameter estimation. This method minimizes the function based on how the function values are evaluated. The exact pattern search algorithm this method uses is called *'coliny_pattern_search'.* More information on this algorithm can be found in the Dakota technical manual [2].

For a non-gradient parameter estimation, the user will select Optimization under 'Dakota Method Category' and use the 'Derivative-Free Local Search" method. The gradient free parameter estimation follows the same workflow as sensitivity analysis and parameter estimation expect for the first tab. The following is an explanation of each input seen in figure 4.11:

1. Initial step size: this defines the initial size of the offsets used in the pattern search algorithm
2. Contraction factor: this specifies the ratio of the reduction in the offset size used in the pattern search algorithm
3. Max # model evals: This is a termination criterion. This specifies the maximum number of model evaluations allowed during the search for the optimum parameter values. This sets the total computational budget for the pattern search algorithm.
4. Max # iterations: This is a termination criterion. This specifies the maximum number of iterations allowed in the optimization algorithm. During each iteration of the algorithm, several model evaluations occur in parallel.
5. Variable tolerance: This is a termination criterion. This specifies the maximum permitted change in the value of the parameters being estimated from one iteration to the next.
6. Convergence tolerance: This is a termination criterion. This specifies the maximum permitted change in the value of the objective function from one iteration to the next.

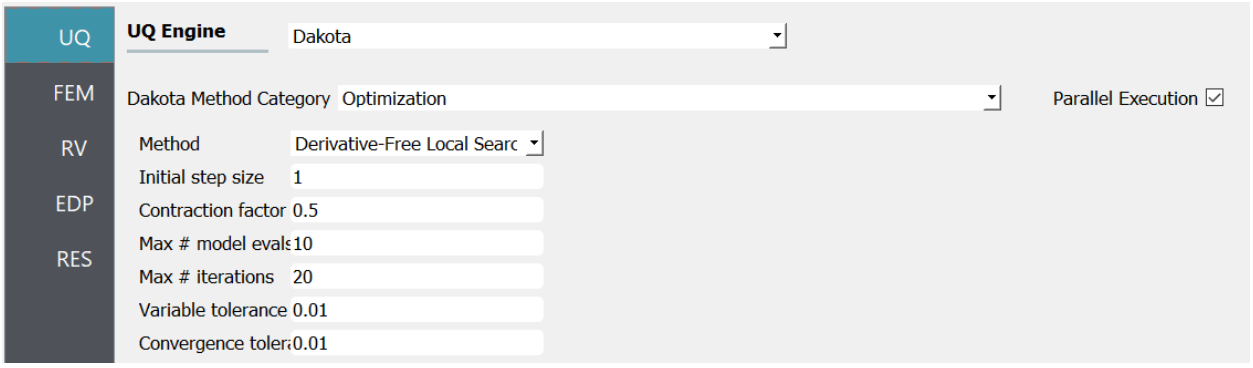

Figure 4.11 *Non-Gradient Parameter Estimation set up*

4.6 Workflow

There are four workflows to consider; i) local desktop for single OpenSees run and post process, ii) Jupyter hub single OpenSees run and post process, iii) quoFEM setup and run, iv) Post quoFEM Jupyter hub process. Each workflow has its own purpose and use in the research being presented. Each workflow can be represented by the flow charts at the end of the section. The following will discuss each workflow in detail.

The first workflow is for the purpose of getting quick results. Unlike on DesignSafe where when you run a job, you are put in a queue for your job to run on your desktop with OpenSees downloaded, you can start your job immediately. The main goal of this workflow is to see how changing a variable or convergence script may affect the results of the simulation. Since it is running on a local desktop/laptop, a single run will be slower than on TACC computers, but the setup and process will be quicker.

To start the workflow it is assumed the user has OpenSees and Jupyter notebook installed and apart of file path environmental variables and the scripts used for this research downloaded. The first step is run Jupyter notebook in the folder where the scripts are located. Once the Jupyter notebook browser is up, select the model creator script. In this script, the only user input is the index number(s) for the wall that will be modeled. For specific wall indices see appendix C. There are options to create a single wall or multiple walls at once in the script. Once these models have been created, they will be stored in a subfolder of tcl_files (If this folder is not already created, one will be created in the same directory as the script). The subfolder is named after the year, month, day, and hour represented in seconds and if multiple walls were created they will all be stored in the subfolder with their corresponding unique id and date. Next step is to go to each wall folder and run OpenSees in folder path, type “source *filename*.tcl” and hit enter. Once OpenSees has finished, go back to Jupyter notebooks and select a postprocessing script to run. All postprocessing images or interactive graphs will be stored in the corresponding wall folder.

The second workflow is for the purpose of running a single wall or multiple walls without requiring any memory or RAM from a local desktop or laptop. It has a similar workflow as the first one, but everything is done through the Jupyter hub on DesignSafe. To get the Jupyter hub, sign into DesignSafe, select Workspace then Tools & Applications and then click on Jupyter (not

HPC) The options are then to select updated Jupyter image or classic Jupyter image. The scripts are created in the classic Jupyter image so select that. Assuming that the scripts are copied to the users local file system on design safe, follow the same workflow above except when using OpenSees. Select the file path of wall to simulate, select the OpenSees script and input necessary information for the job and then run. The rest of the workflow will mirror above. Only difference is this will be on the users local DesignSafe system.

The third and fourth workflows could be a single workflow but they are split up into a desktop workflow for quoFEM which is setup and run, and then a DesignSafe workflow for quoFEM which is the postprocessing.

Since quoFEM is an application that is directly installed to local computer, the wall that will be used on quoFEM needs to be created on the local computer. So use the first part of workflow #1 to create the model, then use the python error function (for max strength or displacement capacity) and corresponding text file for calibration for the input files in quoFEM. After following section 4.3.3 for a sensitivity analysis or 4.3.4 for a parameter estimation, run the job.

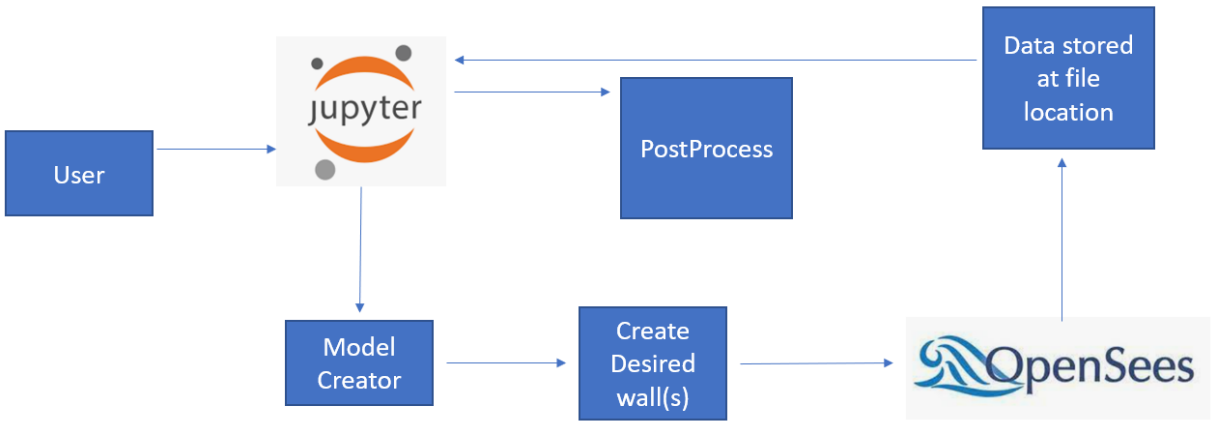

Figure 4.12 *Local Run*

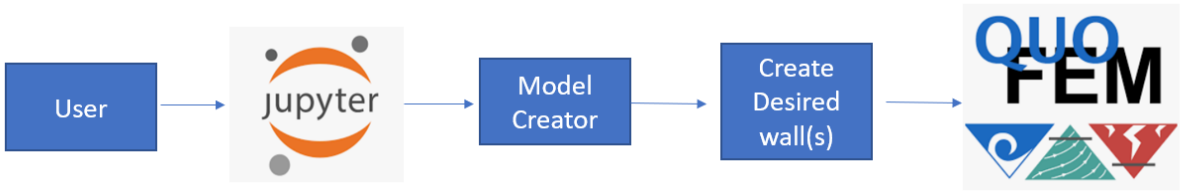

Figure 4.13 *Setting up quoFEM job*

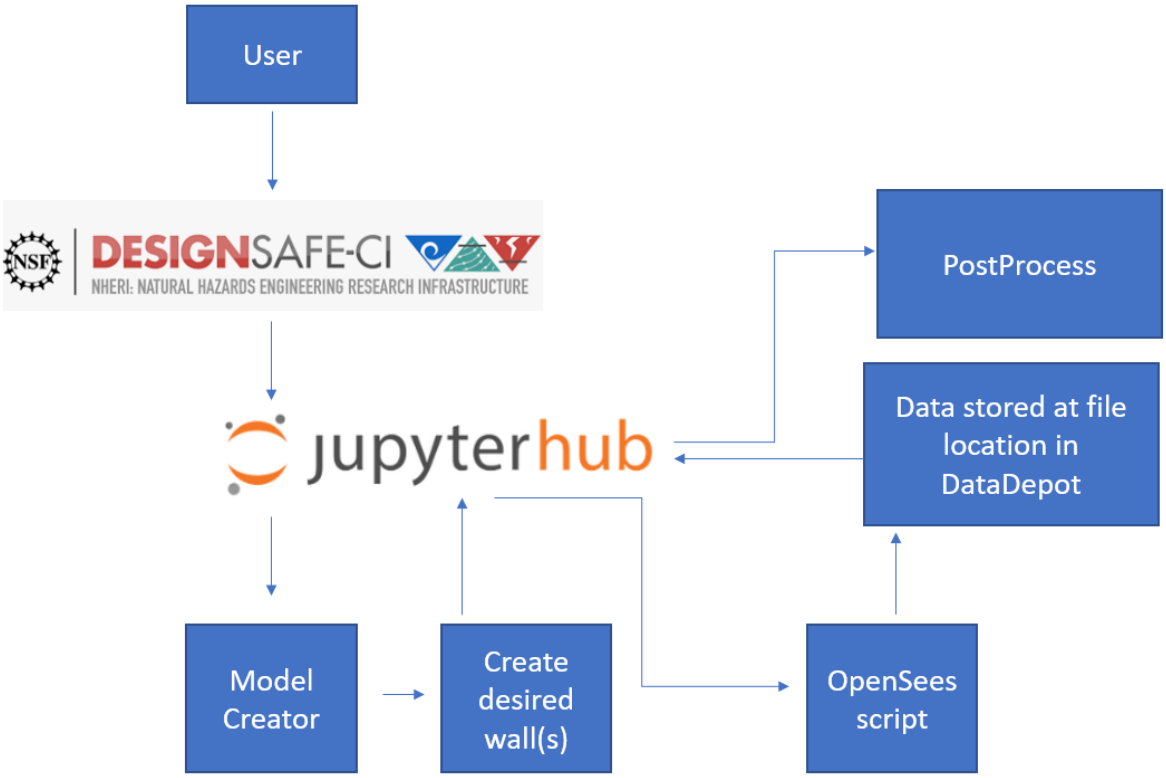

Figure 4.14 *Setting up OpenSees on DesignSafe*

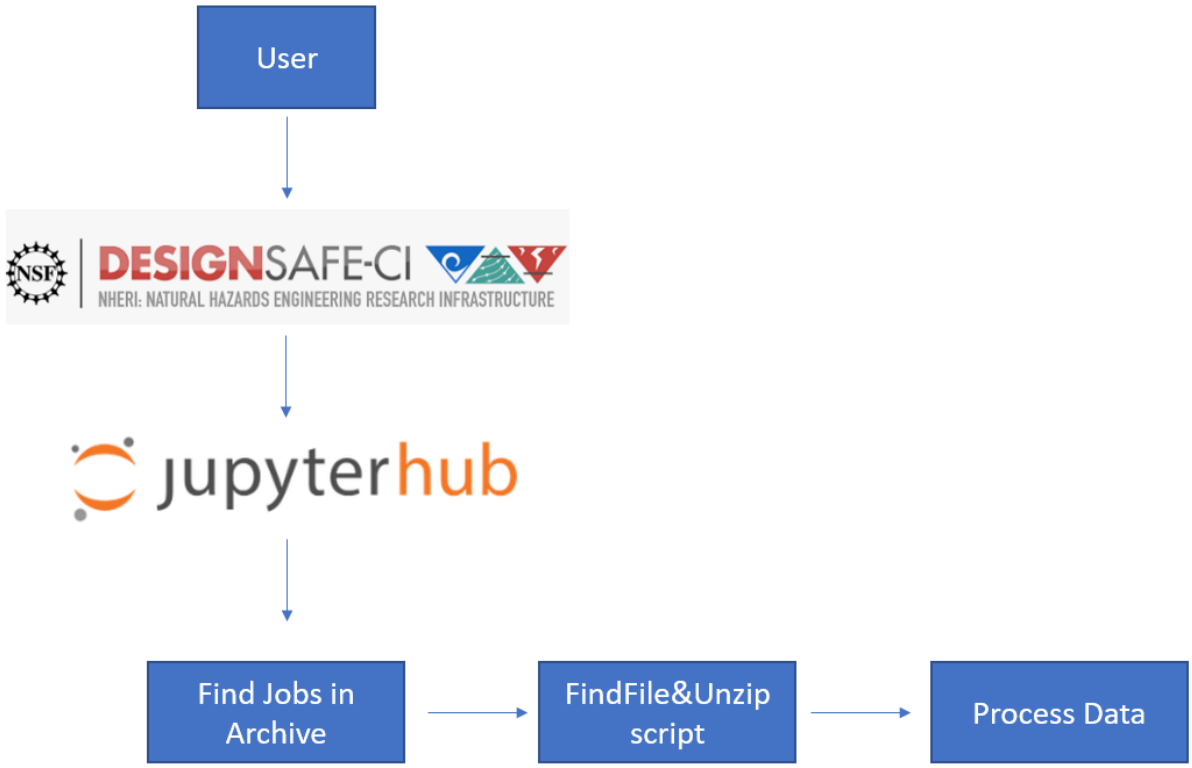

Figure 4.15 *Downloading QuoFEM data*

4.7 Conclusion

This chapter presented the software that was utilized in this research as well described the Jupyter notebooks that assisted in building the model, post processing the data and created the error functions that aid a quoFEM run, and described the multiple workflows that can be used on a local machine and on the SimCenter workbench. The next chapter will conduct sensitivity analysis and parameter estimations for the calibration set and use the preferred values in the validation set to determine if the model can accurately predict strength and drift capacity of the various wall models.

Chapter 5. Calibration and Validation

5.1 Introduction

This chapter presents calibration of three model parameters that are not well-defined by experimental data: shear retention factor (stc), ratio of confined to unconfined crushing energy (rev), and steel rupture strain reduction factor (srs). Calibration is accomplished using the quoFEM software and the calibration dataset, which comprises approximately half of the experimental test specimens, spans a range of specimen design parameters, and includes an approximately equal number of specimens exhibiting the compression-buckling failure mode and the buckling-rupture failure. For each wall specimen, the calibration process starts with calibration of the shear retention factor to achieve accurate simulation of wall specimen strength. Then, for walls exhibiting compression-buckling failure, the ratio of unconfined to confined concrete crushing energy is calibrated and for walls exhibiting buckling-rupture failure, the streel rupture strain reduction factor is calibrated for walls exhibiting the buckling-rupture failure mode. Regardless of failure mode, this second calibration process seeks the model parameter value that results in accurate simulation of drift capacity, defined as the drift at onset of significant strength loss. Average values of the three critical model parameters are compute for the calibration data dataset. These average model parameters are validated via comparison of simulate and measured response quantities for the validation data set, where the validation data set comprises approximately half of the experimental test specimens and spans a range of specimen design parameters.

The calibration and validation processes and results are presented in Sections 5.2 through 5.5 of this thesis as follows. Section 5.2 reintroduces the error functions used in the calibration and validation process and discusses their use with the quoFEM software. Section 5.3 presents calibration of the shear retention factor, crushing energy ratio, and steel rupture strain ratio using quoFEM and the calibration data set as well as comparison of simulated and measured response quantities for the calibration data set, with simulated values computed using the average of the calibrated model parameters. Section 5.4 compares simulated and measured response quantities for the validation data set, with simulated values computed using the average calibrated model parameters. Section 5.5 compares, for the validation data set, results for the case of average

model parameters as computed using the calibration and validation data sets as well as the case of wall-specific values.

5.2 Error Functions

The error functions presented in Chapter 4 were used with quoFEM to determine preferred values for the shear retention factor, ratio of confined to unconfined crushing energy, and steel rupture strain reduction factor. Preliminary evaluation of the model in chapter 3, indicated that the shear retention factor had significant impact on maximum wall strength; this is attributed to the fact that larger values of shear retention result in increased shear transfer parallel to concrete crack surfaces, which can increase wall flexural and shear capacity if concrete cracks at the base of the wall are not horizontal. Thus, this parameter was calibrated to achieve accurate prediction of maximum wall strength. Previous research Lowes [10] and Pugh [17] has demonstrated that unconfined and confined concrete crushing energies and steel rupture strain ratio determine simulated deformation capacity. Thus, the displacement capacity error function (cite and equation that presents this), was used to calibrate these quantities.

When running a sensitivity analysis, the goal is to see in what range of values does a wall get close to the actual value (whether that be max strength of simulated to experimental or displacement capacity of simulated to experimental). When running a parameter estimation, the goal is finding the exact value that gives you the same response of the experimental. So, when running a parameter estimation, quoFEM is set up to get within a 0.01 error percentage and the goal would get the error as close to 0 as possible so the error function used here is the simulated output subtracted by experimental result divided by experimental result. In the following sections, stiffness, max strength, and displacement capacity error functions will be calculated in tables for best values resulting from sensitivity analysis or parameter estimation results in quoFEM. The error function for both the sensitivity analysis and parameter estimation is simulated/measured.

5.3 Model Parameter Calibration

The shear retention factor was calibrated first, as preliminary analyses demonstrated that this value determines maximum strength and the accuracy with which the measured response envelope is simulated. Error is maximum strength was used to calibrate the shear retention factor. Preliminary analyses indicated that a shear retention factor in excess of 0.2 commonly resulted in convergence problems as well as simulated response histories with excessive strength. Thus, the shear retention factor was limited to 0.01 to 0.15 for the parameter estimation analyses.

5.3.1 Shear Retention Factor Calibration

Table 5 1 *Shear Retention Factor Calibration Results*

Author	ID	Shear Retention Factor	Error	Failure Mode
Dazio	WSH1	0.058	0.0014	BR
Dazio	WSH3	0.046	0.0004	BR
Wallace	RW1	0.034	0.008	BR
Wallace	RW2	0.06	0.002	CB
Liu	W1	0.01	0.002	CB
Liu	W2	0.022	0.0016	BR
Lu	C1	0.039	0.01	BR
Lu	C2	0.037	0.004	BR
Lu	C3	0.039	0.004	BR
Tran	S38	0.06	0.001	CB
Oh	WR20	0.056	0.002	CB
Hube	W8	0.14[1]	0.123	CB
Hube	W9	0.136[1]	0.0422	CB
Zhang	SW7	0.024	0.0037	CB
Zhang	SW9	0.03	0.0021	CB
Shegay	C10	0.107[1]	0.0022	CB
	Average	0.056	0.013	
	COV %	67.09	230.77	

1-Defined as an outlier

The average shear retention factor was found to be 0.056 with a COV of 67.1% and average error of 0.013. Twelve of the 16 walls had shear retention factors ranging from 0.02 and 0.06. The Hube walls both required relative high values to get close to best match of max strength and even then, those two walls showed the highest error. It is evident that the Hube walls are not sensitive to the shear retention factor like the other walls. Shegay also showed massive understrength for the Hube wall when simulating a response [18]. The Liu walls posted the lowest shear retention factors and even though the low error suggests that the walls are sensitive to shear retention factor in regards to max strength, it is unknown why these walls are exhibiting higher simulation strength with higher values of the shear retention factor. Other studies that use these walls Lowes [10], Pugh [17], and Shegay [21] were able to predict max strength accurately.

A shear retention factor of 0.056 was used for all models for all subsequent analyses.

5.3.2 Steel Rupture Strain Ratio and Crushing Energy Ratio Calibration

The steel rupture strain and confined concrete crushing energy ratios determine onset of significant strength loss for walls exhibiting steel-controlled buckling rupture (BR) failure and concrete controlled crushing-buckling (CB) failure, respectively. As discussed in the Chapter 3, Marafi [10] recommends a steel rupture strain ratio of 0.25 and a ratio of unconfined crushing energy to confined crushing energy of 2.0 for use with fiber-type beam-column elements. These values were used at the starting values for the quoFEM parameter estimation analyses, with walls exhibiting a BR failure used to calibrate the steel rupture strain ratio and walls exhibiting a CB failure used to calibrate the crushing energy ratio. Other important inputs of the parameter estimation include max number of simulations allowed in the estimation and convergence tolerance which means when the error is below this value the parameter estimation is completed.

Each quoFEM run on the TACC stampede supercomputer has a maximum runtime of 48 hours and if the job takes longer than this, it will be terminated along with any results. Preliminary analyses resulted in maximum runtimes, for individual walls in the calibration dataset of approximately five (5) hours. Thus, parameter estimation runs were batched with ten walls each and jobs submitted in parallel; it should be noted that if the run time for one of these “batched” jobs exceeded the 48-hour limit, only the data for the final wall specimen in the dataset were lost.

Figures 5.1 and 5.2 show the error value for sequential analyses in the quoFEM parameter estimation analysis for two walls each exhibiting BR and CB failure modes; note that individual data points are numbered to identify their place in the analysis sequence. These data show the optimization function predicting the minimal error by taking parameter values on either side of the starting value to determine what will increase the error and what will decrease the error, based on those results, it will continue to do this until the error falls below the convergence tolerance or the max number of simulations is reached. These data show also that the optimization continues until the error is less than 0.01 and start running parallel simulations of a +/- value of the parameter to hone in on the expected value. RW1 and RW2 exhibit this well. W9 shows in uptick in error at a crushing energy ratio of around 2.1. This is common among the walls as at certain values the wall will fail due to a convergence error causing it to fail early than expected. The parameter estimation can overcome this since it is not gradient based and can narrow down on either side of the expected value so if a simulation does fail due to convergence, it does not have a big impact on the next step of the parameter estimation. All the parameter estimation graphs can be found in appendix G.

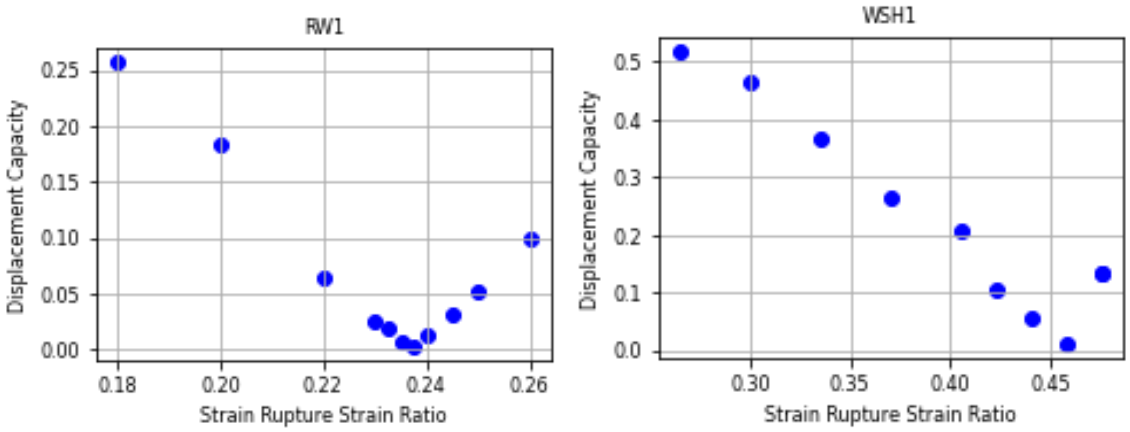

Figure 5.1 *Parameter Estimation Results for RW1 and WSH1*

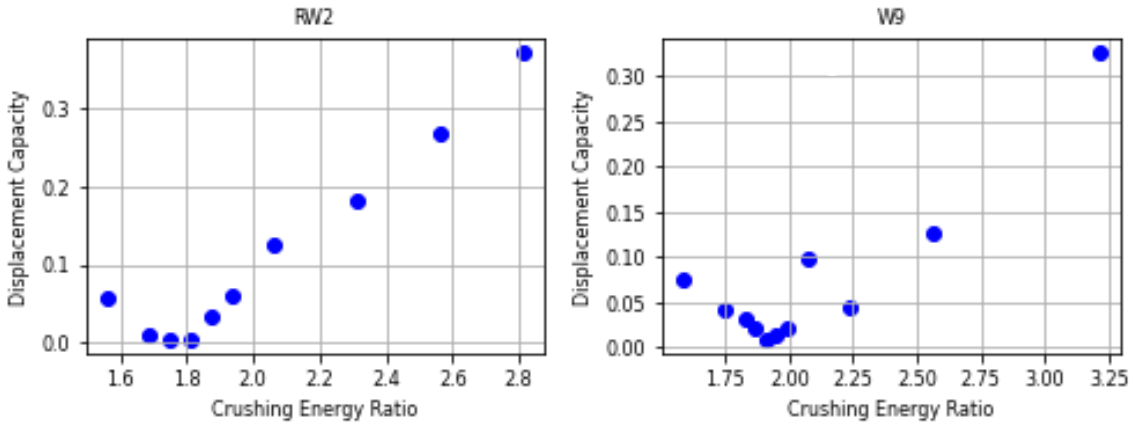

Figure 5.2 *Parameter Estimation Results for RW2 and W9*

Table 2.2 presents the results of the parameter estimation analyses for each wall. The data in Table 2.2 show that 12 of 16 analyses converged; exceptions were WSH1 and W2 (BR failures) and C10 and W8 (CB failures). Of these four walls, WSH1, W2, and C10 still showed in table 5.2 that they were sensitive to the parameters but failed to localize the parameter to a single value that fell below the convergence tolerance. Based on this it can be suggested that the parameter estimation analysis likely would have converged if there were more than 48 hours allotted to each of these walls. Table 5.2 also show that the drift capacity of wall specimen W8 was not sensitive to the crushing energy. This may have something to do with the fact that it is significantly understrength and that it is unable to represent the experimental wall with the deformation capacity and failure mechanism as well.

Table 5 2 *Steel Rupture Strain Ratio and Crushing Energy Ratio Calibration Results*

ID	Steel Rupture Strain Ratio	Error	ID	Crushing Energy Ratio	Error
WSH1	0.46[1]	0.012	**RW2**	1.81	0.004
WSH3	0.32	0.009	**S38**	2.56	0.009
RW1	0.24	0.003	**WR20**	3.1	0.01
W2	0.15	0.03	**W1**	1.93	0.006
C1	0.26	0.005	**W8**	3[1]	0.97
C2	0.295	0.006	**W9**	1.91	0.01
C3	0.29	0.001	**C10**	6.4[1]	0.017
			SW7	2.05	0.008
			SW9	1.35	0.002
Avg	0.29	0.01		2.56	0.01
COV %	32.59	103.71		64.74	55.26

5.3.3 Simulation Results of Calibration set with Calibrated data

The average values of the model parameters presented above and repeated here:

- Shear retention factor = 0.056
- Steel rupture strain ratio = 0.29
- Concrete confined concrete crushing energy ratio = 2.6

were used to simulate the response of all of the walls in the calibration data set.

Table 1.3 lists measured and simulated response quantities of interest for these walls and provides statistics for the entire dataset. Quantities in Table 5.3 are determined as follows:

- Stiffness: Simulation of initial stiffness is evaluated at the point in which the extreme fibers of the concrete reaches -0.003 strain in the simulation and the displacement at that point is compared to the displacement in the measured at which it reaches the same load.
- Strength: Simulation of strength is the max strength that the wall exhibits in the experimental and in the simulation.
- Deformation capacity: Simulation of deformation capacity is at the point in which the wall exhibits a 20% or more strength loss.
- Failure Mode: simulation of failure mechanism of the model. This is determined by a compression buckling failure or a bar rupture failure. If it is a bar rupture failure, the steel stress will go to zero in tension after the strain reaches the steel rupture strain and if is a compression buckling failure, the concrete and steel stress will go to zero in compression after exceeding the crushing strain of the concrete.

Table 5 3 *Simulated Results of Calibration Set*

		Stiffness			Strength			Deformation			Failure Mode	
Author	**Wall ID**	**Exp. Δy**	**Sim. Δy**	**Error**	**Exp. Mb/Mn**	**Sim. Mb/Mn**	**Error**	**Exp. Δ_u**	**Sim. Δ_u**	**Error**	**Exp.**	**Sim.**
		--	--	--	--	--	--	%	%	--	--	--
Dazio	**WSH1**	0.39	0.65	1.67	1.03	1.01	0.98	1.04	0.69	0.66	BR	BR
Dazio	**WSH3**	0.56	0.8	1.43	1.1	1.1	1	2.03	1.83	0.9	BR	CB
Wallace	**RW1**	0.58	0.89	1.53	0.99	1.12	1.13	2.1	2.57	1.22	BR	CB
Liu	**W2**	0.8	0.98	1.23	0.99	1.27	1.28	2.87	4.72	1.64	BR	CB
Lu	**C1**	0.62	1.35	2.18	0.98	1.34	1.37	2.46	2.59	1.05	BR	BR
Lu	**C2**	0.11	0.66	6	1.08	1.12	1.04	1.23	1.39	1.13	BR	BR
Lu	**C3**	0.15	0.59	3.93	1.05	1.11	1.06	0.82	1.09	1.33	BR	BR
Wallace	**RW2**	0.79	0.79	1	1.14	1.18	1.04	2.25	2.29	1.02	CB	BR
Tran	**S38**	0.46	0.78	1.7	1.32	1.3	0.98	3.1	3.34	1.08	CB	CB
Oh	**WR20**	0.19	0.46	2.42	1.04	1.06	1.02	2.45	1.65	0.67	CB	CB
Liu	**W1**	0.95	0.87	0.92	1.01	1.2	1.19	3.05	2.78	0.91	CB	CB
Hube	**W8**	0.5	0.83	1.66	1.48	1.25	0.84	2.71	3.7	1.37	CB	CB
Hube	**W9**	0.37	0.57	1.54	1.184	1.25	1.06	2.68	4.08	1.52	CB	BR
Zhang	**SW7**	0.34	0.51	1.5	1.12	1.3	1.16	2	3.15	1.58	CB	BR
Zhang	**SW9**	0.27	0.3	1.11	1.37	1.72	1.26	2	4.01	2.01	CB	--
Shegay	**C10**	0.15	0.21	1.4	1.22	1.15	0.94	0.85	0.61	0.72	CB	CB
Average		0.45	0.7	1.95	1.13	1.22	1.08	2.1	2.53	1.18		
COV %		56.17	39.14	66.33	13.14	13.49	12.79	35.98	49.6	32.46		

Error = Simulated/Experimental

The data in Table 5.3 evident that wall stiffness, strength and deformation capacity are not accurately predicted when average values of shear retention factor, steel rupture strain ratio, and confined crushing energy ratio are used:

Simulation of initial stiffness: This inaccuracy in stiffness is attributed to shrinkage cracking of concrete and bond-slip between concrete and vertical reinforcing steel; neither of which are included in the simulations. In the laboratory and field, shrinkage cracking of concrete occurs during the curing process as concrete shrinkage is restrained by reinforcing steel. This cracking is likely greater in laboratory test specimens that field specimens, where concrete sections are thinner and surface area to volume is greater.

Simulation of maximum strength: The results of this study are only slightly higher. Error in simulated strength may be attributed to myriad factors including aspect of wall construction and loading that are not accurately represented in the model as well as model inaccuracy. Here is should be noted also that the error in simulated wall strength is correlated with the error in simulated deformation capacity ($R^2 = 0.19$). Thus, some of the error in simulated strength can be attributed to the fact that i) the walls exhibit hardening in the post yield regime and ii) where wall deformation capacity is overpredicted, strength is also overpredicted due to this hardening (figure below shows this)

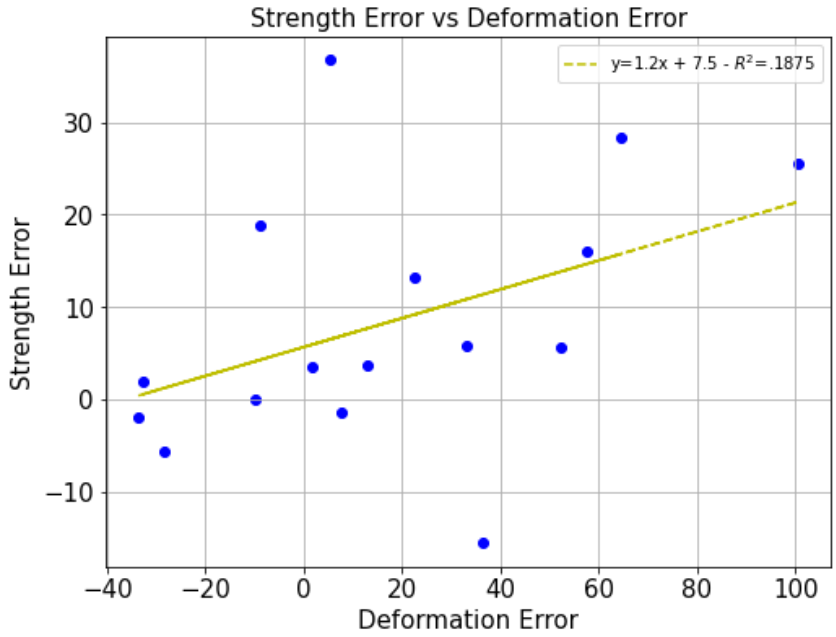

Figure 5.3 *Strength vs Deformation Error Comparison*

Simulation of deformation capacity: Simulation of deformation capacity was over predicted by 18% for the calibration set with a COV percentage of 32.5%. This is a high error and is evident the calibrated values did not represent the deformation capacity correctly. Looking back at the calibrated results for the quoFEM simulations, there is a high COV for all three parameters. This amount of variation is a large factor into why there was such a difference in the calibration set.

Simulation of failure mode: Less than two thirds of the calibration set failed in accordance with the experimental counterpart. This is likely due to the high error and variation of the deformation

capacity. Where these walls were calibrated due to how they failed in the lab, the calibrated parameter opposite of its failure mode ended up being the driving factor for many of the walls.

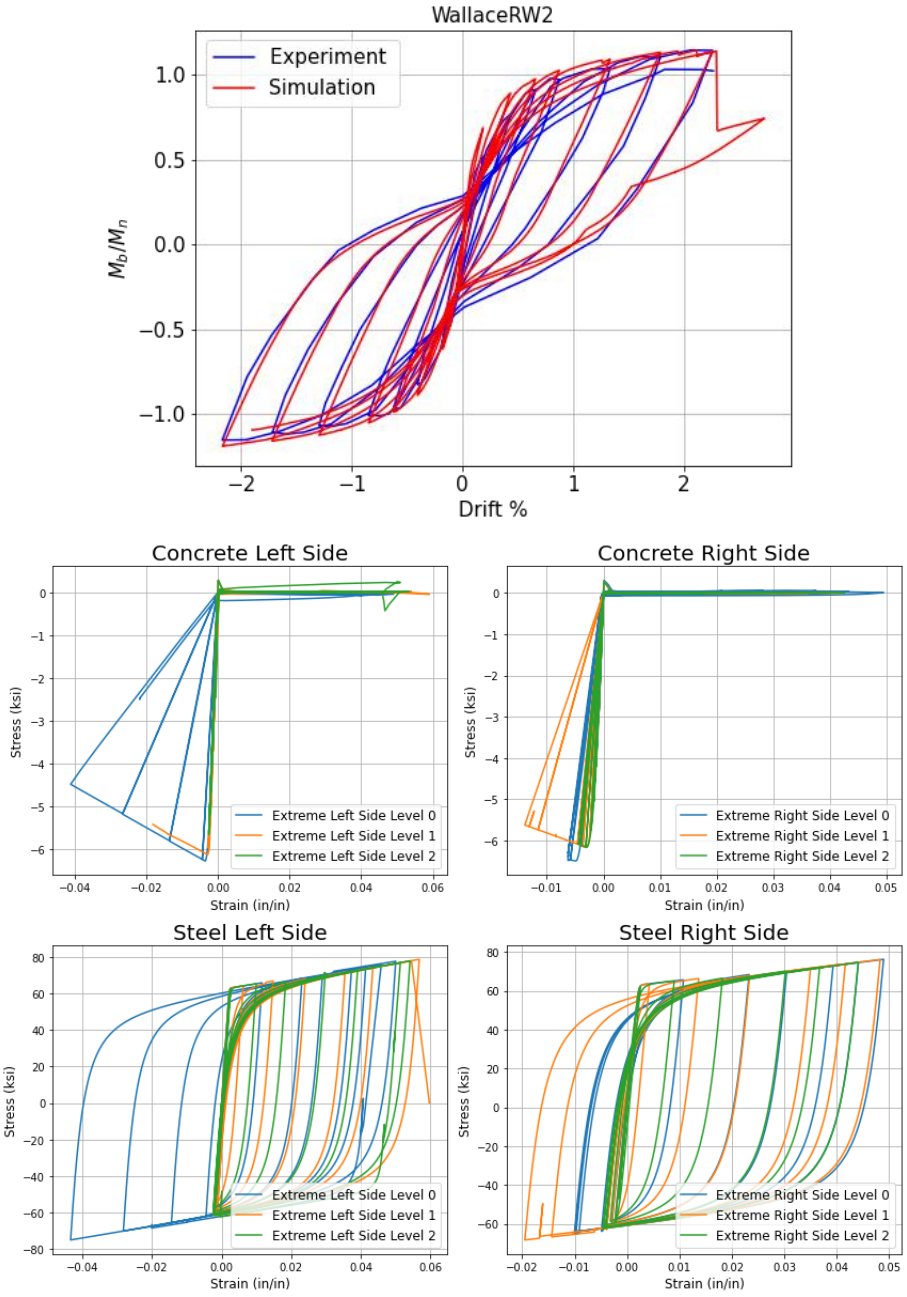

Figure 5.4 *RW2 simulated response and stress vs strain graphs of boundary region for the concrete and vertical steel.*

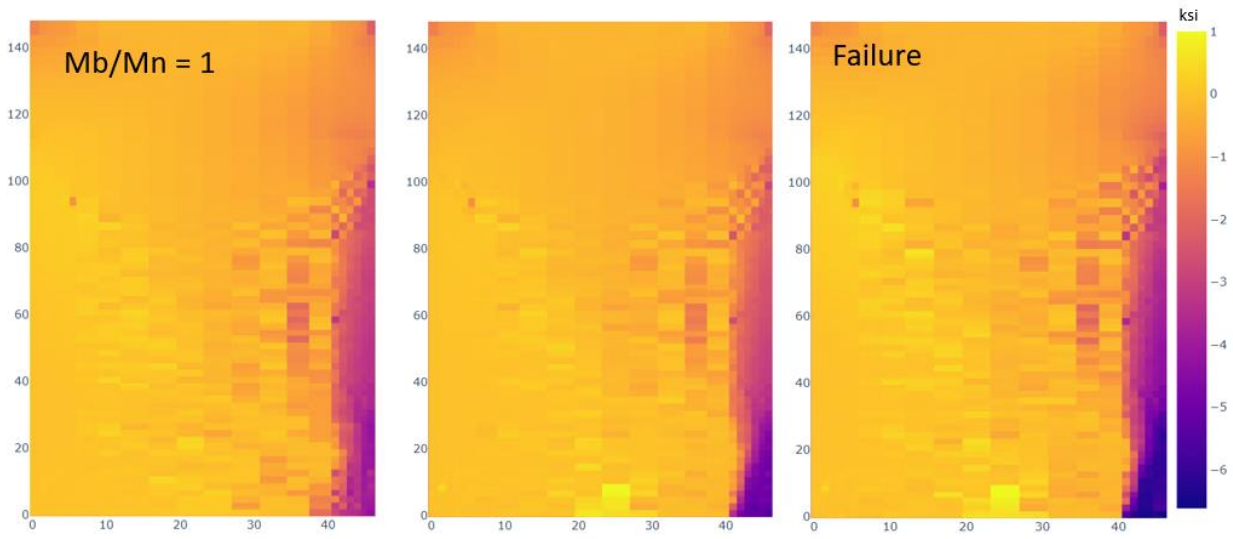

Figure 5.5 *Vertical stress profile of wall for Mb/Mn = 1, middle of simulation, and right before failure. Note that wall dimensions are in inches*

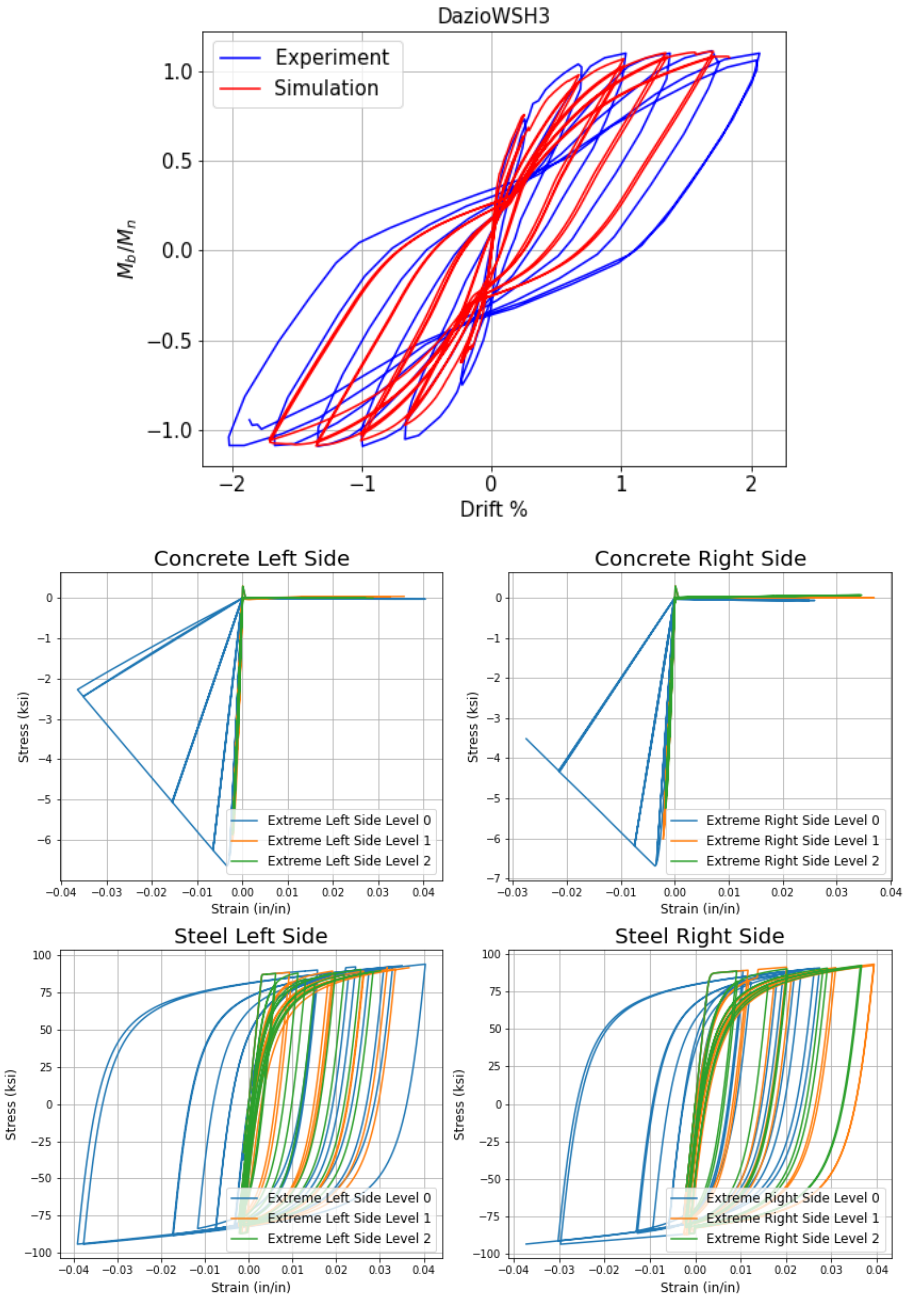

Figure 5.6 *WSH3 simulated response and stress vs strain graphs of boundary region for the concrete and vertical steel.*

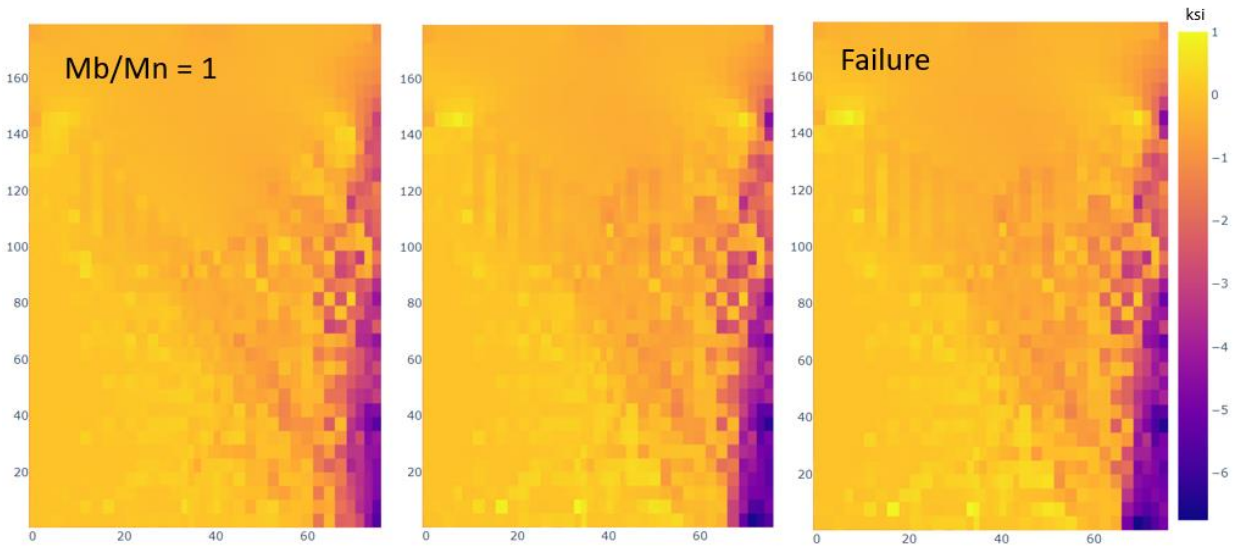

Figure 5.7 *Vertical stress profile of wall for Mb/Mn = 1, middle of simulation, and right before failure. Note that wall dimensions are in inches*

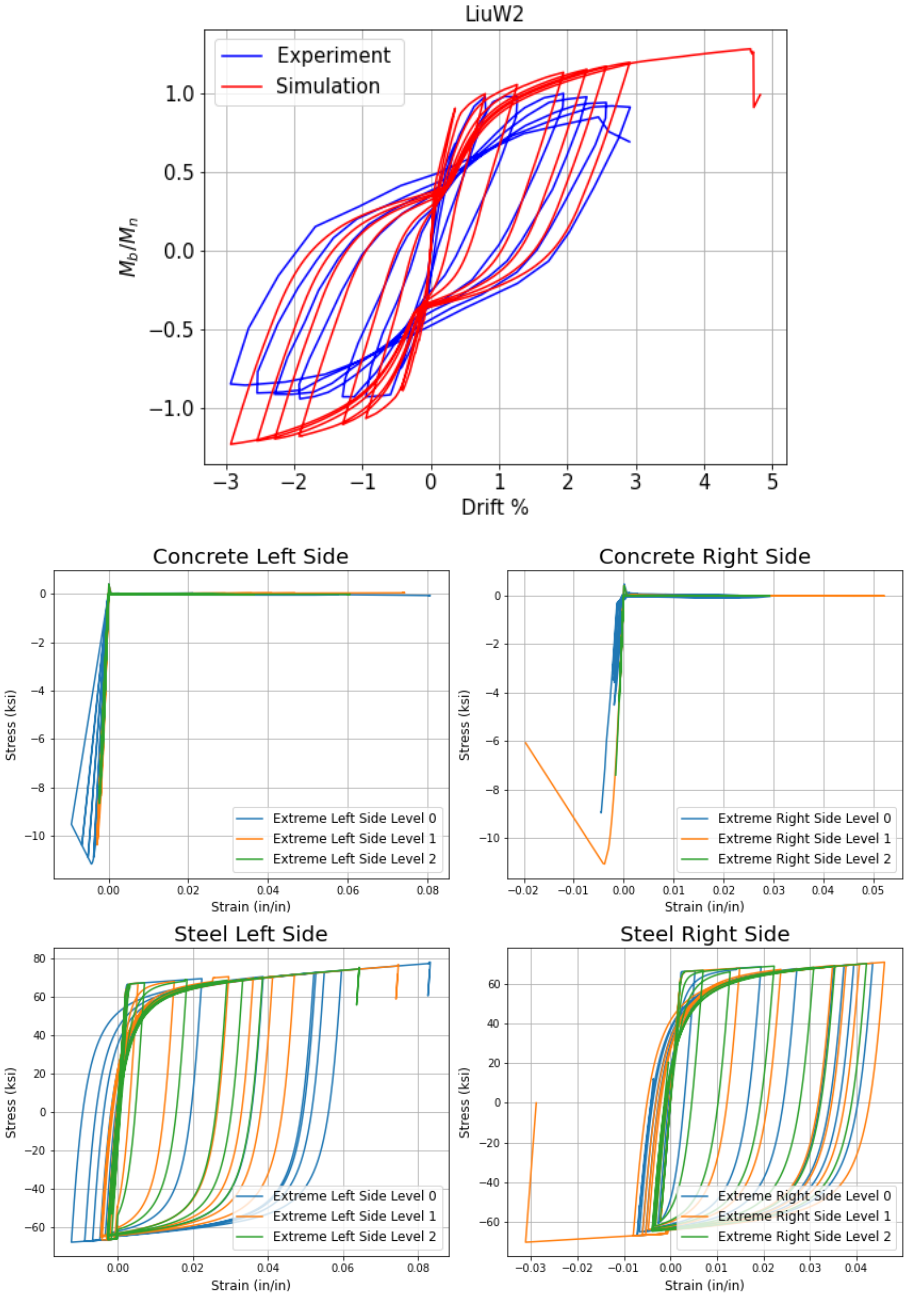

Figure 5.8 *W2 simulated response and stress vs strain graphs of boundary region for the concrete and vertical steel.*

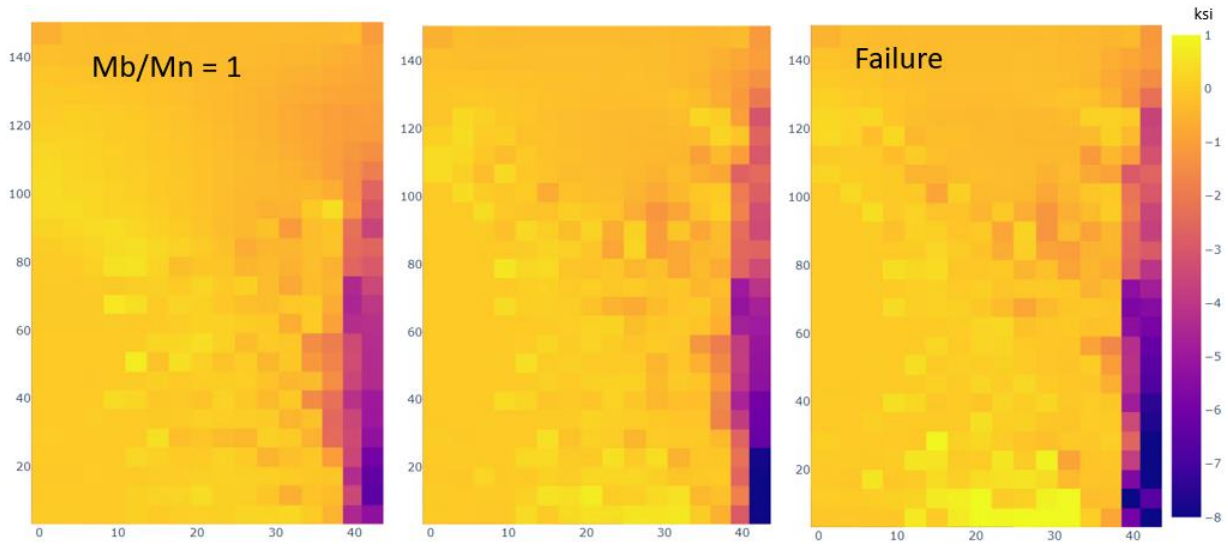

Figure 5.9 *Vertical stress profile of wall for Mb/Mn = 1, middle of simulation, and right before failure. Note that wall dimensions are in inches*

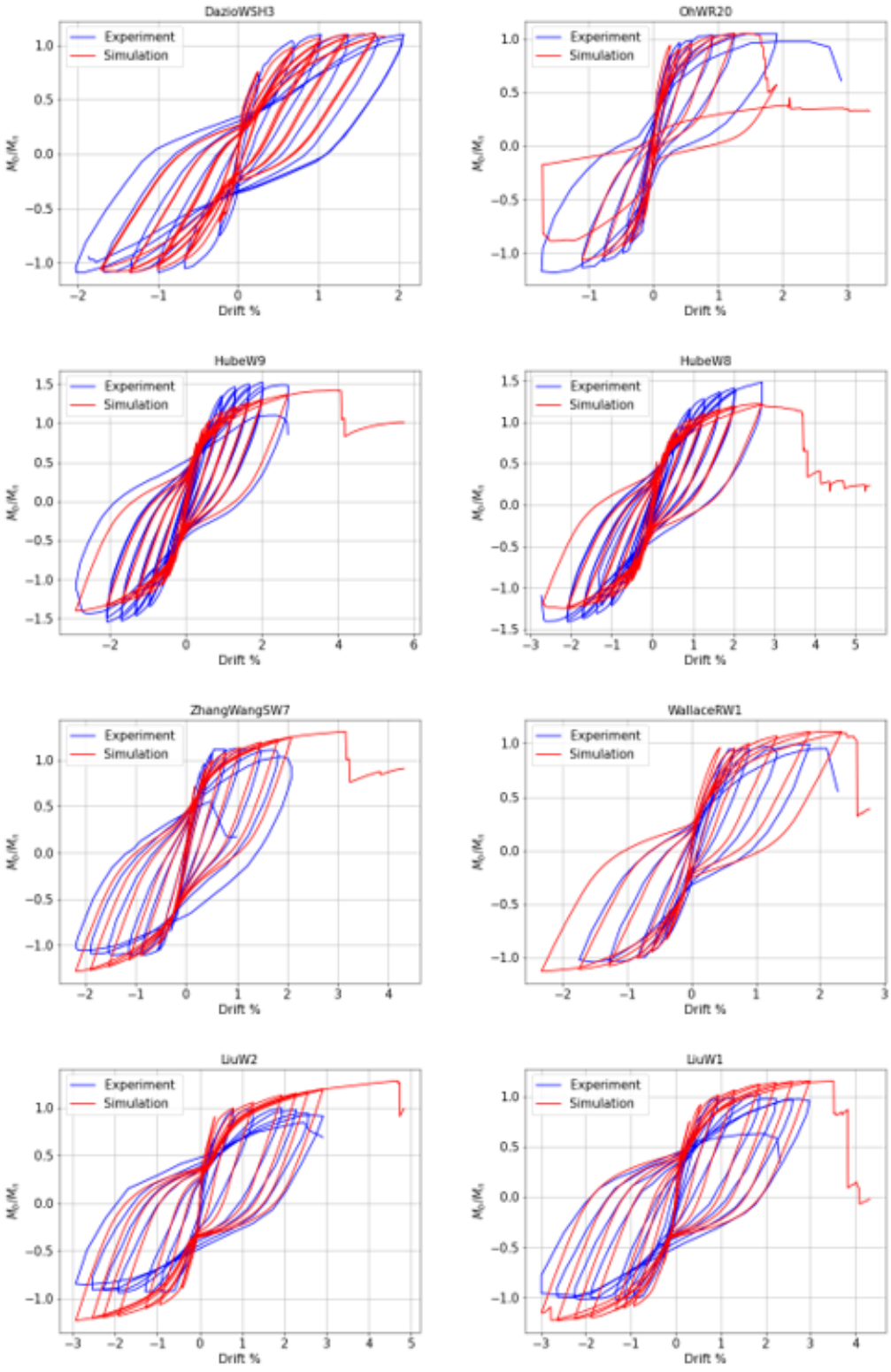

Figure 5.10 *Calibration Walls that Exhibited CB Failures*

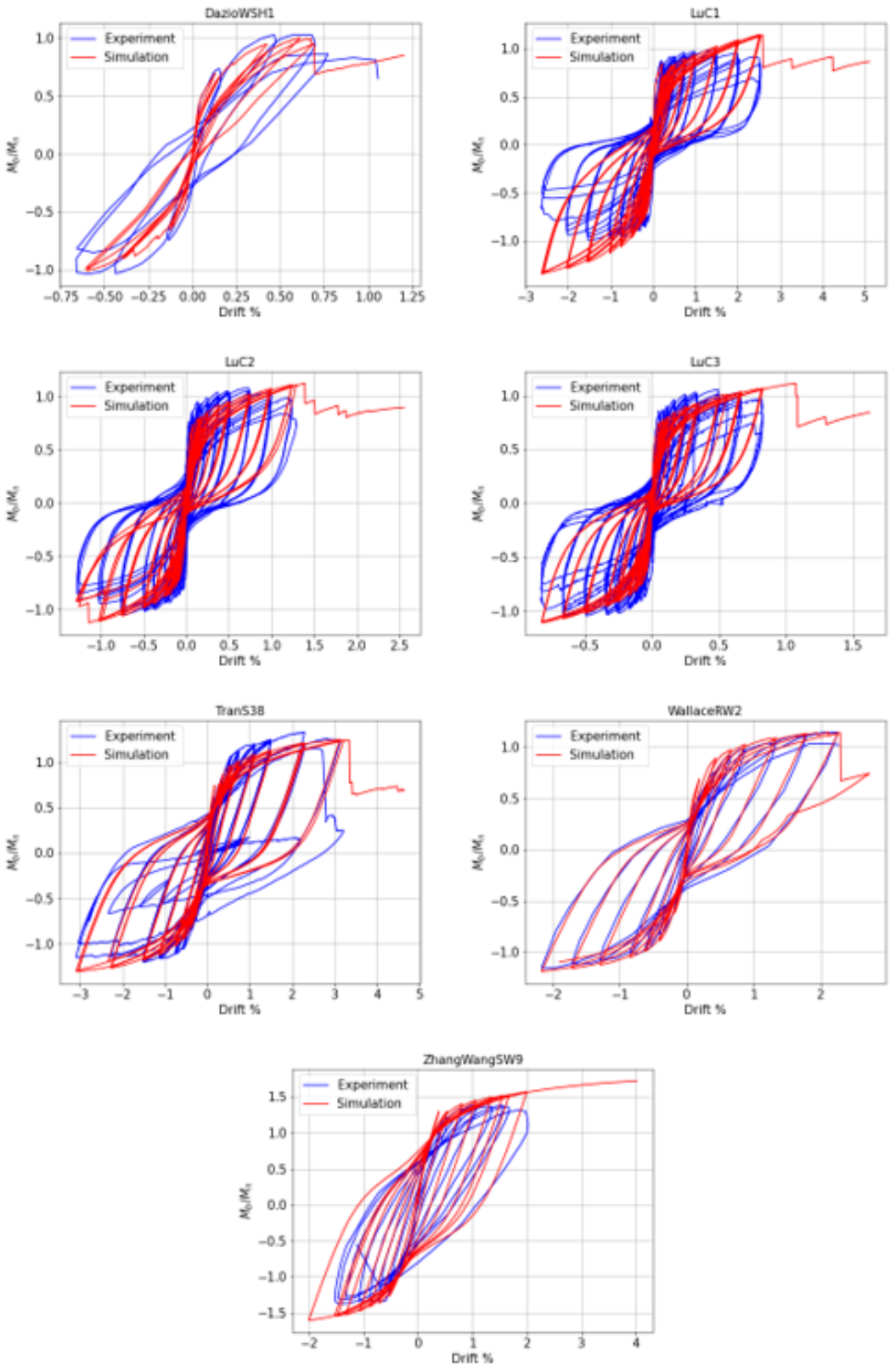

Figure 5.11 *Walls That Exhibited BR Failures*

5.4 Simulation Results of Validation set with Calibrated data

The validation set was ran using the preferred values from the calibrated set. This is using the shear retention factor of 0.056, a steel rupture strain reduction factor of 0.29, and a crushing energy ratio of 2.56. The results are seen below in table 5.2.

Table 5 4 *Simulation Results for Validation Set*

		Stiffness			Strength			Deformation			Failure Mode	
Author	**Wall ID**	**Exp. Δy**	**Sim. Δy**	**Error**	**Exp. Mb/Mn**	**Sim. Mb/Mn**	**Error**	**Exp. Δ_u**	**Sim. Δ_u**	**Error**	**Exp.**	**Sim.**
		--	**--**	--	**--**	**--**	--	**%**	**%**	--	--	--
Dazio	**WSH2**	0.63	0.79	1.25	1.13	1.15	1.02	1.42	0.98	0.69	BR	BR
Dazio	**WSH5**	0.28	0.65	2.32	1.1	1.09	0.99	1.35	0.85	0.63	BR	CB
Shegay	**A10**	0.17	0.21	1.24	1.24	1.16	0.94	0.98	0.58	0.59	BR	CB
Lu	**C4**	0.21	0.32	1.52	0.78	1.11	1.42	1.47	1.85	1.26	BR	BR
Lu	**C5**	0.18	0.85	4.72	1.19	1.41	1.18	1.94	2.26	1.16	BR	CB
Lu	**C6**	0.24	0.77	3.21	1.03	1.09	1.06	1.2	1.22	1.02	BR	BR
Segura	**WP6**	0.11	0.21	1.91	0.94	1.16	1.23	0.9	0.46	0.51	BR	BR
Segura	**WP7**	0.25	0.18	0.72	1.06	1.12	1.06	0.96	0.54	0.56	BR	CB
Dazio	**WSH6**	0.37	0.57	1.54	1.18	1.25	1.06	2.07	1.81	0.87	CB	BR
Oh	**WR10**	0.36	0.56	1.56	1.09	1.26	1.16	2.82	1.74	0.62	CB	CB
Shegay	**A14**	0.16	0.18	1.13	1.2	1.2	1	0.79	0.45	0.57	CB	CB
Shegay	**A20**	0.08	0.12	1.5	1.44	1.38	0.96	0.65	0.44	0.68	CB	CB
Tran	**S63**	0.61	0.54	0.89	1.21	1.15	0.95	3	1.31	0.44	CB	CB
Zhang	**SW8**	0.16	0.36	2.25	1.53	1.59	1.04	1.5	2.38	1.59	CB	BR
Hube	**W5**	0.17	0.36	2.12	1.92	1.25	0.65	1.1	1.91	1.74	CB	CB
Hube	**W7**	0.49	0.77	1.57	1.27	1.17	0.92	2.3	3.1	1.35	CB	CB
Lowes	**PW4**	0.41	0.29	0.71	1.53	1.86	1.22	0.6	0.82	1.37	CB	CB
Average		0.28	0.47	1.84	1.21	1.22	1.04	1.53	1.37	0.89		
COV		60.55	54.25	53.38	21.51	11.14	15.92	46.48	59.58	45.96		

Table 5.2 shows the simulated results for the validation set using the preferred values from the calibration set. As expected, stiffness, strength, deformation, and failure mode were not predicted accurately just like the calibration set. The average errors were similar to that of the calibration set with the stiffness error in the validation set being 90% compared to 96% of the calibration, the strength error being 11.4% compared to the 11.5% of the calibration, the deformation error being 37.2% compared to 31.7% of the calibration, and the failure mode prediction being 65% compared to 63% of the calibration. In the calibration set, C10 saw a drift capacity much lower than the simulation (error of -28%) the estimated crushing energy ratio for this wall was 6.4. As shown in the validation set, all the other Shegay walls drift capacities were similar, A10 at -41%, A14 at -43%, and A20 at -32%. Only one wall came within 10% error of drift capacity and that was Lu C6 which also had the correct failure mode.

5.5 Conclusion

In this chapter, the shear retention factor, steel rupture strain reduction factor, and crushing energy were calibrated and the preferred values were run in the calibration set and validation set. For both sets the deformation capacity and failure mode were poorly represented. The strength was close in simulated compared to measured, but for all measures, the variation was very high. It is evident that the model did not do a good job modeling multiple reinforced concrete walls to accurately simulate strength, deformation capacity, and failure mode. Future work will need to be done to understand how to improve this model.

Chapter 6. Conclusion and Future Works

The research presented in this thesis employed data from the experimental database assembled by Shegay [21] of laboratory tests of planar reinforced concrete walls subjected to constant axial and quasi-static cyclic lateral loading as well as the quoFEM software tool developed by the SimCenter [18] and computing resources provided by DesignSafe to evaluate three and calibrate one of the layered shell element formulations available in the OpenSees platform as well as the planar concrete constitutive model developed by Lu [8] for use with these models.

The primary objectives of the study were:

1. Develop a modeling technique that utilizes the layered shell elements, planar concrete constitutive model as well as other commonly used element formulations and material constitutive models concrete to simulate the nonlinear response of planar and nonplanar walls subjected multi-dimensional loading.
2. Create and publish a Jupyter notebook based computational framework for building wall models, executing OpenSees simulations, visualizing simulation results that utilizes NHERI DesignSafe computing resources as well as NHERI SimCenter computational tools.
3. Use the computational framework, a published data set [Shegay], and SimCenter and DesignSafe software and computational resources to evaluate the shell-element models for simulating wall response as well as to calibrate the wall model to provide accurate simulation of stiffness, strength, deformation capacity, failure mode, and cyclic response for a large set of test specimens with a range of design and load characteristics.
4. Provide recommendations and calibrated model parameters to advance modeling of flexure-controlled reinforced concrete walls subjected to constant axial and cyclic lateral loading.
5. Evaluate the functionality of DesignSafe and SimCenter computational resources and tools and provide feedback to drive advancement of these resources.

6.1 Research Summary

6.1.1 Model Development and Evaluation

Using the experimental database assembled by Shegay et al [21], modeling recommendations were developed for planar concrete walls, that utilize the material models and element formulation developed by others and incorporated in the OpenSees platform. The three shell element formulations available in the OpenSees platform (DKGQ and NLDKGQ developed by Lu [8] and MITC4 developed by Dvorkin and Bathe[5] and implemented by Love) were evaluated; DKGQ was found to be the most stable and least prone artificial strength gain due to the combination of plane membrane element and a plate bending element. This element formulation was used in conjunction with the planar concrete constitutive model, planestressusermaterial, developed and implemented by Liu as well as the OpenSees Steel01 model. Constitutive model parameters, specifically the concrete shear retention factor and confined concrete crushing energy used with the concrete constitutive model and the steel strain capacity used with the reinforcing steel model, were calibrated to provide accurate simulation of response for approximately 33 planar wall laboratory test specimens included in the Shegay data set.

It was possible to calibrate constitutive model parameters for approximately 10 of 16 walls to achieve accurate simulation of wall strength, and 12 of 16 walls to achieve accurate simulation of deformation capacity and failure mode. Only 1 wall did not fail in the correct failure mode when calibrating deformation capacity and 7 of the 16 walls it was not possible to calibrate the model to achieve accurate simulation of failure mode. Previous efforts by researchers at the UW, employing fiber beam-column elements [17] and continuum models [10] have achieved much better accuracy with respect to simulation of strength, deformation capacity and failure mode.

The calibration set produced a shear retention factor of 0.056, a crushing energy ratio of 2.56, and a steel rupture strain reduction factor of 0.29 from the sensitivity analysis and parameter estimation on quoFEM. These values resulted in overstrength of the model by an average of 8% for the calibration set and 4% for the validation set. The deformation capacity was also over predicted for the calibration set by an average of and underpredicted in the validation set by an

average of 12%. Overall, only 2/3rds of the walls for the calibration and validation set failed in accordance to their correct failure mode.

6.1.2 SimCenter Software, DesignSafe Resources and Jupyter Notebooks

Integral to the research project was use of Jupyter notebooks, the quoFEM software developed by the NHERI SimCenter to support sensitivity analysis and model calibration, and NHERI DesignSafe computing and data-storage resources. A series or Jupyter notebooks was created to automate creation, execution and evaluation of OpenSees models of each wall test specimen included in the study. These notebooks are also used on the JupyterHub on DesignSafe were they can access HPC resources and direct access to archived folders from quoFEM jobs. During the course of the project, hundreds of OpenSees models were created for each wall to investigate different element formulations and levels of mesh refinement as well as to calibrate model parameters to achieve accurate simulation of observed response. These notebooks are published in GitHub and the DesignSafe DataDepot.

The SimCenter quoFEM was downloaded as an application on windows and used for sensitivity analysis for the shear retention factor which takes a range for the parameter input and a total number of simulations and runs a sweep of simulations across that range and outputs a corresponding error against the parameter value. The gradient based parameter estimation was used originally to predict the value of a parameter but this version did not work as when it calculated the gradient, it took a minimal step forward of the parameter and this caused a slight error as the output of the parameter estimation was inaccurate with such a small step so a non-gradient based parameter estimation was created which takes a starting value and then calculates errors on either side of this value to determine in which direction the error is being minimized. This version was used to calibrate the crushing energy ratio and steel rupture strain reduction factor.

Using a set of walls called the calibration set, the preferred values for the shear retention factor, steel rupture strain ratio, and the crushing energy ratio that were averaged across the calibration set from sensitivity studies and parameter estimations were: 0.056 for the shear retention factor, 0.29 for the steel rupture strain ratio, and 2.56 for the crushing energy ratio. Using these values for the entire calibration set gave an error of 98% for the stiffness, 11% for the strength capacity,

and 38% for the deformation capacity. Strength capacity was the smallest and effected by the shear retention factor. The deformation capacity was affected by the steel rupture strain ratio for walls that exhibit a bar rupture failure and crushing energy ratio for walls that exhibit a compression buckling failure. Using these values for the validation set showed very similar results in the errors. The validation set was run with a parameter estimation and the outcome gave the same average for the steel rupture strain ratio of 0.29 but many of the walls that exhibit compression buckling were unable to calibrate a value for the crushing energy that met the convergence tolerance.

6.2 Future Work

Work that can be done to further this research are:

Investigate correlation between optimal model parameters (i.e. shear retention, crushing energy and buckling strain factor) and wall design parameters

Using the values that were found for in the parameter estimations and comparing them with multiple design parameters to see if there are any correlations with how a wall is responding based on how it is designed with the shear retention factor, steel rupture strain ratio, and crushing energy ratio.

Further use of QuoFEM and Use of OpenSeesPy:

As the gradient free parameter estimation was just created and with the possibility of increased time used on an HPC systems, the use of quoFEM can be utilized more when running a parameter estimation on a sweep of walls at once to determine a minimum error over multiple parameters in a single run. Also, OpenSeesPy has been developed more and could be used to minimize the workflows in this research.

Effect on Non-Planar walls:

Most walls in real structures are non-planar with three-dimensional configurations. The layered shell element model considered in this study is ideal for modeling non-planar walls as it can simulate the nonlinear strain profiles that develop in nonplanar walls (cite Kamal Ahmed) as well as simulate in- and out-of-plane response. Thus, there is an opportunity to repeat a study similar

the study presented here that employs walls with nonplanar configurations such as I-, T-, L- and C-shaped walls.

References

ACI Committee 318, and American Concrete Institute. 2011. Building Code Requirements for Structural Concrete (ACI 318-11) and Commentary. Farmington Hills, MI: American Concrete Institute.

Adams, B.M., Bohnhoff, W.J., Dalbey, K.R., Ebeida, M.S., Eddy, J.P., Eldred, M.S., Hooper, R.W., Hough, P.D., Hu, K.T., Jakeman, J.D., Khalil, M., Maupin, K.A., Monschke, J.A., Ridgway, E.M., Rushdi, A.A., Seidl, D.T., Stephens, J.A., Swiler, L.P., and Winokur, J.G., "Dakota, A Multilevel Parallel Object-Oriented Framework for Design Optimization, Parameter Estimation, Uncertainty Quantification, and Sensitivity Analysis: Version 6.15 User's Manual," Sandia Technical Report SAND2020-12495, November 2021.

Berry, Matt, Dawn Lehman, and Laura Lowes. 2008. "Lumped-Plasticity Models for Performance Simulation of Bridge Columns." ACI Structural Journal 105 (3). doi:10.14359/19786.

Dazio, Alessandro, Katrin Beyer, and Hugo Bachmann. 2009. "Quasi-Static Cyclic Tests and Plastic Hinge Analysis of RC Structural Walls." Engineering Structures 31 (7): 1556–71. doi:10.1016/j.engstruct.2009.02.018.

Dvorkin,Bathe, A continuum mechanics based four node shell element for general nonlinear analysis, Eng.Comput.,1,77-88,1984 (shell element chapter 3)

Henry, Richard S. et al. "Lightly reinforced and precast concrete walls: Recent research and design recommendations." (2016). (Lu)

Liu, H. 2004. "Effect of Concrete Strength on the Response of Ductile Shear Walls." MS thesis, Montreal, QB: Dept. of Civil Engineering and Applied Mechanics, McGill University.

Lu XZ, Xie LL, Guan H, Huang YL, Lu X, A shear wall element for nonlinear seismic analysis of super-tall buildings using OpenSees, Finite Elements in Analysis & Design, 2015, 98: 14-25.

M.A. Hube, A. Marihuén, J.C. de la Llera, B. Stojadinovic, Seismic behavior of slender reinforced concrete walls, Engineering Structures, Volume 80, 2014, Pages 377-388, ISSN 0141-0296

Marafi, Nasser & Ahmed, Kamal & Lowes, Laura. (2019). Variability in Seismic Collapse Probabilities of Solid- and Coupled-Wall Buildings. Journal of Structural Engineering. 145. 10.1061/(ASCE)ST.1943-541X.0002311.

Martin, Joshua; Stanton, John; Mitra, Nilanjan; Lowes, Laura N. ACI Materials Journal; Farmington Hills Vol. 104, Iss. 6, (Nov/Dec 2007): 575-584.

McKenna, F. (1997) Object oriented finite element analysis: Frameworks for analysis algorithms and parallel computing. Ph.D. dissertation, University of California, Berkeley. (opensees)

NIST, 2013. “Recommendations for Seismic Design of Reinforced Concrete Wall Buildings Based on Studies of the 2010 Chile Earthquake,” NEHRP Consultants Joint Venture for the National Institute of Standards and Technology, Gaithersburg, MD, Tech. Rep. No. GCR 13-917-25.

Oh, Young-Hun, Sang Whan Han, and Li-Hyung Lee. 2002. “Effect of Boundary Element Details on the Seismic Deformation Capacity of Structural Walls.” Earthquake Engineering & Structural Dynamics 31 (8): 1583–1602. doi:10.1002/eqe.177.

Orakcal, Kutay, and John Wallace. 2006. “Flexural Modeling of Reinforced Concrete Walls - Experimental Verification.” ACI Structural Journal 103 (2). doi:10.14359/15177.

Palermo, Dan, and Frank J. Vecchio. 2007. “Simulation of Cyclically Loaded Concrete Structures Based on the Finite-Element Method.” Journal of Structural Engineering 133 (5): 728–38. doi:10.1061/(ASCE)0733-9445(2007)133:5(728).

Pugh, Josh. 2012. “Numerical Simulation of Walls and Seismic Design Recommendations for Walled Buildings.” Ph.D. dissertation, Seattle, WA: Dept. of Civil and Environmental Engineering, University of Washington.

Rathje, E., Dawson, C. Padgett, J.E., Pinelli, J.-P., Stanzione, D., Adair, A., Arduino, P., Brandenberg, S.J., Cockerill, T., Dey, C., Esteva, M., Haan, Jr., F.L., Hanlon, M., Kareem, A., Lowes, L., Mock, S., and Mosqueda, G. 2017. "DesignSafe: A New Cyberinfrastructure for Natural Hazards Engineering," ASCE Natural Hazards Review, doi:10.1061/(ASCE)NH.1527-6996.0000246.

Saatcioglu, Murat and Salim R. Razvi. "Strength and Ductility of Confined Concrete." *Journal of Structural Engineering-asce* 118 (1992): 1590-1607.

Segura, C. (2017). Seismic Performance Limitation of Slender Reinforced Concrete Structural Walls. *UCLA*. ProQuest ID: Segura_ucla_0031D_16051. Merritt ID: ark:/13030/m5004xp1.

Shegay, Alex & Motter, Christopher & Henry, Richard & Elwood, Kenneth & Lowes, Laura. (2018). Impact of Axial Load on the Seismic Response of Rectangular Walls. Journal of Structural Engineering. 188. 10.1061/(ASCE)ST.1943-541X.0002122. (Shegay)

The authors acknowledge the Texas Advanced Computing Center (TACC) at The University of Texas at Austin for providing HPC resources that have contributed to the research results reported within this paper. URL: http://www.tacc.utexas.edu

Tran, Thien Anh. 2012. "Experimental and Analytical Studies of Moderate Aspect Ratio Reinforced Concrete Structural Walls." Ph.D. dissertation, Los Angeles, CA: Dept. of Civil and Environmental Engineering, University of California, Los Angeles.

Thomas Kluyver, Benjamin Ragan-Kelley, Fernando Pérez, Brian Granger, Matthias Bussonnier, Jonathan Frederic, Kyle Kelley, Jessica Hamrick, Jason Grout, Sylvain Corlay, Paul Ivanov, Damián Avila, Safia Abdalla, Carol Willing, Jupyter Development Team. "Jupyter Notebooks – a publishing format for reproducible computational workflows "(1): 87-90. doi: 10.3233/978-1-61499-649-1-87

Wallace, John W., and John H. Thomsen IV. 1995. "Seismic Design of RC Structural Walls. Part II: Applications." Journal of Structural Engineering 121 (1): 88–101. doi:10.1061/(ASCE)0733-9445(1995)121:1(88). 157

Wong, P. S., F. J. Vecchio, and H. Trommels. 2013. Vector2 & formworks user's manual. Toronto, ON: Vector Analysis Group.

Zhang, Y. & Wang, Z.. (2000). Seismic behavior of reinforced concrete shear walls subjected to high axial loading. ACI Structural Journal. 97. 739-750.

Appendix A– Material and Wall Demands

Table C - 1 Material for Wall Set

Author	ID	Material								
		f'_c	$f_{y,be}$	$E_{s,be}$	$f_{u,be}$	$\epsilon_{u,be}$	$f_{y,v}$	$E_{s,v}$	$f_{u,v}$	$\epsilon_{u,v}$
		ksi	ksi	ksi	ksi	in/in	ksi	ksi	ksi	in/in
Dazio et al.	WSH1	6.53	79.38	29000	89.91	0.046	84.64	29000	87.12	0.023
Dazio et al.	WSH2	5.87	84.57	29000	108.40	0.077	70.33	29000	77.52	0.058
Dazio et al.	WSH3	5.69	87.16	29000	105.22	0.077	82.55	29000	101.55	0.073
Dazio et al.	WSH5	5.55	84.66	29000	103.61	0.079	75.26	29000	81.03	0.055
Dazio et al.	WSH6	6.61	83.54	29000	97.88	0.073	84.66	29000	103.61	0.079
Liu	W1	4.80	66.38	29000	91.41	0.180	67.35	29000	84.25	0.165
Liu	W2	10.25	66.38	29000	91.41	0.180	67.35	29000	84.25	0.165
Lowes et al.	PW4	4.27	67.10	29000	109.50	0.120	75.70	29000	77.00	0.055
Thomsen et al.	RW1	4.58	63.00	29000	93.00	0.100	65.00	29000	85.00	0.080
Thomsen et al.	RW2	4.93	63.00	29000	93.00	0.100	65.00	29000	85.00	0.080
Oh et al.	WR20	4.77	65.12	29000	89.49	0.176	47.72	29000	64.54	0.176
Oh et al.	WR10	5.05	65.12	29000	89.49	0.176	47.72	29000	64.54	0.176
Shegay et al.	C10	4.74	78.76	29000	98.34	0.160	73.53	29000	94.71	0.143
Shegay et al.	A10	4.74	78.76	29000	98.34	0.160	73.53	29000	94.71	0.143
Shegay et al.	A14	6.18	78.76	29000	98.34	0.160	73.53	29000	94.71	0.143
Shegay et al.	A20	6.34	78.76	29000	98.34	0.160	73.53	29000	94.71	0.143
Tran et al.	S38	6.83	68.40	29000	88.90	0.150	65.30	29000	95.90	0.122
Tran et al.	S63	7.05	69.20	29000	92.40	0.144	64.20	29000	102.60	0.190
Zhang et al.	SW7	4.82	58.74	29000	70.49	0.120	44.24	29000	53.08	0.120
Zhang et al.	SW8	5.20	62.66	29000	75.19	0.120	44.24	29000	53.08	0.120
Zhang et al.	SW9	5.75	54.39	29000	65.27	0.120	44.24	29000	53.08	0.120
Segura et al.	WP6	6.71	77.00	29000	107.60	0.111	83.90	29000	105.30	0.103
Segura et al.	WP7	12.48	62.84	29000	92.39	0.100	121.25	29000	121.40	0.100
Lu et al.	C1	5.58	43.60	29000	66.98	0.126	43.60	29000	66.98	0.126

Author	ID	Material								
		f'_c	$f_{y,be}$	$E_{s,be}$	$f_{u,be}$	$\epsilon_{u,be}$	$f_{y,v}$	$E_{s,v}$	$f_{u,v}$	$\epsilon_{u,v}$
		ksi	ksi	ksi	ksi	in/in	ksi	ksi	ksi	in/in
Lu et al.	C2	5.00	43.60	29000	66.98	0.126	43.60	29000	66.98	0.126
Lu et al.	C3	5.25	43.60	29000	66.98	0.126	43.60	29000	66.98	0.126
Lu et al.	C4	5.03	43.60	29000	66.98	0.126	43.60	29000	66.98	0.126
Lu et al.	C5	5.13	43.60	29000	66.98	0.126	43.60	29000	66.98	0.126
Lu et al.	C6	5.41	43.60	29000	66.98	0.126	43.60	29000	66.98	0.126
Hube et al.	W5	3.97	68.02	29000	98.05	0.166	64.63	29000	86.88	0.151
Hube et al.	W7	3.97	68.02	29000	98.05	0.166	64.63	29000	86.88	0.151
Hube et al.	W8	3.97	68.02	29000	98.05	0.166	64.63	29000	86.88	0.151
Hube et al.	W9	3.97	68.02	29000	98.05	0.166	64.63	29000	86.88	0.151

Table C - 2 Loading Data Wall Set

Author	Specimen	Loading				Results	
		CSAR	Shear Span	ALR	$V_{max}/ (A_{cv}f'^{0.5}_c)$	Δu	FM
		--	--	%	psi	%	--
Dazio et al.	WSH1	13.33	2.28	5.1	2	1.04	BR
Dazio et al.	WSH2	13.33	2.28	5.69	2.25	1.43	BR
Dazio et al.	WSH3	13.33	2.28	5.83	2.92	2.03	BR
Dazio et al.	WSH5	13.33	2.28	12.83	2.81	1.36	BR
Dazio et al.	WSH6	13.33	2.26	10.79	3.49	2.07	CB
Liu	W1	6.07	3.13	7.64	2.31	2.98	CB
Liu	W2	6.07	3.13	3.58	1.67	2.91	BR
Lowes et al.	PW4	20	2	11.7	4.31	1.01	CB
Wallace	RW1	12	3.13	10.23	2.44	2.1	BR
Wallace	RW2	12	3.13	8.99	2.63	2.25	CB
Oh et al.	WR20	7.5	2	8.39	2.71	2.7	CB
Oh et al.	WR10	7.5	2	7.92	2.5	2.82	CB

Author	Specimen	Loading				Results	
		CSAR	Shear Span	ALR	$V_{max}/ (A_{cv}f'_c{}^{0.5})$	Δu	FM
		--	--	%	psi	%	--
Shegay	C10	11.25	4.6	9.17	2.12	3.1	CB
Shegay	A10	11.25	4.6	9.17	2.11	3.1	BR/Global
Shegay	A14	11.25	4.6	14.08	2.15	2.5	CB
Shegay	A20	11.25	4.6	20.59	2.45	2.05	CB
Tran et al.	S38	8	2	7.32	4.54	3.1	CB
Tran et al.	S63	8	2	7.29	6.88	3	CB
Zhang et al.	SW7	7	2.14	21.44	6.01	2	CB
Zhang et al.	SW8	7	2.14	31.26	6.46	1.5	CB/Global
Zhang et al.	SW9	7	2.14	21.44	8.31	2	CB
Segura et al.	WP6	12	3.57	7.46	2.2	3.55	BR
Segura et al.	WP7	10	3.51	7.1	1.63	3.7	CB
Lu et al.	C1	9.33	2	3.59	1.6	2.5	BR
Lu et al.	C2	9.33	4	4	0.87	2.5	BR
Lu et al.	C3	9.33	6	3.81	0.54	2.5	BR
Lu et al.	C4	9.33	2	0	0.93	1.5	BR
Lu et al.	C5	9.33	2	7.47	2.28	1.98	BR
Lu et al.	C6	9.33	4	3.7	0.8	2.45	BR
Hube et al.	W5	7	1.9	14.96	6.21	1.45	CB
Hube et al.	W7	7	2.5	14.96	4.62	2.3	CB
Hube et al.	W8	7	2.5	14.96	5.13	2.71	CB
Hube et al.	W9	7	2.5	14.96	4.69	2.68	CB

Appendix B – Experimental Data

Author	ID	Flexural Data						Shear Data				Drift Data		
		ALR	My	Mn	Mb,max	Mb,max/Mn	Vn, ACI	Vb,max	vmax	Vb,max/Vn	Δy	Δu		FM
		%	kip-ft	kip-ft	kip-ft	--	kip	kip	--	--	%	%		--
Dazio et al.	WSH1	5.1	930	1088	1124	1.03	174	75	2.00	0.43	0.24	1.04		BR
Dazio et al.	WSH2	5.69	960	1060	1201	1.13	153	80	2.25	0.52	0.23	1.43		BR
Dazio et al.	WSH3	5.83	1140	1376	1530	1.11	153	102	2.92	0.67	0.36	2.03		BR
Dazio et al.	WSH5	12.83	1210	1316	1458	1.11	157	97	2.81	0.62	0.2	1.36		BR
Dazio et al.	WSH6	10.79	1530	1651	1956	1.18	163	132	3.49	0.81	0.28	2.07		CB
Liu	W1	7.64	615	712	714	1.00	150	59	2.31	0.39	0.64	2.98		CB
Liu	W2	3.58	650	769	756	0.98	191	62	1.67	0.33	0.55	2.91		BR
Lowes et al.	PW4	11.7	3660	1624	2436	1.50	247	203	4.31	0.82	0.4	1.01		CB
Thomsen et al.	RW1	10.23	330	400	396	0.99	67	32	2.44	0.47	0.48	2.1		BR
Thomsen et al.	RW2	8.99	330	387	443	1.14	68	35	2.63	0.52	0.55	2.25		CB
Oh et al.	WR20	8.39	790	639	857	1.34	130	87	2.71	0.67	0.35	2.7		CB
Oh et al.	WR10	7.92	795	741	814	1.10	151	83	2.50	0.55	0.47	2.82		CB
Shegay et al.	C10	9.17	2561	2818	3409	1.21	311	102	2.12	0.33	--	3.1		CB
Shegay et al.	A10	9.17	2561	2757	3378	1.23	312	101	2.11	0.32	0.35	3.1		BR/Global
Shegay et al.	A14	14.08	3231	3331	3997	1.20	331	118	2.15	0.36	0.46	2.5		CB

Author	ID	Flexural Data					Shear Data				Drift	
		ALR	My	Mn	Mb,max	Mb,max/Mn	Vn, ACI	Vb,max	vmax	Vb,max/Vn	Δy	Δu
		%	kip-ft	kip-ft	kip-ft	--	kip	kip	--	--	%	%
Shegay et al.	A20	20.59	3818	3185	4538	1.42	347	136	2.45	0.39	0.31	2.05
Tran et al.	S38	7.32	680	651	864	1.33	108	108	4.54	1.00	0.53	3.1
Tran et al.	S63	7.29	1135	1094	1331	1.22	160	166	6.88	1.04	0.63	3
Zhang et al.	SW7	21.44	191	198	223	1.13	70	45	6.01	0.64	0.4	2
Zhang et al.	SW8	31.26	211	160	249	1.56	75	51	6.46	0.67	0.37	1.5
Zhang et al.	SW9	21.44	283	244	337	1.38	89	68	8.31	0.77	0.56	2
Segura et al.	WP6	7.46	3128	3438	4194	1.22	128	122	2.20	0.95	0.59	4.08
Lu et al.	C1	3.59	259	363	352	0.97	90	39	1.60	0.43	0.55	2.5
Lu et al.	C2	4	255	338	368	1.09	90	20	0.87	0.22	0.52	2.5
Lu et al.	C3	3.81	257	332	350	1.05	90	13	0.54	0.14	0.68	2.5
Lu et al.	C4	0	103	251	194	0.77	85	21	0.93	0.25	0.27	1.5
Lu et al.	C5	7.47	368	411	481	1.17	101	53	2.28	0.53	0.76	2
Lu et al.	C6	3.7	248	343	354	1.03	84	19	0.80	0.23	1	2.5
Hube et al.	W5	14.96	155	127	244	1.92	50	42	6.21	0.85	0.31	1.45
Hube et al.	W7	14.96	127	142	181	1.27	50	32	4.62	0.63	0.36	2.3
Hube et al.	W8	14.96	129	136	202	1.48	50	35	5.13	0.70	0.42	2.71
Hube et al.	W9	14.96	122	121	184	1.51	50	32	4.69	0.64	0.34	2.68

Appendix C – Data Structure

Structure Level 1	2	3	4	5	Variable type	Variable description
Authors					Cell Array	Representative author of the study
SpecimenID					Cell Array	Specimen ID as classified by author
UniqueID					Cell Array	Unique specimen ID - amalgamation of Author and SpecimenID
WallType					Structure	General wall overview
	Shape				Cell Array	Cross sectional shape of the wall ('Rect' or 'Flanged' or 'Barbell')
	SteelLayout				Cell Array	BE or Dist
Geometry					Structure	Wall geometrical details
	t				Double	Wall web thickness (in)
	h				Double	Clear height of specimen (between foundation block and capping block, if present) (in)
	l				Double	Length of the wall edge to edge (in)
	h_v				Double	Effective specimen height, base moment divided by base shear (in)
	l_be				Double	Length of the boundary element measured as the cumulative center to center distance of the bars in the BE plus cover to the bar centerlines either side (in). For flanged section, this is 0 if there is no BE in the web portion.
	endCover				Double	Clear cover to the confinement reinforcement at end of wall (in)
	sideCover				Double	Clear cover to the confinement reinforcement at face of wall (in)
	t_f				Double	Flange thickness (in)
	b_f				Double	Width of the flange (in)
	AspectRatio				Double	Clear height of wall divided by length of wall (h/l)
	ShearSpan				Double	Shear span ratio. Base moment/base shear/length of wall (h_v/l)
	SlenderRatio				Double	Cross-sectional aspect ratio. Length of wall/thickness of web (l/t)
	BeRatio				Double	Area of both boundary elements (BEs) divided by the gross cross sectional wall area
	WallVolume				Double	thickness x length x clear height (t x l x h) (in^3)
	WallSurfaceArea				Double	(t x h + l x h)x2 for most walls. Calculation for T-section and barbell walls is appropriately adjusted
	Area				Double	Gross cross sectional wall area
	numStory				Double	Number of stories constructed
	Igross				Double	Gross moment of inertia (in^4)
	h_measured				Double	Height at which lateral displacement is measured in the experiment
	l_bef				Double	Length of the boundary element in the flange of the wall (if present), measured as the center to center distance of the bars in the BE plus cover to the bar centerlines either side (in)
	LoadingDirection				Double	Indicates the direction towards which the load is initially loaded in the protocol: + 1: load is applied which puts the 'right' boundary element in compression -1: load is applied which puts the 'left' boundary element in compression The 'right' and 'left' definitions are consistent with the section data entered in the Layers section of the SectionAnalysis part of the database. i.e., for T-sections, +1 puts the flange in compression at start of test.
	BuildingAspectRatio				Double	This is the aspect ratio of the wall in the building design. Often this is larger than the shear span ratio because the shear span ratio is based on an effective height, which is 60-70% of the actual wall design to be used in a building. This parameter is needed for some code comparisons

Structure Level 1	2	3	4	5	Variable type	Variable description
Variable Name						
Reinf					Structure	Wall reinforcement detailing
	rho_be				Double	Reinforcement ratio in the BE (area of longitudinal reinforcement in the BE divided (l_be*t)
	rho_v				Double	Vertical reinforcement ratio in the web of the wall (area of longitudinal reinforcement in the web divided (l*t -2l_be*t)
	rho_v_all				Double	Vertical reinforcement ratio of the entire cross section (area of all longitudinal reinforcement divided by l*t)
	rho_h				Double	Horizontal reinforcement ratio of the wall in the web (area of horizontal reinforcement divided by spacing*t)
	rho_z				Double	Reinforcement ratio of the confinement legs in the BE (area of BE hoops and ties divided by spacing*l_be)
	rho_h_be				Double	Reinforcement ratio of the horizontal confinement hoops in the BE (area of BE hoops and ties divided by spacing*t)
	NoCH				Double	Number of curtains of longitudinal reinforcement in the horizontal direction
	NoCV				Double	Number of curtains of longitudinal reinforcement in the vertical direction
	s_h				Double	Spacing of horizontal web reinforcement (in)
	s_v				Double	Spacing of the vertical longitudinal reinforcement in the web (in)
	s_hoop				Double	Hoop spacing in the BE (in)
	d_be				Double	Diameter of longitudinal bars in the BE (in)
	d_v				Double	Diameter of longitudinal bars in the web (in)
	d_h				Double	Diameter of the horizontal reinforcement in the web (in)
	d_hoop				Double	Diameter of the hoops in the BE (in)
	rho_vol				Double	Transverse reinforcement volumetric ratio (volume of one layer of hoops/ties in BE divided by (l_be*s_hoop*t)
	Confinement				Structure	Confinement reinforcement detailing of the wall
		UniqueID	cTog		Double	1 or 0 to indicate of wall does (1) or does not (0) have confinement reinforcement in the BE, respectively
			xdir	bars	2D Matrix	2 column matrix with single confinement leg area in first column (in^2) and yield strength in the second column (ksi). The number of rows corresponds to the number of confinement legs in the BE crossing the longitudinal axis of the wall cross section
				b	Double	The length of the boundary element to the outside of the peripheral confinement/transverse reinforcement legs
				s1	Double	Spacing of longitudinal reinforcement in the BE. This is averaged if the number value fluctuates (hoops or cross ties)
				sHoop	Double	Vertical spacing of the confinement hoops/ties
			ydir	bars	2D Matrix	2 column array with single confinement leg area in first column (in^2) and yield strength in the second column (ksi). The number of rows corresponds to the number of confinement legs in the BE crossing the transverse axis of the wall cross section
				b	Double	The length of the boundary element to the outside of the peripheral confinement/transverse reinforcement legs
				s1	Double	Spacing of longitudinal reinforcement in the BE. This is averaged if the number value fluctuates (hoops or cross ties)
				sHoop	Double	Vertical spacing of the confinement hoops
			webcTog		Double	1 or 0 to indicate of wall does or does not have confinement reinforcement in the web, respectively
			web_xdir	bars	2D Matrix	2 column matrix with single confinement leg area in first column (mm^2) and yield strength in the second column (Mpa). The number of rows corresponds to the number of confinement legs in the BE crossing the longitudinal axis of the wall cross section
				s1	Double	Spacing of longitudinal reinforcement in the web. This is averaged if the number value fluctuates (hoops or cross ties)
				sHoop	Double	Vertical spacing of the web confinement reinforcement
			web_ydir	bars	2D Matrix	2 column array with single confinement leg area in first column (mm^2) and yield strength in the second column (Mpa). The number of rows corresponds to the number of confinement legs in the BE crossing the transverse axis of the wall cross section
				s1	Double	Spacing of longitudinal reinforcement in the web. This is averaged if the number value fluctuates (hoops or cross ties)
				sHoop	Double	Vertical spacing of the web confinement reinforcement
			minHookAngle		Double	Number indicating the WORST hook shape in the BE. 1 if the worst shape is a hoop corner or a 180-180 hook. 0.5 if the worst shape has a 90 degree hook. This is used to reduce effectiveness of confinement. See: Shegay, A. V. (2019). Seismic Performance of Reinforced Concrete Walls Designed For Ductility. Ph.D. Thesis. University of Auckland. Welt, T. S. (2015). Detailing for Compression in Reinforced Concrete Wall Boundary Elements: Experiments, Simulations, and Design Recommendations. Ph.D. Thesis, University of Illinois at Urbana-Champaign.
			asymTog		Double	Number to indicate if the cross section of the wall is symmetrical (0) or asymmetrical (1)
	s_hoop_e				Double	Hoop spacing in the BE (in) of the opposite side (in case where wall detailing is assymetrical)
	rho_be_e				Double	Reinforcement ratio in the BE of the opposite side (in case where wall detailing is assymetrical)
	d_be_e				Double	Diameter of longitudinal bars in the BE (in) of the opposite side (in case where wall detailing is assymetrical)
	d_v_e				Double	Diameter of longitudinal bars in the web (in) of the opposite side (in case where wall detailing is assymetrical)
	d_h_e				Double	Diameter of the horizontal reinforcement in the web (in) of the opposite side (in case where wall detailing is assymetrical)
	d_hoop_e				Double	Diameter of the hoops in the BE (in) of the opposite side (in case where wall detailing is assymetrical)
	rho_vol_e				Double	Transverse reinforcement volumetric ratio of the opposite side (in case where wall detailing is assymetrical)

Structure Level 1	2	3	4	5	Variable type	Variable description
Material						
	age				Double	Age of concrete when test was conducted (days)
	fc				Double	Measured concrete compressive strength (psi)
	eps				Double	Strain at peak concrete compressive stress
	Ec				Double	Measured Youngs modulus of concrete (psi)
	fr				Double	Measured rupture stress of concrete (if available) (psi)
	fsp				Double	Measured splitting stress of concrete (if available) (psi) - split cylinder test
	fy_be				Double	Measured yield strength of BE longitudinal reinforcement (ksi)
	fu_be				Double	Measured ultimate strength of BE longitudinal reinforcement (ksi)
	fy_v				Double	Measured yield strength of vertical web longitudinal reinforcement (ksi)
	fu_v				Double	Measured ultimate strength of web vertical longitudinal reinforcement (ksi)
	fy_h				Double	Measured yield strength of horizontal web reinforcement (ksi)
	fu_h				Double	Measured ultimate strength of horizontal web reinforcement (ksi)
	fy_hoop				Double	Measured yield strength of hoop reinforcement (ksi)
	fu_hoop				Double	Measured ultimate strength of hoop reinforcement (ksi)
	eps_ult_be				Double	Strain at ultimate stress of BE longitudinal reinforcement
	eps_ult_v				Double	Strain at ultimate stress of vertical web longitudinal reinforcement
	eps_ult_h				Double	Strain at ultimate stress of horizontal web reinforcement
	eps_max				Double	Strain at rupture of longitudinal BE reinforcement
	fyt_web				Double	Measured yield strength of web confinement reinforcement (ksi)
	fut_web				Double	Measured ultimate strength of web confinement reinforcement (ksi)
	fy_be_e				Double	Measured yield strength of BE longitudinal reinforcement (ksi) in the opposite wall end (if the wall is asymmetrical)
	fu_be_e				Double	Measured ultimate strength of BE longitudinal reinforcement (ksi)in the opposite wall end (if the wall is asymmetrical)
	eps_ult_be_e				Double	Strain at ultimate stress of BE longitudinal reinforcement in the opposite wall end (if the wall is asymmetrical)
	eps_ult_hoop				Double	Strain at ultimate stress of BE hoop reinforcement
Loading					Structure	Information on the loading conditions on the test wall during the experiment
	Mtop_Vtop				Double	Applied moment at top of specimen (at height of shear load application) divided by applied shear at top of specimen
	LoadingType				Cell	Horizontal loading condition of the wall. Eitehr 'Cyclic' or 'monotonic'
	AxialLoad				Double	Axial load magnitude (kips)
	TotalAxialLoad				Structure	
		UniqueID			Double	Axial load plus self weight of the specimen (including capping block), calculated using 0.087lb/in^3 (kips)
	CyclicHistory					
		UniqueID			2D Matrix	Loading protocol of the tests determined from raw data or digitized graphs when available. Structure is a 2D array with positive drift steps in 1st column and negative drift steps in second column, including all cycles.

Appendix D – Post Processing of Calibrated Walls

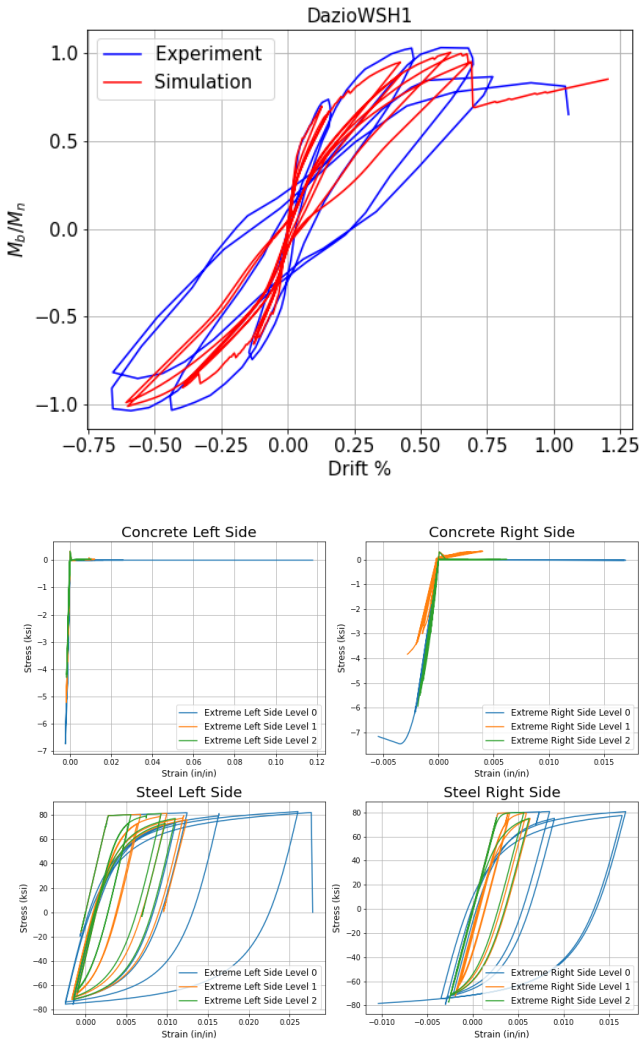

Figure D - 1 WSH1 Load-Displacement and Stress Strain Response

Link to interactive Stress and Strain wall plots:

https://stokljos.github.io/thesis/wsh1_movie.html

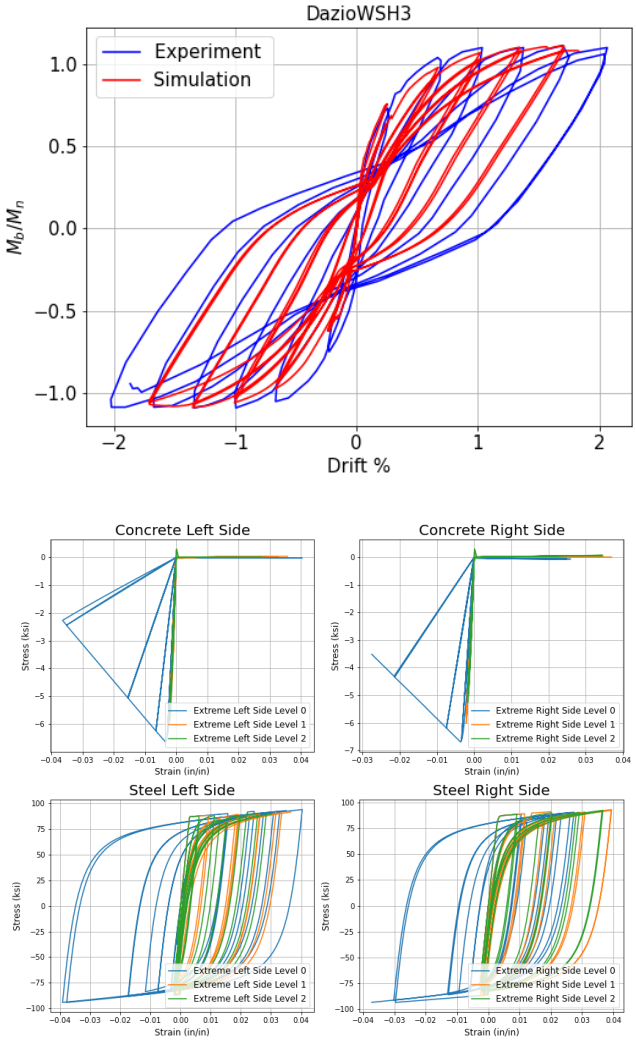

Figure D - 2 WSH3 Load-Displacement and Stress Strain Response

Link to interactive Stress and Strain wall plots:
https://stokljos.github.io/thesis/DazioWSH3_221104203416_movie.html

*Note file is to large to preview and needs to be downloaded to be viewed.

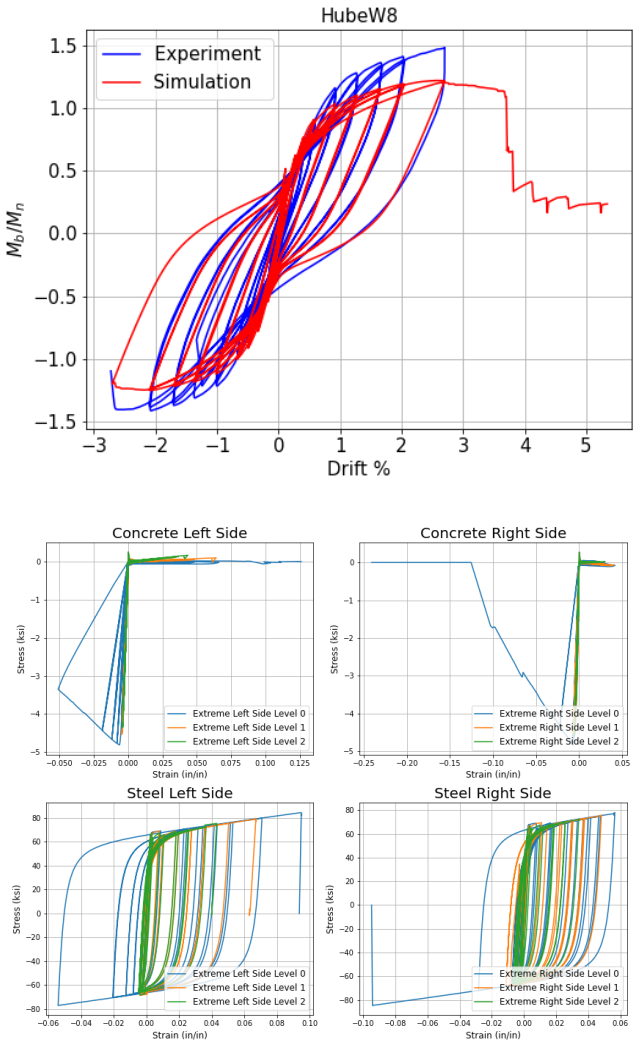

Figure D - 3 W8 Load-Displacement and Stress Strain Response

Link to interactive Stress and Strain wall plots:
https://stokljos.github.io/thesis/HubeW8_221104203424_movie.html

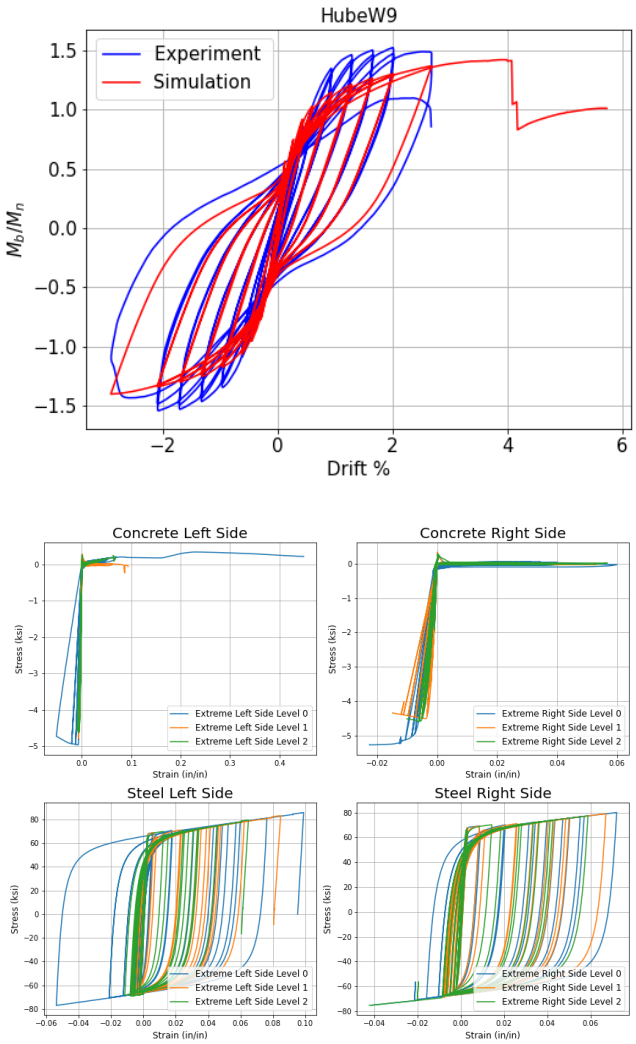

Figure D - 4 W9 Load-Displacement and Stress Strain Response

Link to interactive Stress and Strain wall plots:
https://stokljos.github.io/thesis/HubeW9_230305015202_movie.html

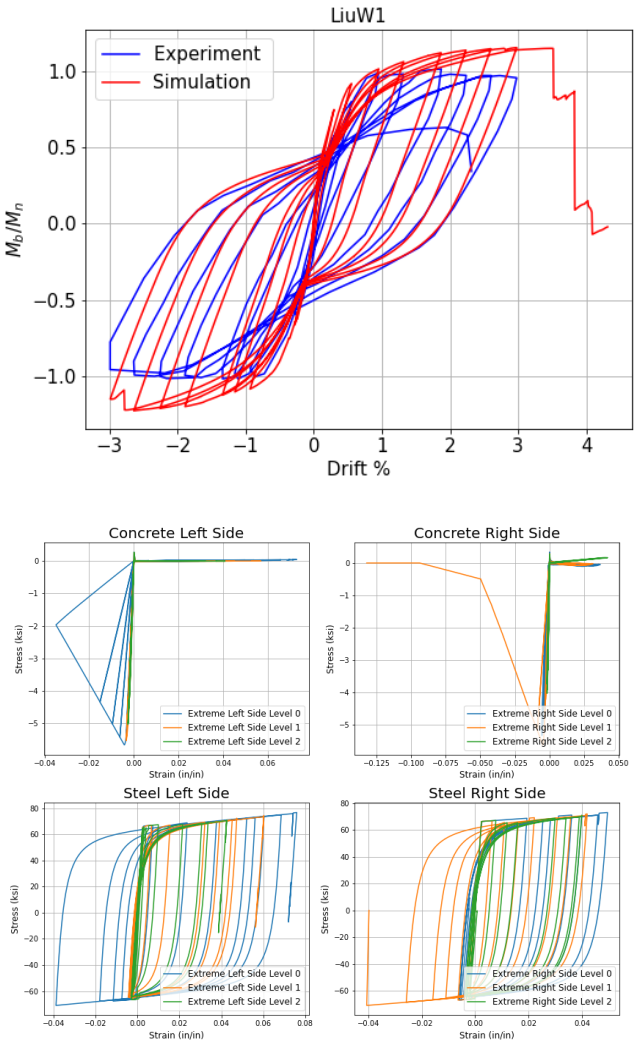

Figure D - 5 W1 Load-Displacement and Stress Strain Response

Link to interactive Stress and Strain wall plots:
https://stokljos.github.io/thesis/LiuW1_221104203417_movie.html

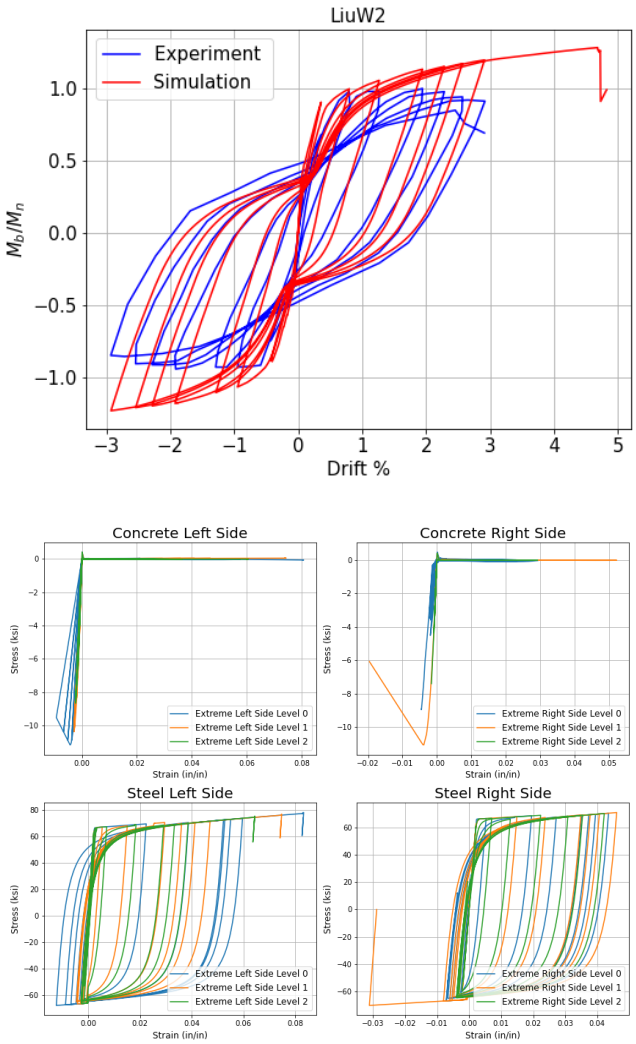

Figure D - 6 W2 Load-Displacement and Stress Strain Response

Link to interactive Stress and Strain wall plots:
https://stokljos.github.io/thesis/LiuW2_221104203418_movie.html

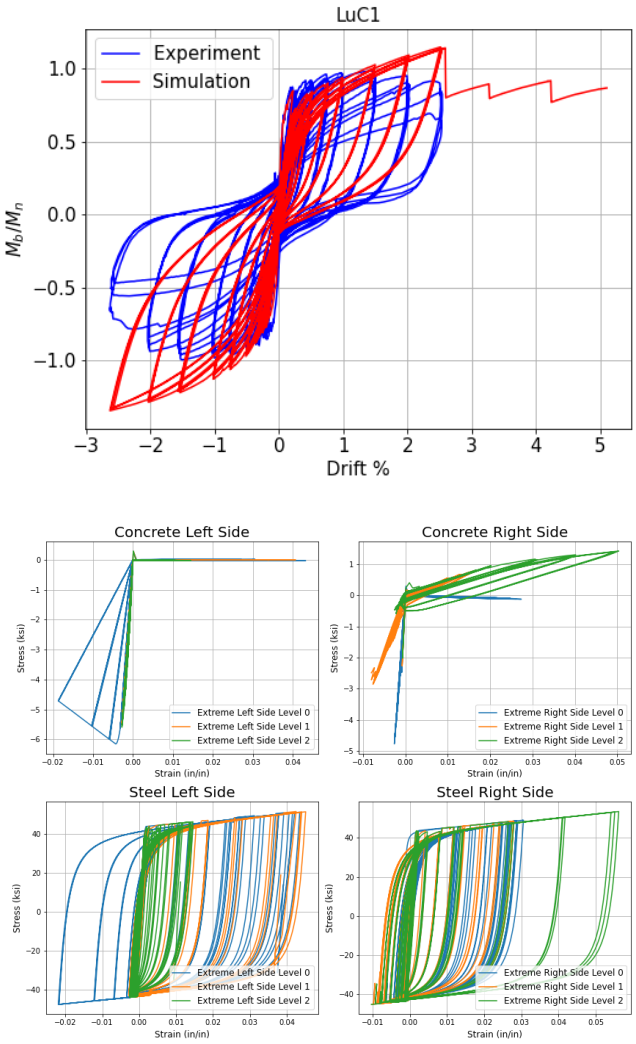

Figure D - 7 C1 Load-Displacement and Stress Strain Response

Link to interactive Stress and Strain wall plots:
https://stokljos.github.io/thesis/LuC1_230305015158_movie.html

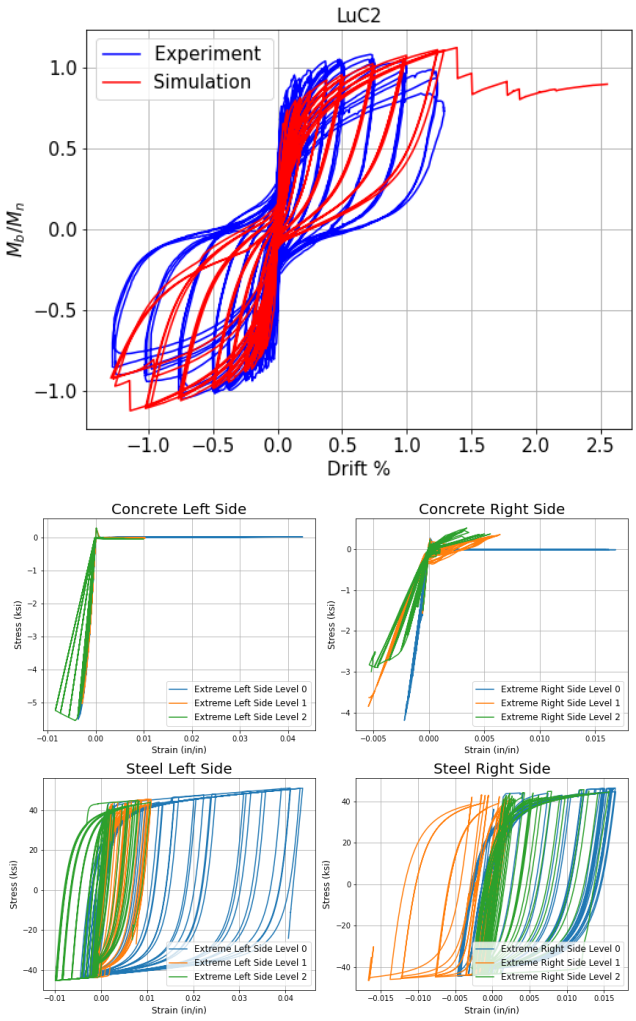

Figure D - 8 C2 Load-Displacement and Stress Strain Response

Link to interactive Stress and Strain wall plots:
https://stokljos.github.io/thesis/LuC2_230305015159_movie.html

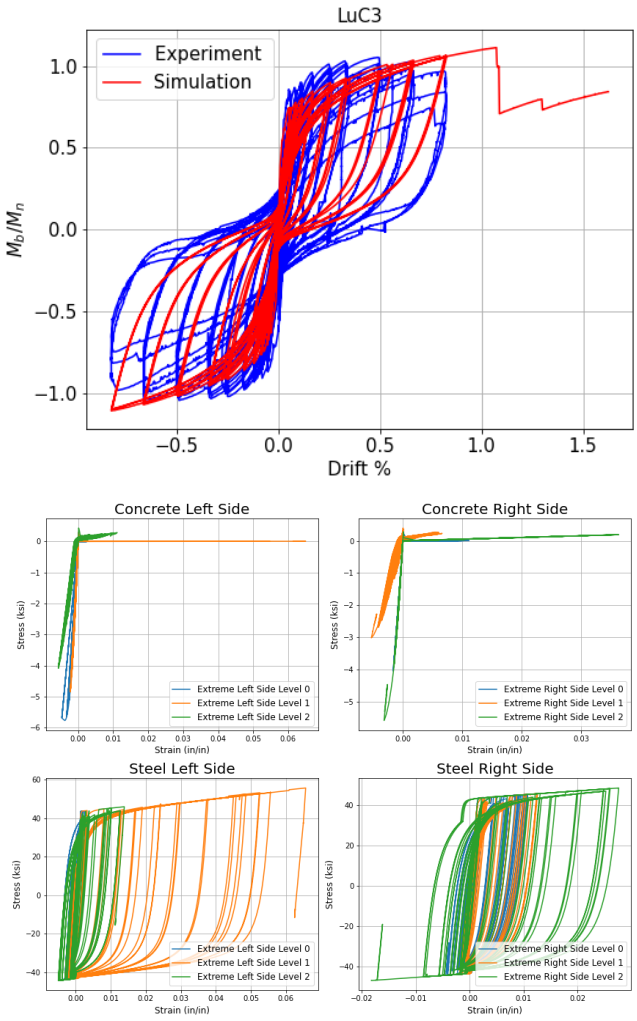

Figure D - 9 C3 Load-Displacement and Stress Strain Response

Link to interactive Stress and Strain wall plots:
https://stokljos.github.io/thesis/LuC3_230305015200_movie.html

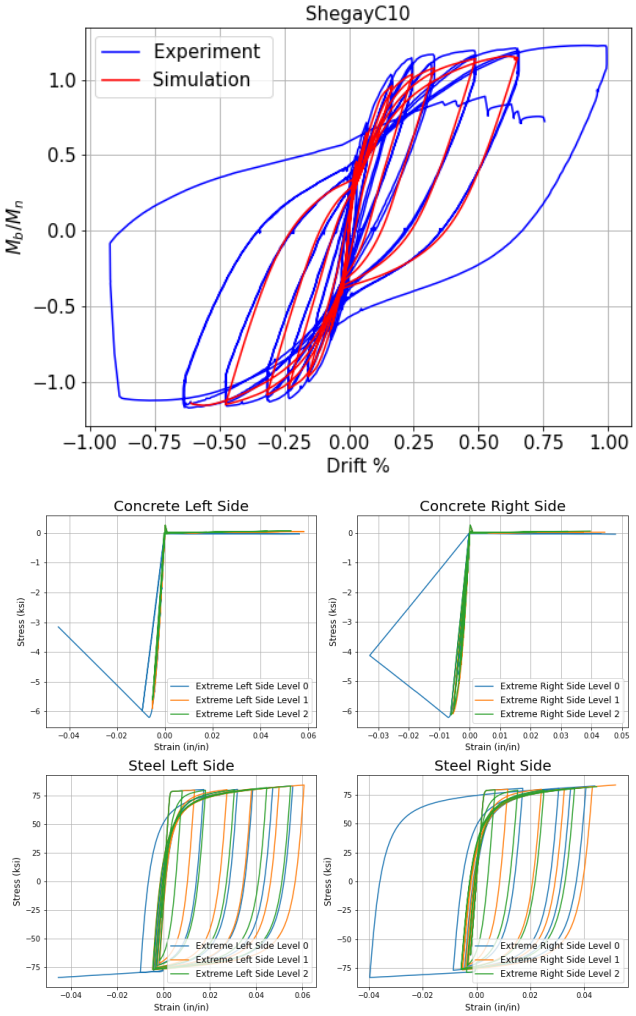

Figure D - 10 C10 Load-Displacement and Stress Strain Response

Link to interactive Stress and Strain wall plots:
https://stokljos.github.io/thesis/ShegayC10_230211125342_movie.html

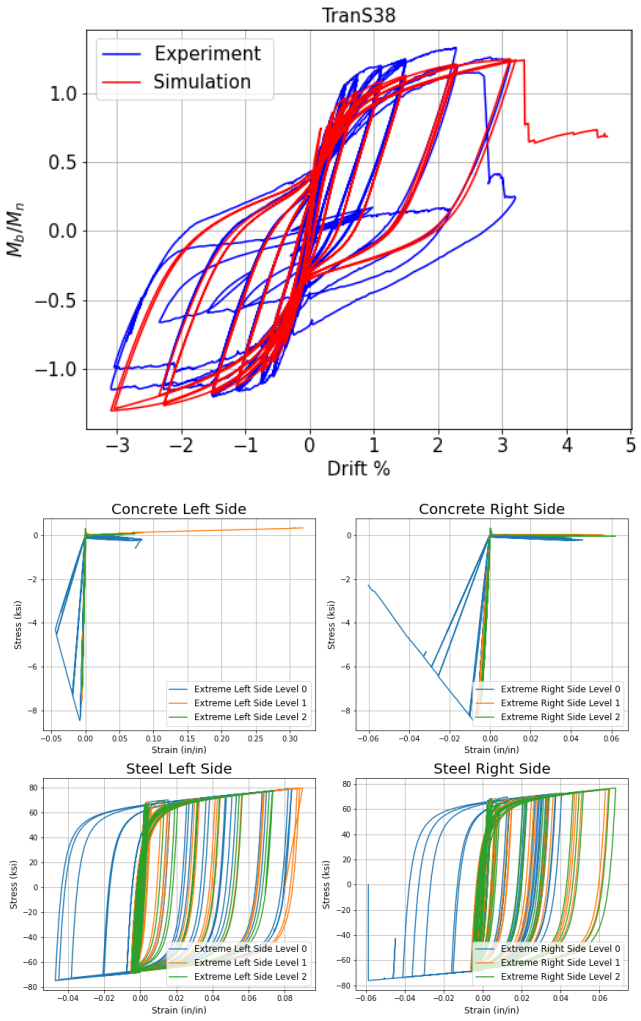

Figure D - 11 S38 Load-Displacement and Stress Strain Response

Link to interactive Stress and Strain wall plots:
https://stokljos.github.io/thesis/TranS38_221104203422_movie.html

*Note file is to large to preview and needs to be downloaded to be viewed.

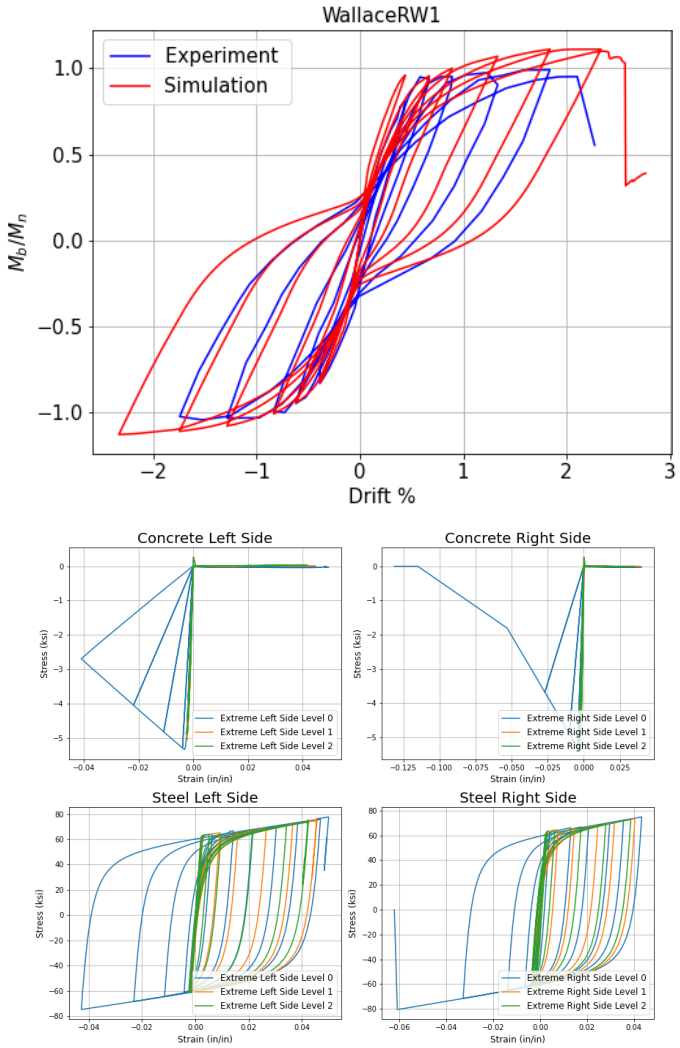

Figure D - 12 RW1 Load-Displacement and Stress Strain Response

Link to interactive Stress and Strain wall plots:
https://stokljos.github.io/thesis/WallaceRW1_221104203419_movie.html

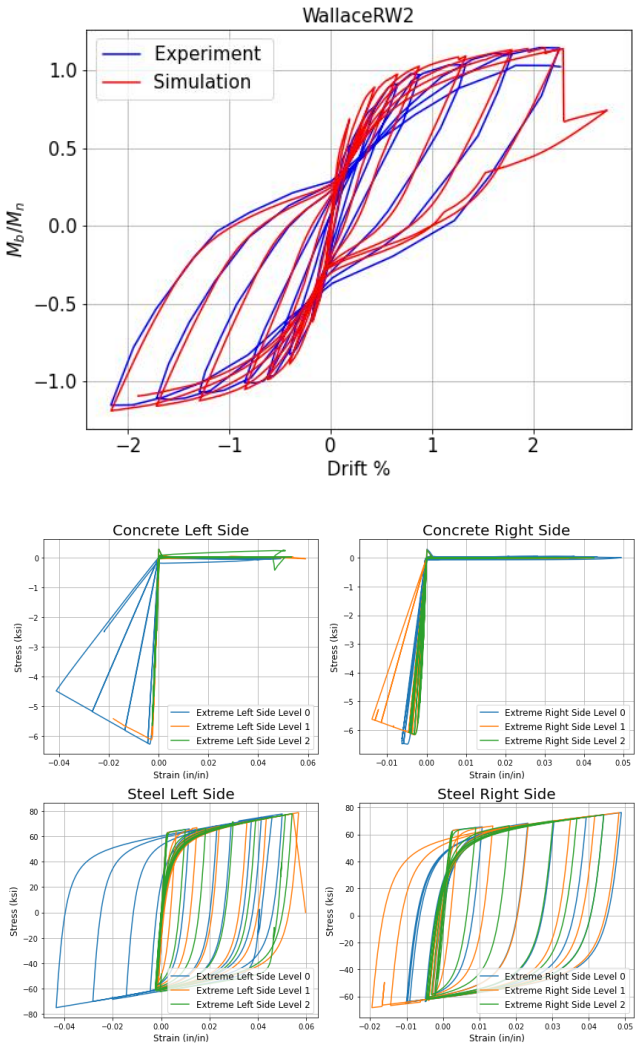

Figure D - 13 RW2 Load-Displacement and Stress Strain Response

Link to interactive Stress and Strain wall plots:
https://stokljos.github.io/thesis/WallaceRW2_230305015041_movie.html

*Note file is to large to preview and needs to be downloaded to be viewed.

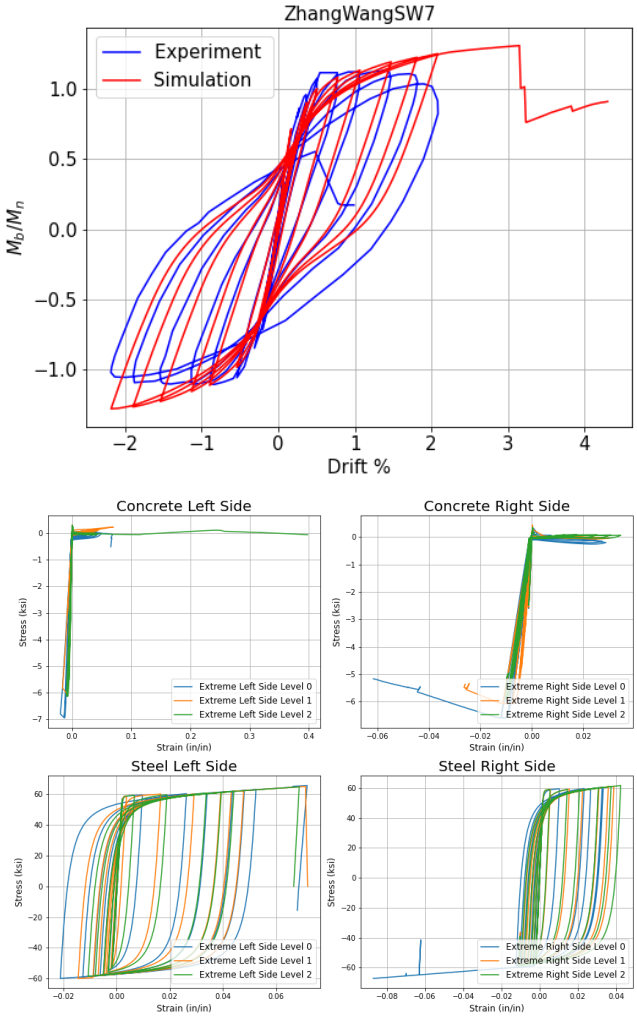

Figure D - 14 SW7 Load-Displacement and Stress Strain Response

Link to interactive Stress and Strain wall plots:
https://stokljos.github.io/thesis/ZhangWangSW7_230211125344_movie.html

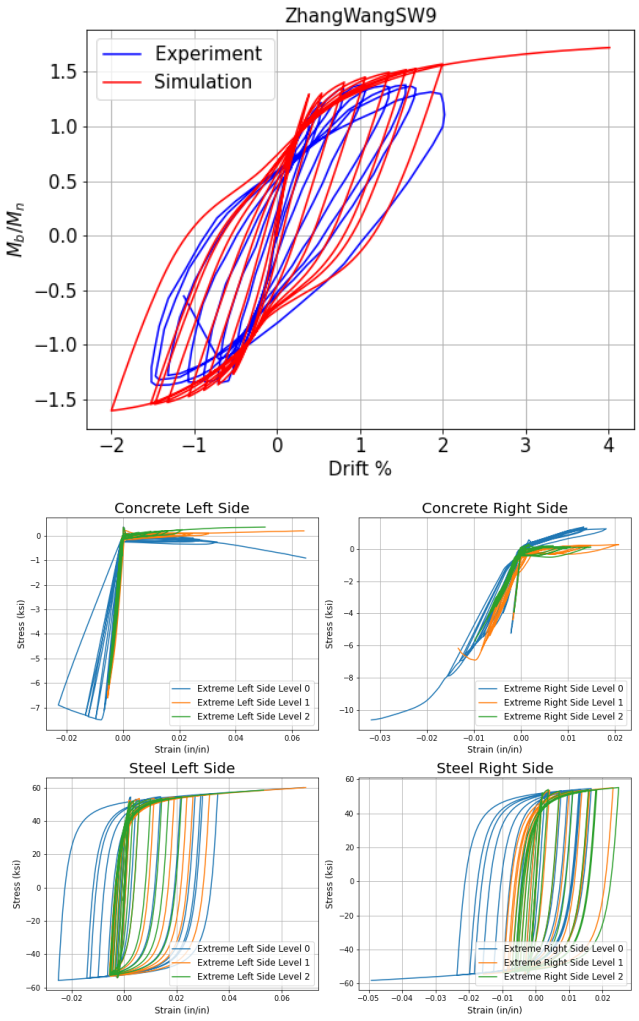

Figure D - 15 SW9 Load-Displacement and Stress Strain Response

Link to interactive Stress and Strain wall plots:
https://stokljos.github.io/thesis/ZhangWangSW9_221104203425_movie.html

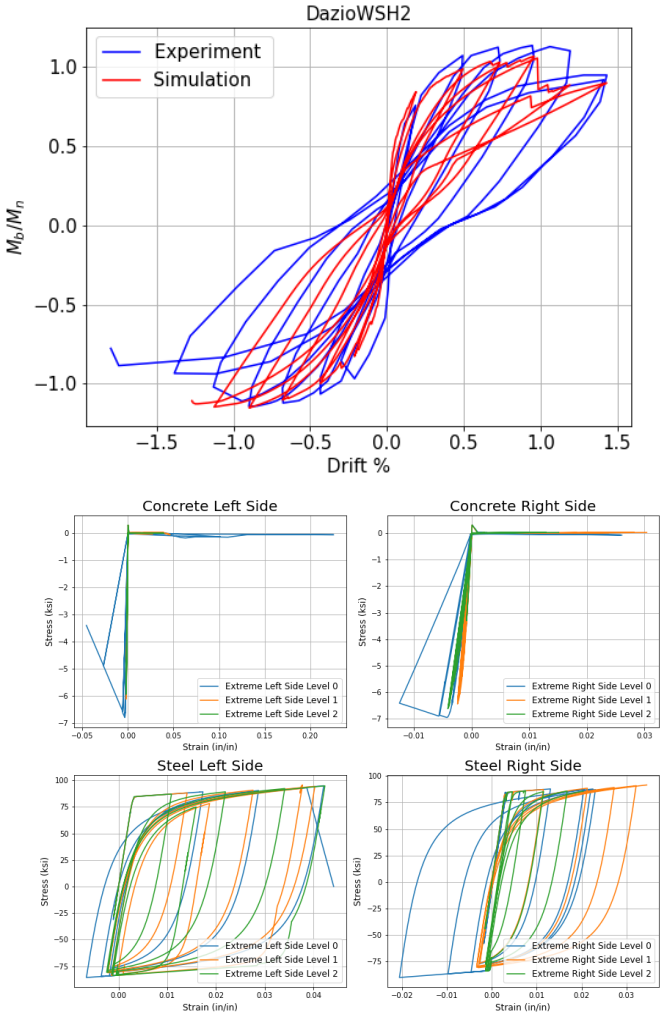

Figure D - 16 WSH2 Load-Displacement and Stress Strain Response

Link to interactive Stress and Strain wall plots:
https://stokljos.github.io/thesis/DazioWSH2_230305015050_movie.html

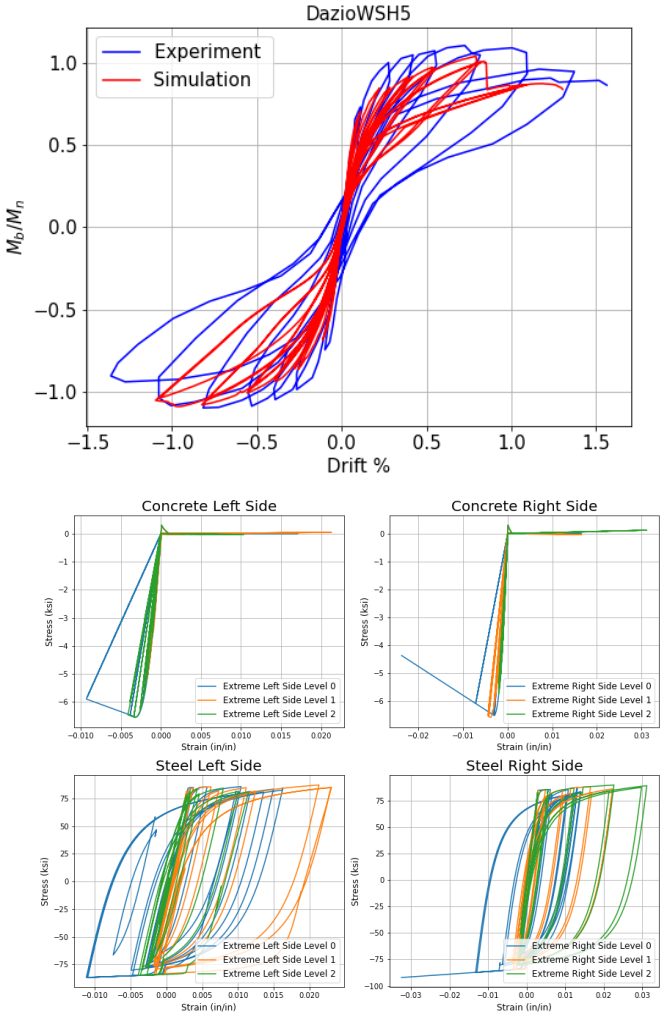

Figure D - 17 WSH5 Load-Displacement and Stress Strain Response

Link to interactive Stress and Strain wall plots:
https://stokljos.github.io/thesis/DazioWSH5_230305015204_movie.html

*Note file is to large to preview and needs to be downloaded to be viewed.

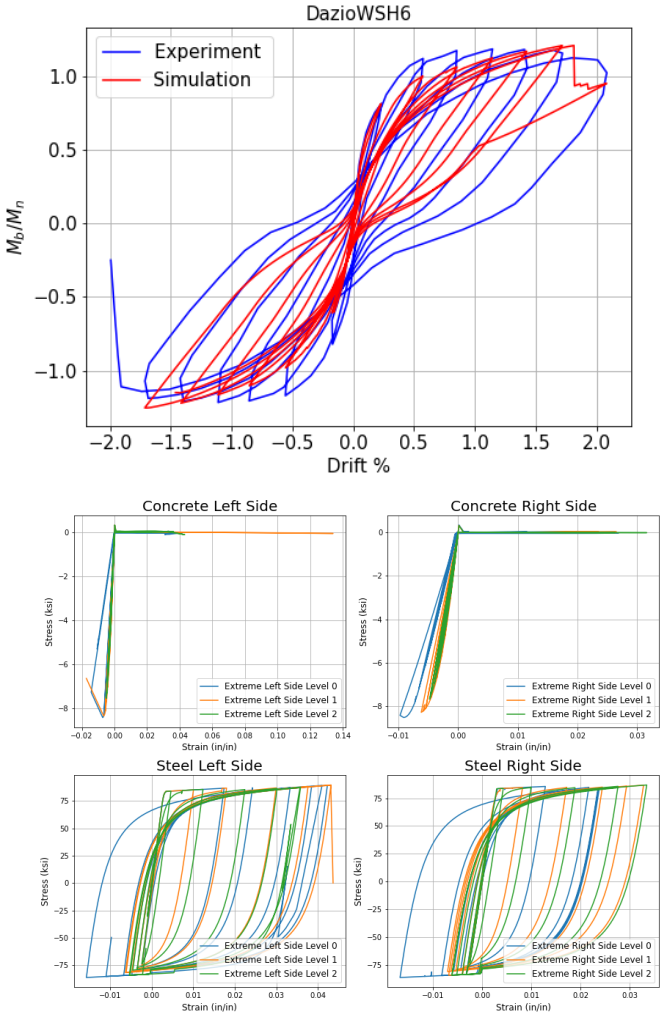

Figure D - 18 WSH6 Load-Displacement and Stress Strain Response

Link to interactive Stress and Strain wall plots:
https://stokljos.github.io/thesis/DazioWSH6_230305015205_movie.html

*Note file is to large to preview and needs to be downloaded to be viewed.

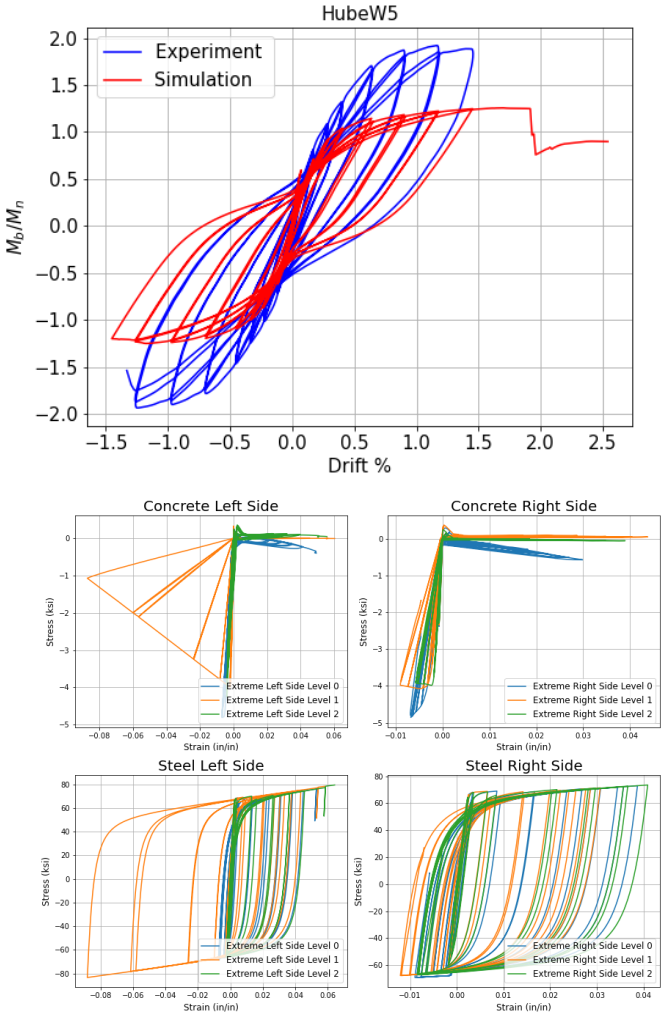

Figure D - 19 W5 Load-Displacement and Stress Strain Response

Link to interactive Stress and Strain wall plots:
https://stokljos.github.io/thesis/HubeW5_230301204159_movie.html

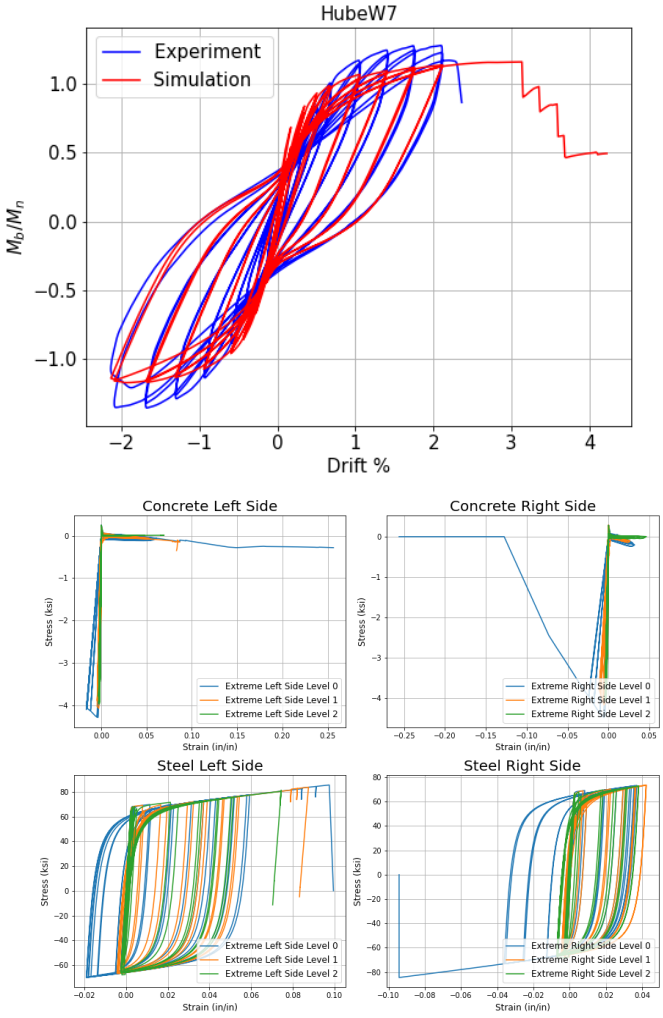

Figure D - 20 W7 Load-Displacement and Stress Strain Response

Link to interactive Stress and Strain wall plots:
https://stokljos.github.io/thesis/HubeW7_230301204200_movie.html

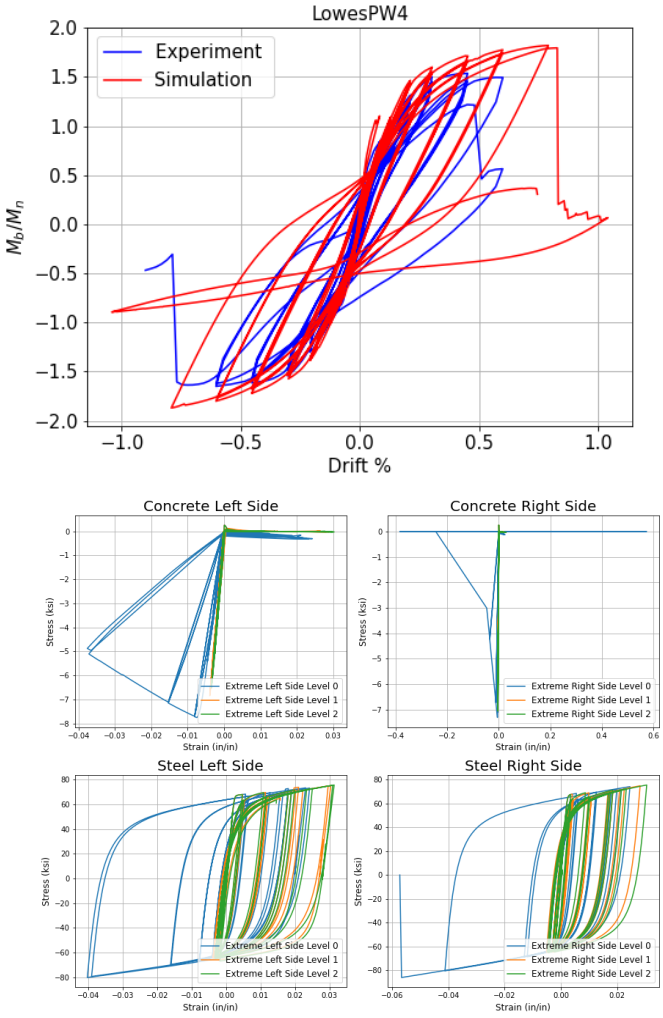

Figure D - 21 PW4 Load-Displacement and Stress Strain Response

Link to interactive Stress and Strain wall plots:
https://stokljos.github.io/thesis/LowesPW4_230304205135_movie.html

*Note file is to large to preview and needs to be downloaded to be viewed.

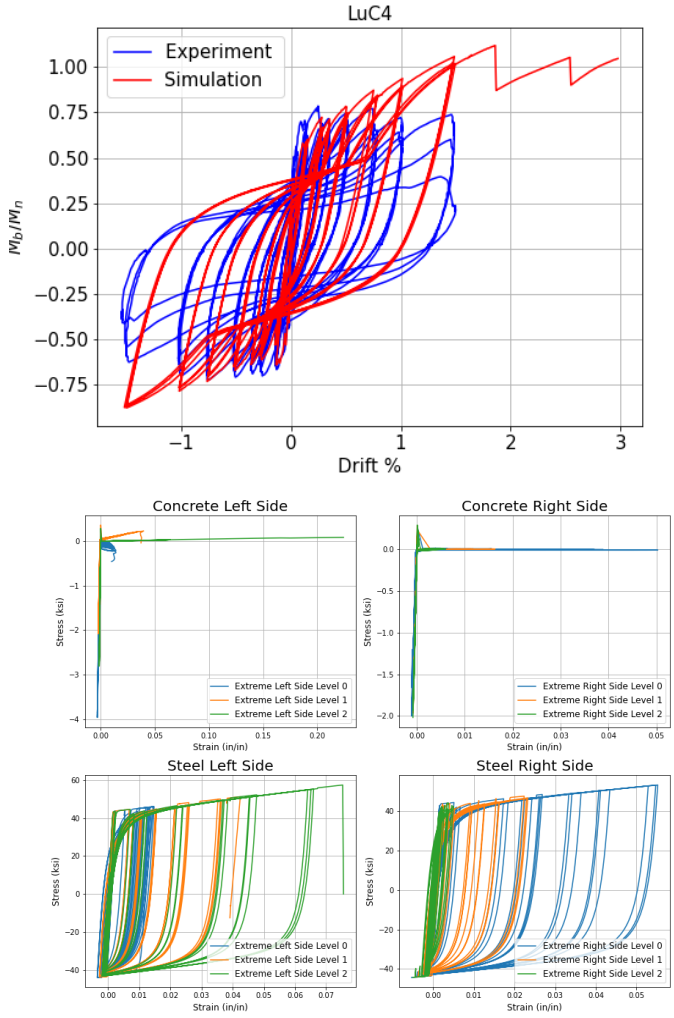

Figure D - 22 C4 Load-Displacement and Stress Strain Response

Link to interactive Stress and Strain wall plots:
https://stokljos.github.io/thesis/LuC4_230305015217_movie.html

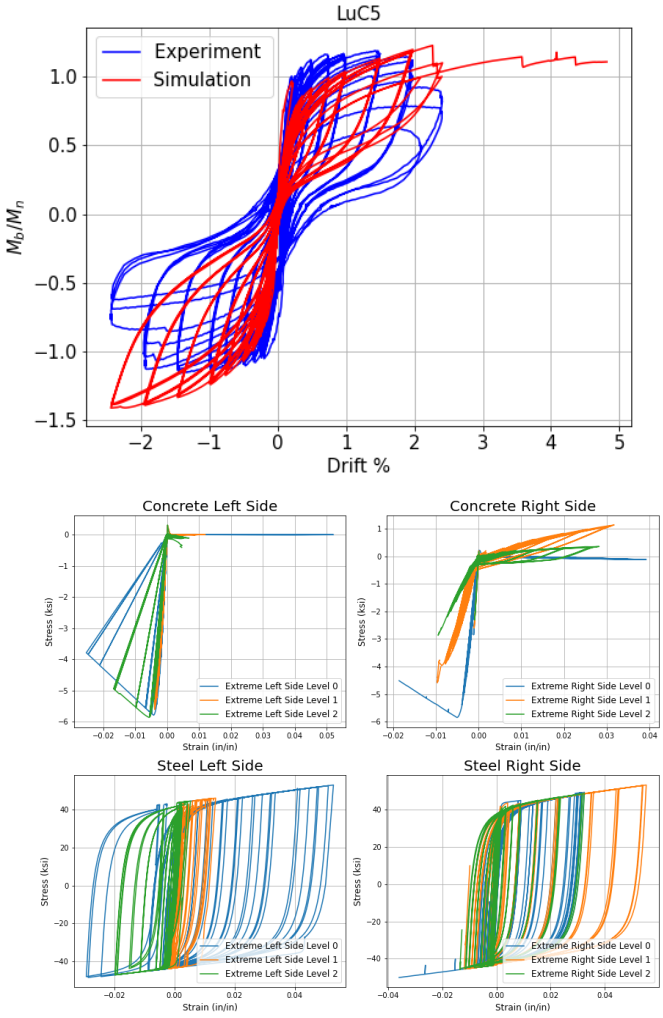

Figure D - 23 C5 Load-Displacement and Stress Strain Response

Link to interactive Stress and Strain wall plots:
https://stokljos.github.io/thesis/LuC5_230305015218_movie.html

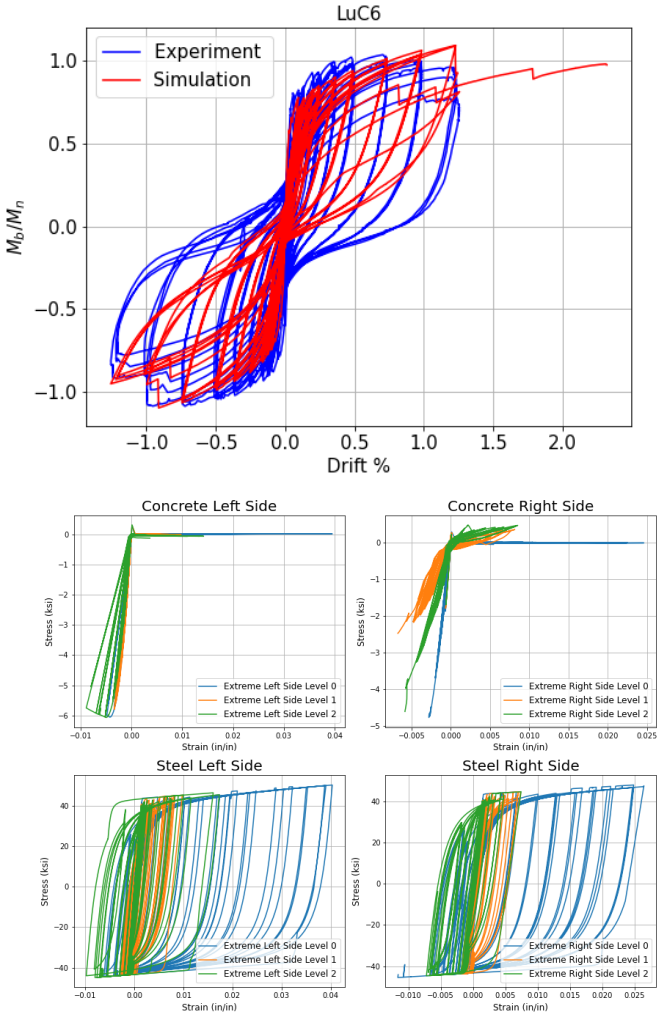

Figure D - 24 C6 Load-Displacement and Stress Strain Response

Link to interactive Stress and Strain wall plots:
https://stokljos.github.io/thesis/LuC6_230305015219_movie.html

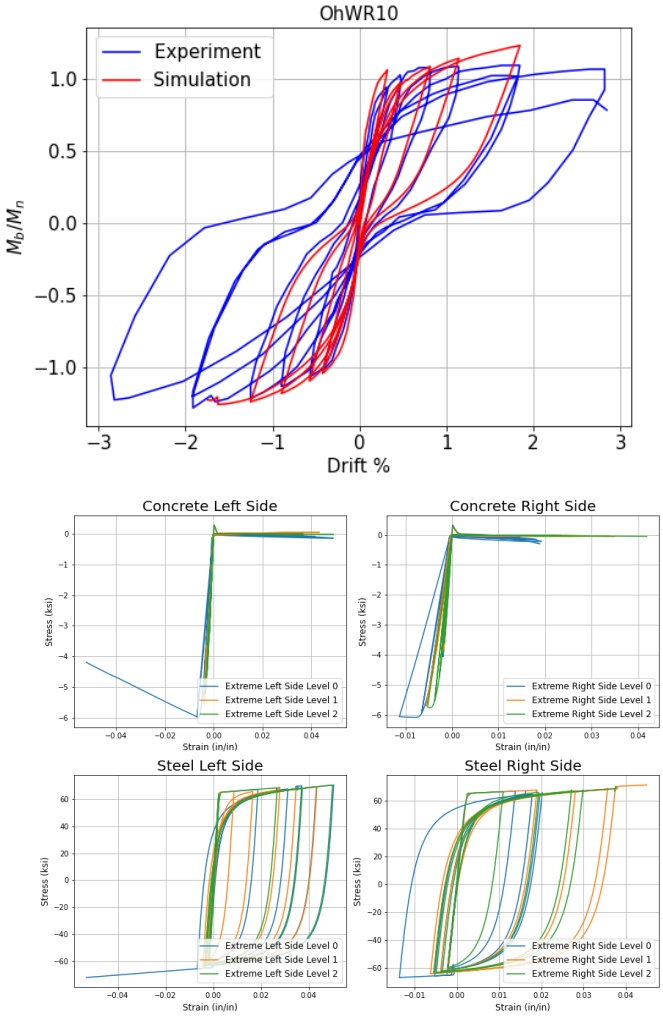

Figure D - 25 WR10 Load-Displacement and Stress Strain Response

Link to interactive Stress and Strain wall plots:
https://stokljos.github.io/thesis/OhWR10_230305015206_movie.html

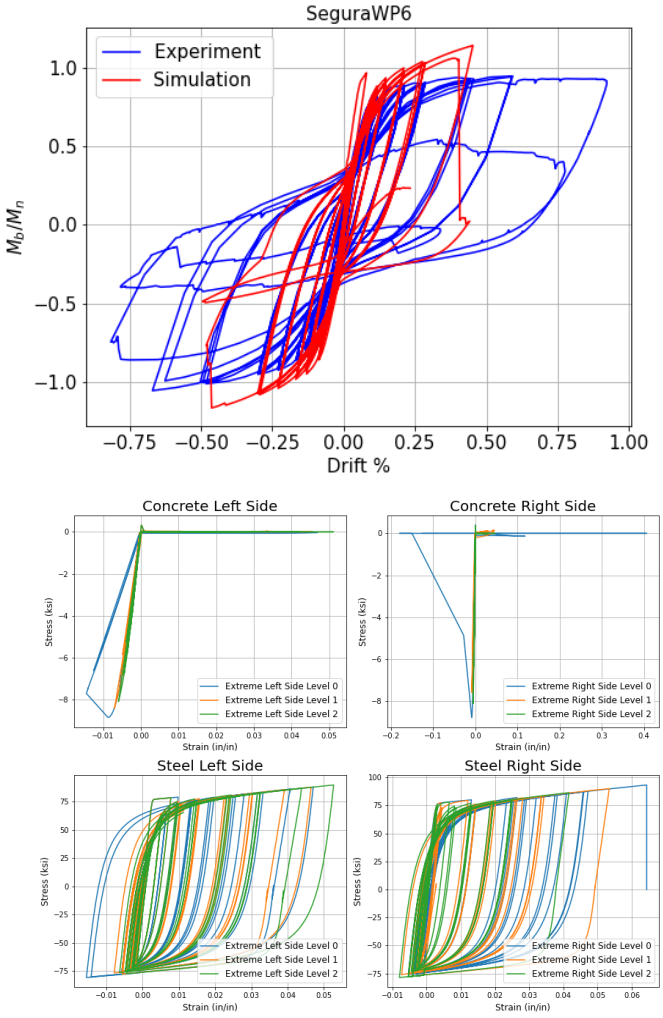

Figure D - 26 WP6 Load-Displacement and Stress Strain Response

Link to interactive Stress and Strain wall plots:
https://stokljos.github.io/thesis/SeguraWP6_230301204151_movie.html

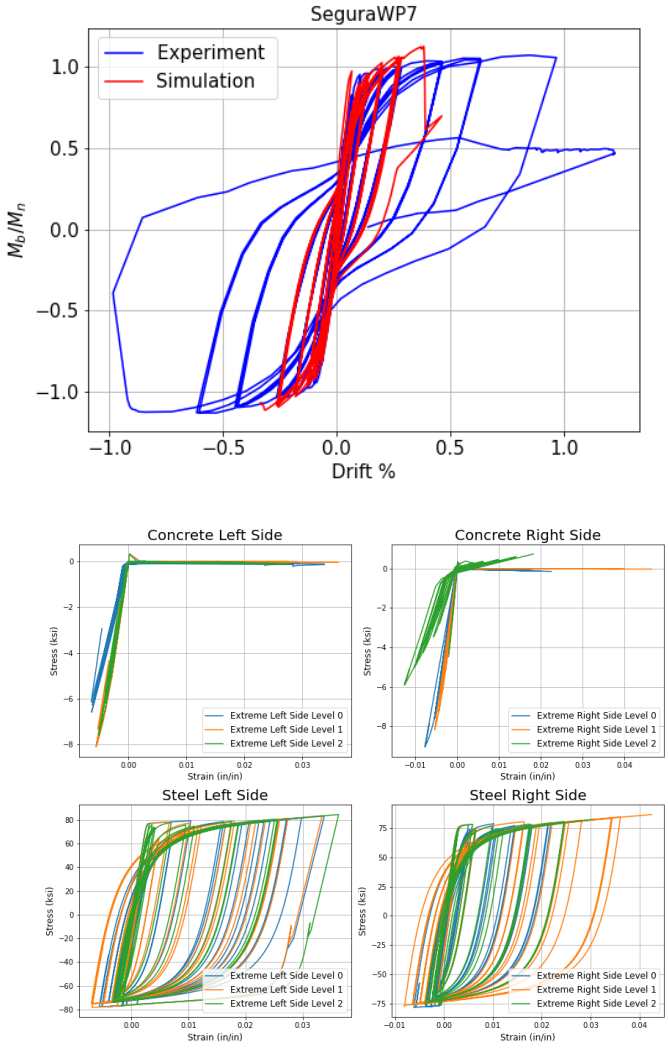

Figure D - 27 WP7 Load-Displacement and Stress Strain Response

Link to interactive Stress and Strain wall plots:
https://stokljos.github.io/thesis/SeguraWP7_230305015217_movie.html

*Note file is to large to preview and needs to be downloaded to be viewed.

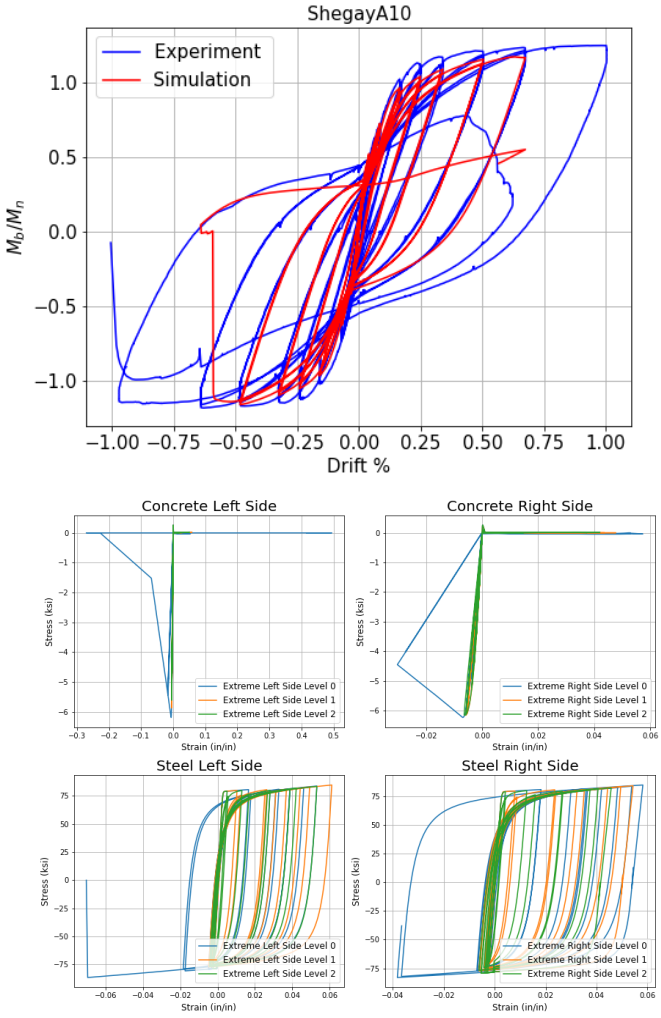

Figure D - 28 A10 Load-Displacement and Stress Strain Response

Link to interactive Stress and Strain wall plots:
https://stokljos.github.io/thesis/ShegayA10_230305015206_movie.html

*Note file is to large to preview and needs to be downloaded to be viewed.

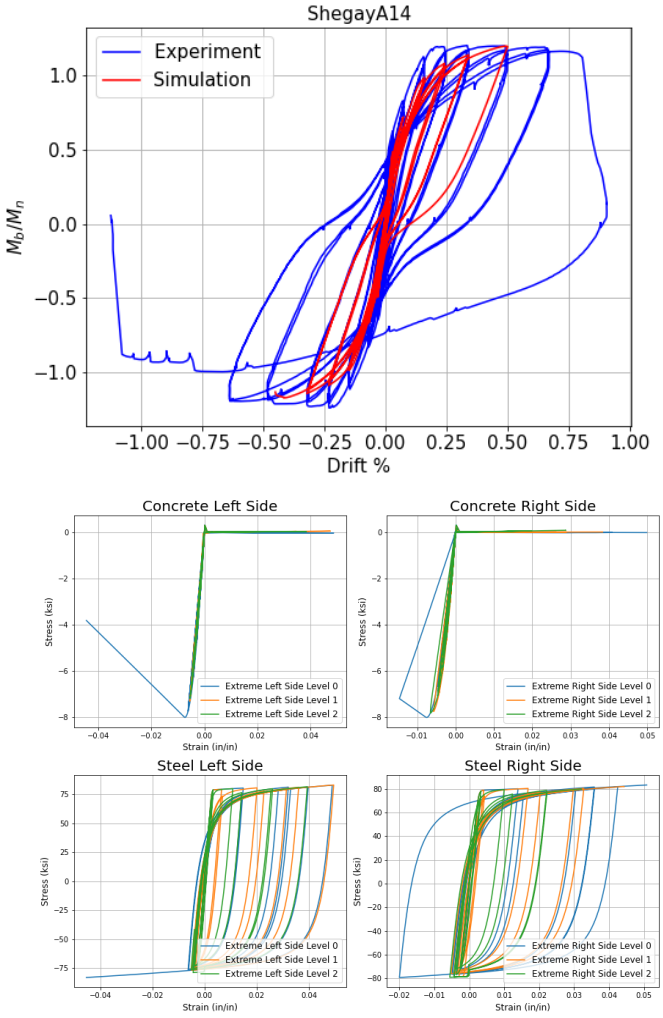

Figure D - 29 A14 Load-Displacement and Stress Strain Response

Link to interactive Stress and Strain wall plots:
https://stokljos.github.io/thesis/ShegayA14_230305015207_movie.html

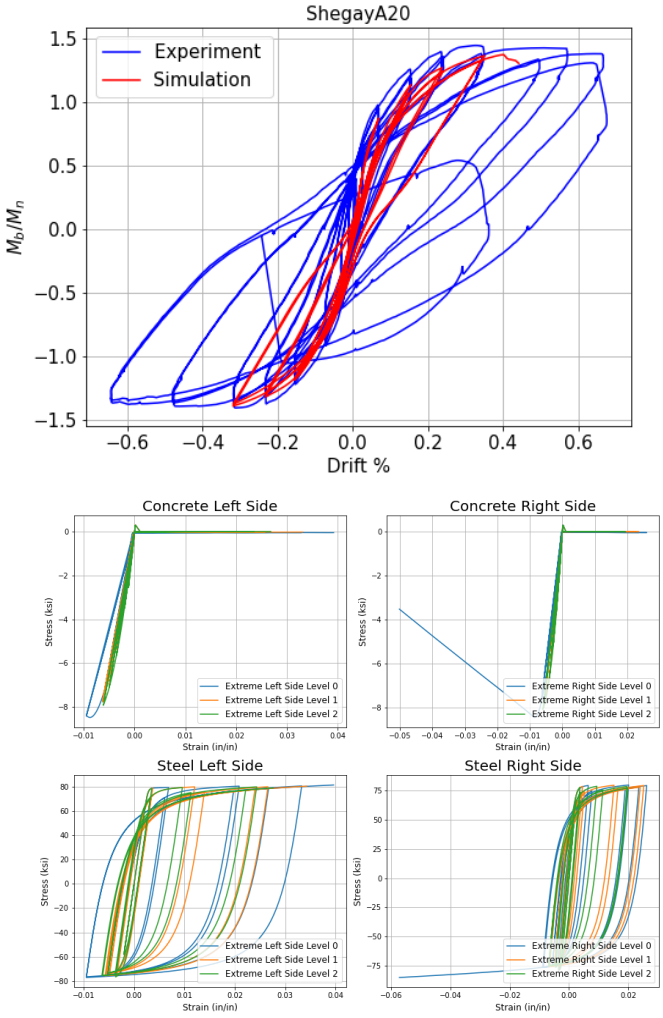

Figure D - 30 A20 Load-Displacement and Stress Strain Response

Link to interactive Stress and Strain wall plots:
https://stokljos.github.io/thesis/ShegayA20_230305015208_movie.html

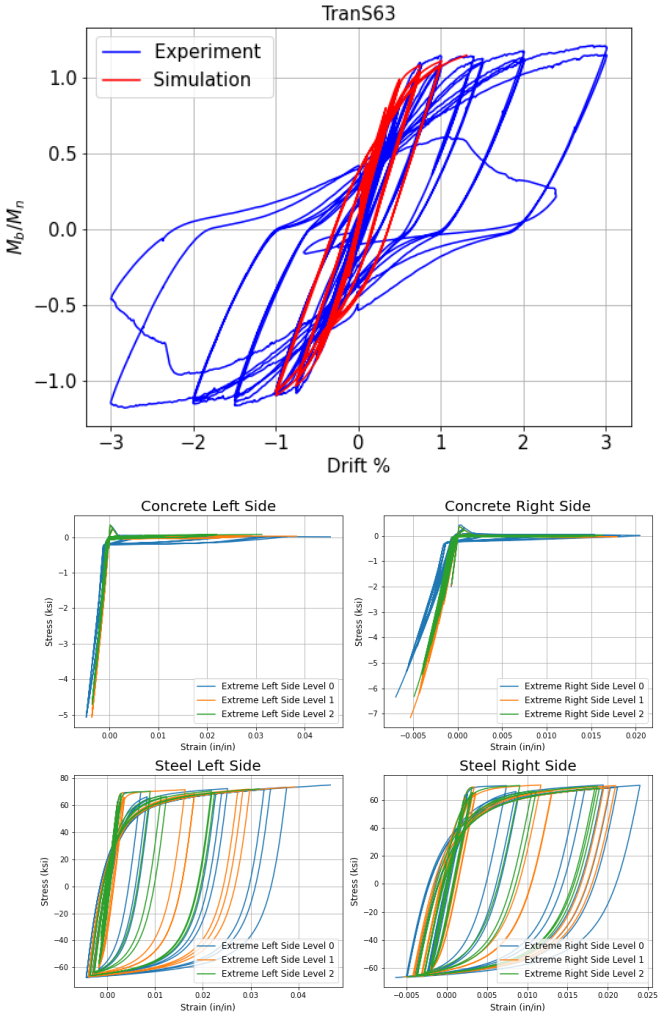

Figure D - 31 S63 Load-Displacement and Stress Strain Response

Link to interactive Stress and Strain wall plots:
https://stokljos.github.io/thesis/TranS63_230305015209_movie.html

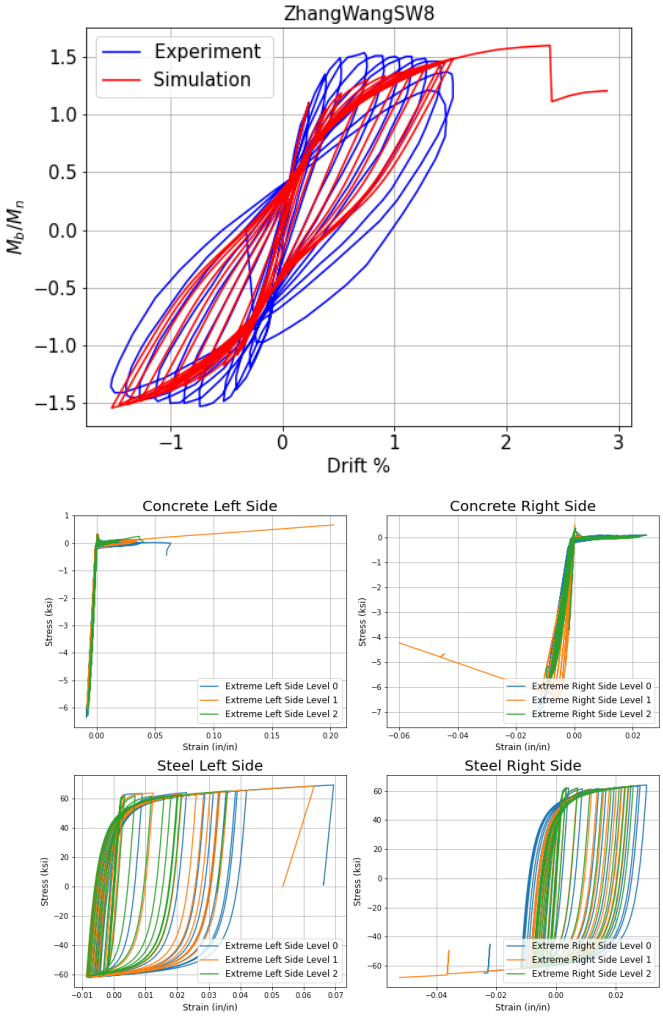

Figure D - 32 SW8 Load-Displacement and Stress Strain Response

Link to interactive Stress and Strain wall plots:
https://stokljos.github.io/thesis/ZhangWangSW8_230301204146_movie.html